

Gold and Gold-Silver Alloy Nanostructures: Synthesis and Applications

A Thesis

Submitted in Partial Fulfillment of the Requirements

for the Degree of

Doctor of Philosophy

by

Ranguwar Rajendra

ID: 20113139



INDIAN INSTITUTE OF SCIENCE EDUCATION AND RESEARCH, PUNE

2017

Dedicated to

My parents and every person who is seeking for the truth



Dr. NIRMALYA BALLAV
Associate Professor (Chemistry)
E-mail: nballav@iiserpune.ac.in
Web: <http://www.iiserpune.ac.in/~nballav/>

Dr. Homi Bhabha Road, Pashan
Pune 411 008, INDIA
Tel: +91 20 2590 8215
Fax: +91 20 2586 5315

CERTIFICATE

Certified that the work incorporated in the thesis entitled “*Gold and Gold-Silver Alloy Nanostructures: Synthesis and Applications*” submitted by *Mr. Ranguwar Rajendra* was carried out by the candidate, under my supervision. The work presented here or any part of it has not been included in any other thesis submitted previously for the award of any degree or diploma from any other university or institution.

Date: 23rd August, 2017

Dr. Nirmalya Ballav
(Research Supervisor)



Declaration

I, **Mr. Ranguwar Rajendra** declare that, this written submission represents my ideas in my own words and where others' ideas have been included; I have adequately cited and referenced the original sources. I also declare that I have adhered to all principles of academic honesty and integrity and have not misrepresented or fabricated or falsified any idea/data/fact/source in my submission. I understand that violation of the above will be cause for disciplinary action by the Institute and can also evoke penal action from the sources which have thus not been properly cited or from whom proper permission has not been taken when needed.

The work reported in this thesis is the original work done by me under the guidance of **Dr. Nirmalya Ballav**.

Date: 23rd August, 2017

Mr. Ranguwar Rajendra
(ID: 20113139)

Acknowledgement

My Ph.D. journey would not have been delightful without the involvement of few people directly or indirectly during my stay in IISER Pune for the last 6 years. I sincerely express my heartfelt gratitude to these people for making me learn many things not only in order to accomplish my Ph.D. but also enhancing my ability to deal with scientific as well as non-scientific problems and thereby making me more confident and optimistic towards life.

I am very much beholden to my thesis supervisor Dr. Nirmalya Ballav without whose everlasting support, encouragement and perseverance to keep my research in the right direction it would not have been possible for me to become a good researcher. I fondly look back on the several fruitful and healthy discussions held with him which gave impetus to my research and not to forget his unwavering faith in me and giving me a free hand in shaping my research. Whenever going got tough for me, brisk conversations with him would lift my spirits up. His unique qualities such as always being optimistic, enthusiastic and altruistic not only improved the quality of doing research but also tremendously influenced my personal life.

I would like to thank my Research Advisory Committee (RAC) members Dr. G. V. Pavan Kumar and Dr. Sudipta Basu for their valuable suggestions and criticism (during RAC meeting) which helped me to improve the quality of my research. I thank Dr. Pavan Kumar and Dr. Janardhan Kundu (NCL) for the measurement of Raman spectroscopy. I also thank Dr. Shilpy Sharma (Department of Biotechnology, Savitribai Phule Pune University) for the cytotoxic study of Au-Ag alloy NPs and Dr. Sreekumar Kurongot (NCL Pune) and Mr. Pranav for the electrocatalysis measurement. I also take this opportunity to thank Prof. N. Ravishankar and Dr. Shalini Tripathi for extending their support in the TEM measurements at times of need. It is my pleasure to thank Prof. Sulabha Kulkarni and Dr. Smita Chaturvedi for allowing me to work with them and making me learn many things about magnetism. Finally, I thank Dr. Prasenjit Ghosh and Ms. Niharika Joshi for teaching me how to do theoretical calculations (computational) by using 'Quantum espresso' and 'Gaussian' software.

I am very grateful to Prof. K. N. Ganesh, Director, IISER Pune for providing excellent lab infrastructure and instrument facility to conduct good scientific research. I am also grateful to Prof. M. Jayakannan, (Chair, chemistry) for his kind support during the early stage of Ph.D.

I am indebted to my lab-mates (former and present) Dr. Barun Dhara, Plawan, Shammi, Kriti, Debashree, Dipayan, Dr. Kaustav Bhattacharji, Dr. Syed Zahid, Hetal, Justin, Srikanth, Shraddha, Siddharth, Mahendra, Vimlesh, Vikas, Anupam, Utkarsh and Jay for being friendly, enthusiastic, co-operative and creating a scientific environment in the lab. I especially thank Barun and Plawan for their enormous support during early days of my Ph.D. since we started our research with the very limited facility. Apart from the technical support from my lab-mates during research, they made me improve my perspective on learning new things.

I am very much grateful to Mr. Anil Prathamshetti for teaching me how to operate FE-SEM instrument which I have used it extensively throughout my Ph.D. I also thank Mahesh Jadhav (T.O), Mayuresh Kulkarni (Admin.), Tushar Kurulkar, Yatish, Nitin Dalvi, Nilesh Dumbre, Ganesh (T.A.) and Praveen Nasa for enormous technical help.

I would like to thank other lab-mates Anant, Gopal, Kiran, Ashok, Mahesh, Arvind, Arun, Indra, Partha Pratim, Sudeb G., Mandar, Sohini, Santhosh.S, Santhosh.P, Rakesh G., Kadlog, Avinash, Abhijeet, Pramod P.S., Shekar (NCL), Tushar (RGB Lab) and Madhanagopal (taught how to synthesise Au NPs at the beginning my research) for their enormous support regarding research. And I am also very much thankful to my NCL friends Krishna Chaitanya (Dr. Majusha lab), Shekar (Dr. Asha lab), Santosh (Dr. Sreekumar lab) and Rangarajan (Dr. Kundu lab) for timely help.

I convey my deepest sense of gratitude to my friends without whom life would not be delightful here, Bapu, Subrahmanyam, Jagdeesh, Rajkumar, Palvai, Satish D., Satish E., Ganesh, Ravikiran, Kishor, Krishna, Venky, Rajesh, Shiva, Mahesh, Ashok N., Reddy, Koti, Harikrishna, Aluri, Mullangi, Narasimha, Veeresh, Mehak, Meghna, Reman, Nanda, Naveen, Jagan, Mohan and Pavan. I specially mention the names of Bapu and Subrahmanyam for their immense support when I was in difficult situations.

It gives me an immense sense of satisfaction to express my sincere gratitude to my school and college teachers. Vinod Siddamshetty (Maths), Shankar (Science), Shankar Kadasa (Science) motivated me a lot regarding the importance of education in life. Gopikrishna (Maths) not only taught me mathematics in intermediate education (11th and 12th) but also encouraged me to cross the barrier of being dumb in the study. The most influencing teacher I met is Dr. Nakka Srinivas who taught me (for few months) chemistry during my B.Sc. 2nd year in such an

excellent way that it became my favorite subject (it was boring before he taught) and also made me choose research as my career.

I owe to my best friends Rakesh samala (tINGU), A. Mahesh, N.R.P., Revoji, Goskula, Kranthi and Suresh for their consistent and honest support is helping me a lot to keep myself excited and joyful.

Words fall short to express my indebtedness towards my mother in her consistent efforts to shape me into a good human being. She has been my first teacher who has not only introduced me to preliminary education but also trained me strictly regarding the importance of moral values in life. My father's unshaken patience in the face of adversities is what I look up to and hope to imbibe.

Ranguwar Rajendra

Table of Contents

Synopsis	i-iv
List of Publications	v
1. Introduction for Noble Metal Nanoparticles	1-33
1.1 Introduction	
1.2 Synthesis and Growth of Metal Nanoparticles	
1.3 Surface Plasmon Resonance (SPR)	
1.4 Anisotropic Au NPs	
1.4.1 Role of Surfactant	
1.4.2 Role of Halides	
1.4.3 Role of Silver	
1.5 High-Index Faceted Metal Nanoparticles	
1.6 Gold Nanowires	
1.7 Bimetallic Nanoparticles	
1.8 References	
2. High-Index Faceted Gold Nanocrystals (Au NCs)	
A: Synthesis and Applications of Convex Au NCs	34-50
2A.1 Introduction	
2A.2 Materials and Methods	
2A.3 Results and Discussion	
2A.4 Summary and Conclusions	
2A.5 References	
B: Synthesis and Characterization of Convex Au NCs	51-57
2B.1 Introduction	
2B.2 Materials and Methods	
2B.3 Results and Discussion	
2B.4 Summary and Conclusions	
2B.5 References	
3. Synthesis and Characterization of Gold Nanowires	58-66
4. Synthesis, Characterization and Applications of Au-Ag alloy NPs	67-88

Synopsis

The thesis entitled “*Gold and Gold-Silver Alloy Nanostructures: Synthesis and Applications*” includes 4 chapters.

Nobel metal nanostructures have received a considerable research attention in the view of diverse applications promise ranging from drug-delivery, photonics, optoelectronics, surface enhanced Raman scattering (SERS), to catalysis and electro-catalysis. Among various nanoscale structures, gold (Au) and silver (Ag) nanoparticles (NPs) are widely studied, perhaps due to their shape, size, and composition dependent optical properties and catalytic activities. However, the development of effective synthetic protocols for the precise control of size, shape, and composition of such NPs has always been challenging.

Our work primarily aimed at developing facile wet-chemical synthesis of Au and Au-Ag alloy NPs with controllable physiochemical properties. We have successfully used tannic acid and ammonium hydroxide (NH₄OH) as one of the reagents in course of producing various Au-based nanostructures. Specifically, tannic acid was used as a mild reducing agent for the dimension controlled synthesis of convex and concave Au NPs enclosed with high-index facets (represented by a set of Miller indices, *h*, *k*, and *l*, having at least one index greater than unity). High-index faceted Au NPs were employed for SERS studies and electro-catalytic oxidation of formic acid (HCOOH). The reducing power of tannic acid was further extended to produce Au nanowires. Finally, NH₄OH was utilized to synthesize composition tuneable, chemically stable, and homogeneously alloyed Au-Ag alloy NPs at relatively higher concentrations, above the solubility product of silver chloride (AgCl).

Chapter-1. *Introduction for Metal Nanoparticles*

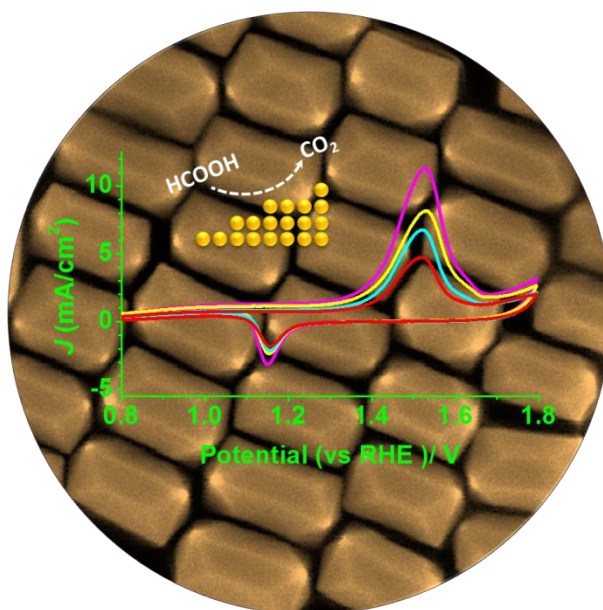
This chapter comprises of general introduction for the metal nanoparticles, properties, and growth mechanism of spherical nanoparticles in bottom-up approach. Seed-mediated growth method has been discussed extensively regarding the proposed growth mechanisms for Au nanorods (also applicable to other metal nanostructures) and the important roles of each chemical species present in the growth solution. Introduction to various high-index faceted, bimetallic, and 1D metal nanostructure is also discussed.

Chapter-2. *High-Index Faceted Gold Nanocrystals (Au NCs)*

This chapter has been divided in to two parts as Chapter-2A and Chapter-2B.

Chapter-2A. *Synthesis, Characterization and Applications of Convex Au NCs*

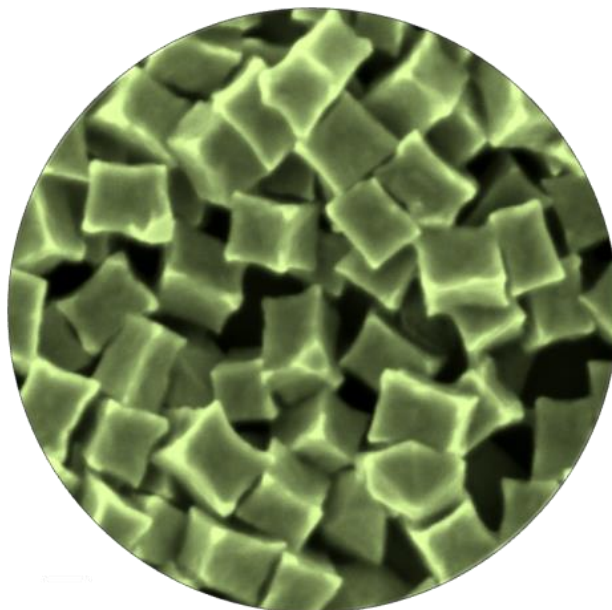
In this section, we have successfully explored for the first time, tannic acid as mild reducing agent in seed mediated growth method for the synthesis of elongated tetrahedra (ETHH) Au NCs with precisely controlled size. Additionally, electrocatalytic activity (formic acid oxidation) and SERS applications of ETHH Au NCs were studied.



Reference: High-index faceted Au nanocrystals with highly controllable optical properties and electro-catalytic activity. **Ranguwar Rajendra**, Pranav K. G., Shalini T., Sreekumar K. and Nirmalya Ballav. *Nanoscale* **2016**, 8, 19224-19228.

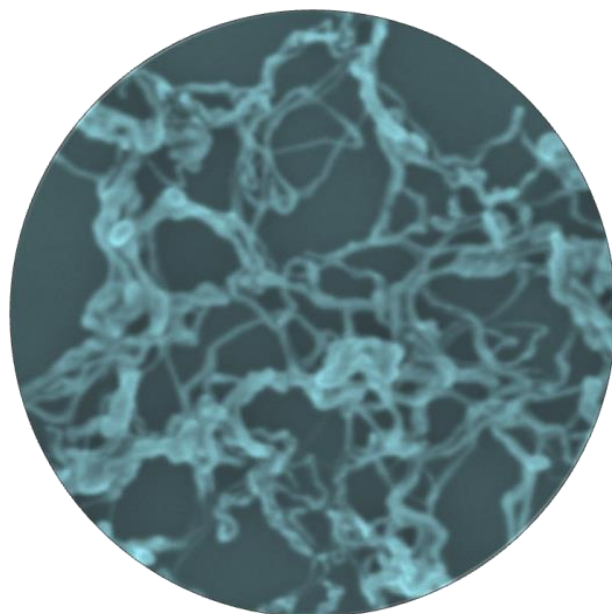
Chapter-2B. *Synthesis and Characterization of Concave Au NCs*

This part encloses the size controlled synthesis of concave cuboid Au NCs through seed mediated growth method by using tannic acid and pre-formed Au NRs as mild reducing agent and seeds, respectively. Characterizations of concave Au nanocuboids have been done with UV-Vis spectrometer, FE-SEM and HR-TEM techniques. (Manuscript under preparation)



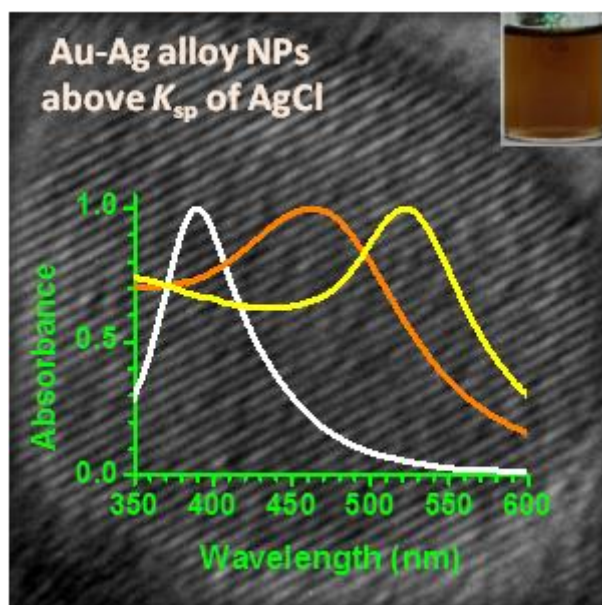
Chapter-3. *Synthesis and Characterization of Gold Nanowires (Au NWs)*

The use of tannic acid has been further extended to the development of simple and robust method for the synthesis of Au NWs. Our method utilizes readily available chemicals and the growth of Au NWs was completed within few minutes. UV-Vis spectrometer, FE-SEM and TEM techniques were used for the characterization of Au NWs. (Manuscript under preparation)



Chapter-4. Synthesis, Characterization and Applications of Au-Ag alloy NPs

The major problem encountered (during the period 2002-2014) in the synthesis of homogeneously alloyed Au-Ag alloy NPs by simple co-reduction of HAuCl_4 and AgNO_3 is the formation of AgCl precipitate (difficult to be reduced) in the reaction mixture. Therefore, it hampered production of Au-Ag alloy NPs with desired composition. Here, we have successfully synthesized homogeneously alloyed Au-Ag alloy NPs as per the feeding moles of HAuCl_4 and AgNO_3 by using NH_4OH as dissolving agent for the AgCl precipitate. These Au-Ag alloy NPs were characterized with various techniques and diverse applications were also studied.



References: (1) Homogeneously-alloyed gold–silver nanoparticles as per feeding moles. **Ranguwar Rajendra**, Parnika Bhatia , Anita Justin, Shilpy Sharma, and Nirmalya Ballav *J. Phys. Chem. C*, 2015, 119 , 5604–561.

(2) Discriminative response of aliphatic and aromatic dithiol in the self-assembly of gold nanoparticles. **Ranguwar Rajendra** and Nirmalya Ballav, *RSC Adv.* 2013, 3, 15622-15625.

List of Publications

1. *High-index faceted Au nanocrystals with highly controllable optical properties and electro-catalytic activity.* **Ranguwar Rajendra**, Pranav K. G., Shalini T., Sreekumar K. and Nirmalya Ballav, *Nanoscale* **2016**, *8*, 19224-19228.
2. *Homogeneously-Alloyed Gold–Silver Nanoparticles as per Feeding Moles.* **Ranguwar Rajendra**, Parnika B., Shilpy S., and Nirmalya Ballav, *J. Phys. Chem. C*, **2015**, *119* (10), 5604–5613.
3. *Highly Hydrophobic and Chemically Rectifiable Surface-Anchored Metal-Organic Framework Thin-Film Devices.* Shammi R., **Ranguwar Rajendra**, Barun D. Plwan K. J., Nirmalya Ballav, *Adv. Mat. Interfaces* **2016**, *3*, 1500738.
4. *Probing bismuth ferrite nanoparticles by hard x-ray photoemission: Anomalous occurrence of metallic* Smita C., Indranil S., Mandar M. S., U-Ser J., Yi-Qi Y., **Ranguwar Rajendra**, Nirmalya Ballav, and Sulabha K. *App. Phys. Lett.* **2014**, *105*, 102910.
5. *Coercivity and exchange bias of bismuth ferrite nanoparticles isolated by polymer coating* Smita C., Mandar M. S., **Ranguwar Rajendra**, Surjeet S., Nirmalya Ballav, and Sulabha K., *J. App. Phys.* **2014**, *115*, 123906.
6. Discriminative response of aliphatic and aromatic dithiol in the self-assembly of gold nanoparticles. **Ranguwar Rajendra** and Nirmalya Ballav, *RSC Adv.* **2013**, *3*, 15622–15625.

Chapter-1

Introduction to Metal Nanoparticles

1.1 Introduction

Noble metals have been of significant interest to human-beings since ages, due to their intriguing properties such as good conductor of electricity and heat, high ductility and tensile strength and most importantly, resistance to corrosion and oxidation at ambient conditions. Thus, such unique physicochemical properties allowed us to use them in art, fine jewellery and coinage etc. The annual production order of widely used noble metals is Silver (Ag) > Gold (Au) > Palladium (Pd) > Platinum (Pt); though Ag is produced more, relatively greater susceptibility to oxidation in air hampered its practical applications. Therefore, Au has become the most important metal in various applications due to its chemical inertness in air. Despite its pretty appearance in bulk, when the size is brought to nanometer size (<100 nm) regime, very interesting and distinct optoelectronic properties can be perceived. In this size range Au nanoparticles (NPs) exhibit surface plasmon resonance (SPR), a phenomenon defined as a collective oscillation of conduction electrons upon interacting with light.¹⁻³ There exists a plethora of articles which explored the variation of SPR with size, shape, stabilizing agent, dielectric constant (of the surrounding media), composition (for example bimetallic) and colloidal stability of NPs. Along with SPR, various fascinating physicochemical properties of metal NPs allow them to be functional in diverse applications such as biomedical, electronic devices, electrochemical, solar energy harvesting, optics, photonics and catalysis.⁴⁻¹¹ However, dealing with materials at nanoscale, for examples, dimension controlled synthesis of anisotropic NPs enclosed with high-index facets and synthesis of homogeneously alloyed NPs remained challenging task, part which has been addressed in this thesis work.

1.2 Synthesis and Growth of Metal Nanoparticles

Usually there are two approaches for the synthesis of metal NPs: i) top-down and ii) bottom-up. Top-down method involves the breakdown of large particles (micro size) of bulk metal into NPs^{12,13} whereas bottom-up approach is associated with the reduction or decomposition of metal ions into atoms followed by their aggregation in to NPs.^{14,15} The latter method is more practical and versatile for the synthesis of diverse NPs of different shapes and sizes. In general, this method requires four precursors, i) appropriate solvent, ii) metal ion salt, iii) capping agent, and iv) reducing agent (sometimes capping agent itself). Furthermore, experimental conditions such

as temperature, pH and concentration of precursor of the reaction mixture have a significant influence on morphology of the final nanoparticle. Most of the synthetic methodologies developed for the fabrication of metal nanoparticles are based on bottom-up approach; wet-chemical, green syntheses, and digestive ripening etc. For the synthesis of Au NPs, Turkevich method is widely used.¹⁶ This method is as follows: aqueous solution of gold (III) chloride (HAuCl_4 (1mM) is heated to boiling with subsequent addition of sodium citrate (Na_3Ct) (resultant concentration is 2.5 mM) to the solution. Eventual change in colour of the solution from pale yellow to wine-red colour within 20 min is observed. Here Na_3Ct acts as a reducing as well as a capping agent. A comprehensive study has been done by Siavash Irvani on the green synthetic methodologies.¹⁷ B. L. V. Prasad and co-workers have explored the digestive ripening method to achieve size uniformity of gold nanoparticles (**Figure 1.1**).¹⁸⁻²¹

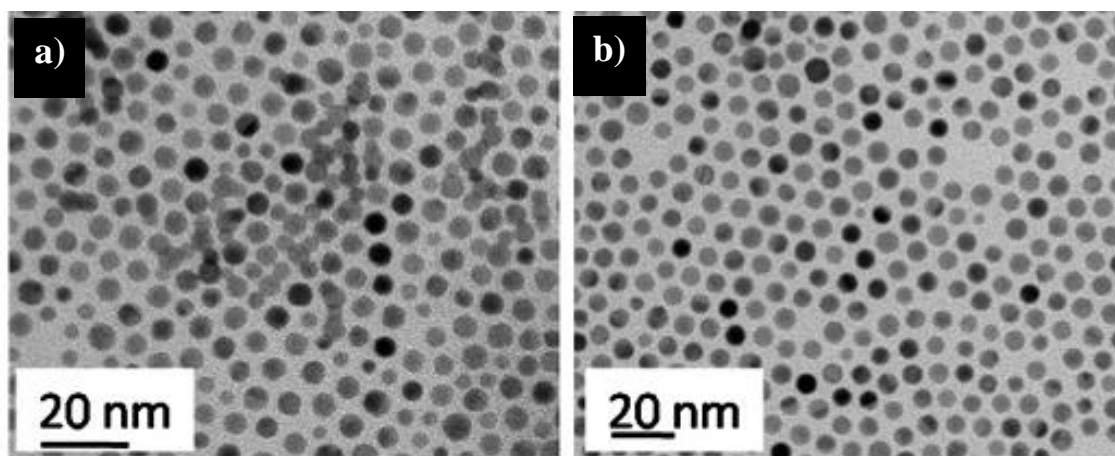


Figure 1.1: TEM images of Au nanoparticles digestively ripened at 110 °C (a) and 180 °C (b) with hexadecanethiol. (adopted from Ref. 19 © Royal Society Chemistry)

To explain the nucleation and growth mechanism of Au NPs, Victor K. La Mer had proposed a theoretical model, –so called ‘classical nucleation theory’.²² According to this theory, when the concentration of Au^0 (after reduction) reaches super saturation level in the solution, it begins the self-nucleation and generate some primary particles which will acts as nuclei centres or seeds in later stages for the deposition of newly formed Au^0 atoms.

Moreover, the number of primary particle increases until the concentration of Au^0 becomes much lower than super-saturation and remain constant till the end of the reaction. Contrary to this

theory, Polte *et al.* has proposed a three phase mechanism for the Au NPs nucleation and growth under different experimental conditions by utilizing small-angle X-ray scattering (SAXS) and X-ray absorption near edge structure (XANES) techniques.²³

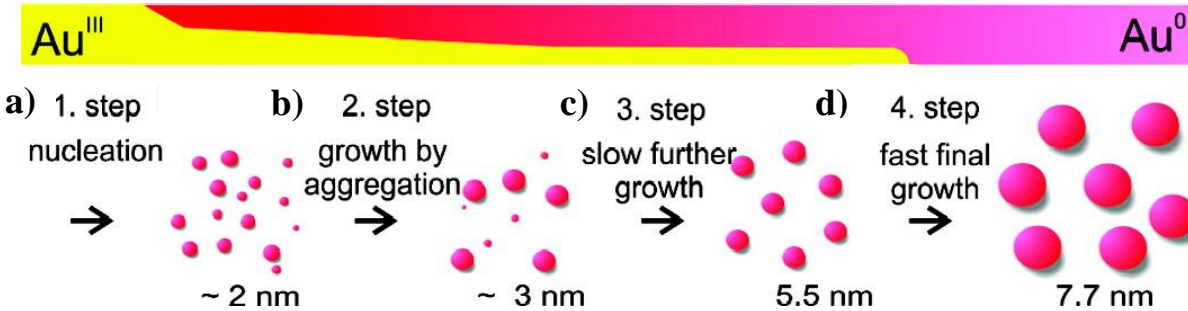


Figure 1.2: Schematic illustration for the deduced process of Au NPs formation. (adopted from Ref. 23 © American Chemical Society)

The three phase of Au NPs formation was interpreted as four-step nucleation and growth where the first phase has been further divided into two steps. The first two steps include rapid nucleation followed by coalescence of nuclei to form bigger particles. The third step consists of slow diffusion growth of the as-formed nuclei in the second step along with the reduction of Au precursor and coalescence. Subsequently, rapid growth takes place to final size accompanied by the complete consumption of Au (III) precursor (**Figure 1.2**). Loh *et al.* have performed real-time transmission electron microscopy (TEM) experiments and theoretical calculations claiming that in the reaction mixture at initial stage, supersaturated Au⁰ solution is formed, followed by spinodal decomposition resulting in gold-rich and gold-poor liquid phases. Consequently, gold-rich phase turned into amorphous gold nanoclusters and then gold nanocrystals (**Figure 1.3**).²⁴

Metal nanoparticles are stabilized in the aqueous solution owing to the capping agent which ligates to the metal surface as well as interacts with the medium. According Derjaguin–Landau–Verwey–Overbeek (DLVO) theory^{25,26} there are mainly four kind of interactions between nanoparticles: i) Van der Waal attraction (V_{vdW}), ii) electrostatic repulsion (V_{elec}), iii) dipole-dipole (V_{dipole}) and iv) dipole-charge ($V_{dipole-charge}$). The total potential (V_T) of nanoparticle is the these four potentials, estimated by the following equation

$$V_T = V_{vdW} + V_{elec} + V_{dipole} + V_{dipole-charge}$$

In general, V_{elec} predominates over the rest of the potentials to keep the nanoparticles well isolated from each other in aqueous colloidal solution whereas in hydrophobic solvents relatively stronger Van der Waals interaction between capping agent and solvent molecules than among metal nanoparticles. Partial removal of capping agent on Au NPs causes asymmetric charge distribution over the surface which induces the dipole moment (positive and negative charge separation) and thus lead to linear agglomeration whereas complete removal or exchange with hydrophobic (dodecanethiol) capping agent would promote the globular type agglomeration; dipole-dipole interaction (V_{dipole}) is anisotropic whereas V_{vdW} and V_{elec} are isotropic. Colloidal stability of metal nanoparticles has a great influence on their optical properties originated from the intrinsic property named as surface plasmon resonance which is discussed in the next section.

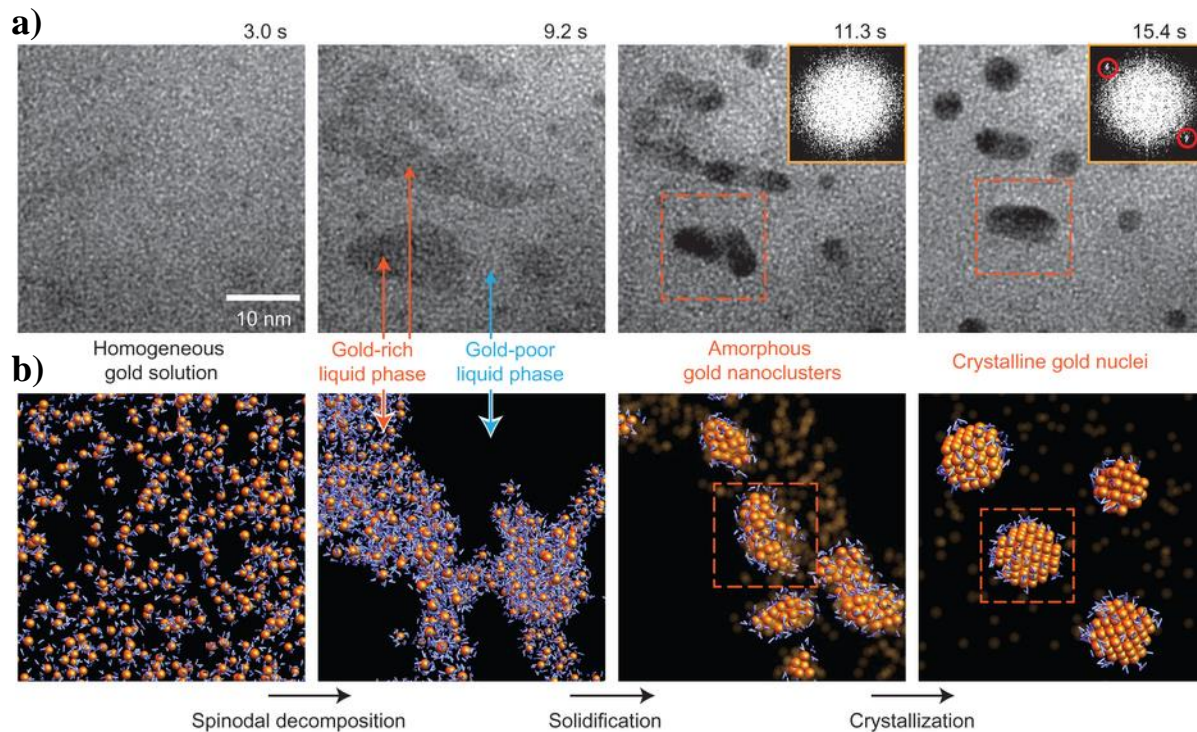


Figure 1.3: a) Real time TEM imaging of gold nanocrystals evolution, images captured at 3, 9.2, 11.3 and 15.4s after Au^0 atoms generated in the solution. Insets shows the Fourier transform of nanocrystals marked with red colour square boxes. b) Schematic of the proposed steps in nucleation (gold as orange spheres, with surrounding water as blue bent lines). (adopted from Ref. 24 © Nature Publishing Group)

1.3 Surface Plasmon Resonance (SPR)

The free electrons in the conduction band of metals such as Ag and Au are free to travel through the material. Since, mean free path of free electrons in Au and Ag is ~ 50 nm, no scattering is expected from the bulk if the dimensions of the particles smaller than the mean free path. Therefore all interactions can occur with the surface. When the wave length of light is much larger than the nanoparticle size it can set up standing resonance conditions as represented in **Figure 1.4**. The oscillating electric field of light causes the conduction electrons (free-electrons/plasmon) in metal to oscillate coherently. Furthermore, coherent oscillation is indeed the result of displacement of electron cloud relative to metal nuclei and the restoring force (created from Coulomb attraction between electron cloud and nuclei) that pull the displaced electron cloud to the nuclear framework.¹⁰

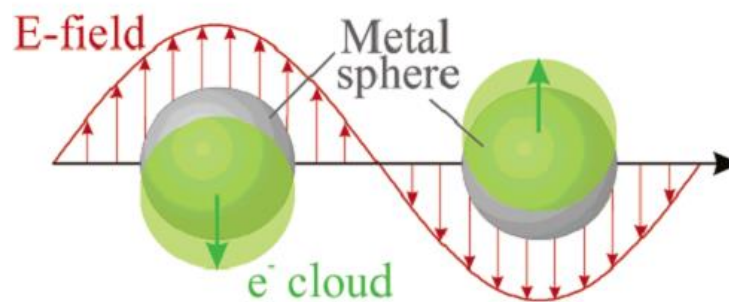


Figure 1.4: Origin of surface plasmon resonance due to coherent interaction of the electrons in the conduction band with light. (adopted from Ref. 10 © The Royal Society of Chemistry)

The oscillation frequency is relies on size and shape of nanoparticle and dielectric constant of surrounding media.^{3,11} Size of the metal nanoparticles has significant influence on SPR band position. As the average size of the particles increases, SPR band red-shifts (**Figure 1.5**) and absorbance would decrease due to increase in scattering portion as compared with absorption upon interaction with light.²⁷ For example, spherical Au NPs exhibit only one SPR band; spherical Au NPs of 27 nm exhibit surface plasmon band (SPR) at 520 nm in UV-vis spectrum¹⁶ and its position varies with the increase or decrease in size (**Figure 1.5a**).

In addition to size variation, shape also has substantial effect on SPR features. Gold nanorods (Au NRs) possess two peaks correspond to transverse (TSPR; at lower wavelength) and longitudinal (LSPR; at higher wavelength) SPR (red curve; **Figure 1.6**). These two peaks at

lower and higher wavelength are attributed to plasmon oscillations perpendicular to and along the length of nanorod respectively. LSPR of Au NRs gets significantly red-shifted as the aspect ratio (AR) of its increases (**Figure 1.5**).²⁸ Au nanoprisms exhibit three SPR peaks in UV-vis spectrum (blue curve; **Figure 1.6**).²⁹

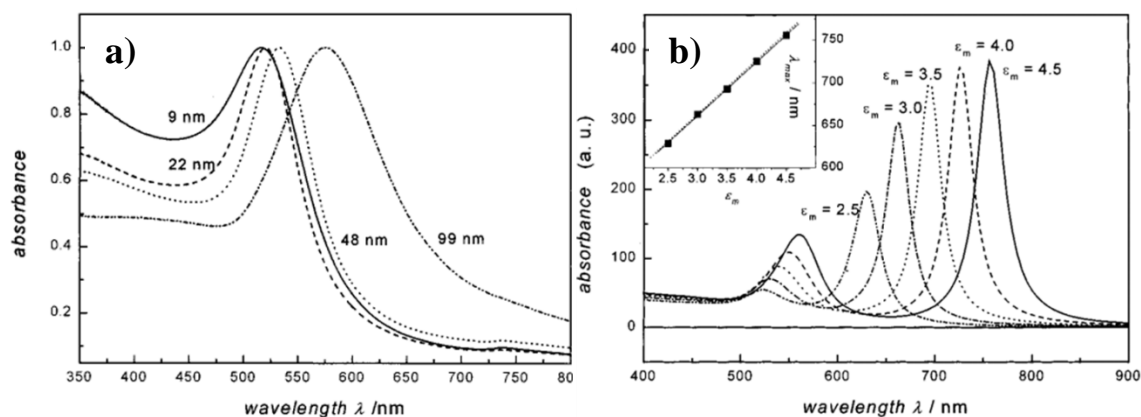


Figure 1.5: a) UV-vis spectra for the spherical Au NPs with different sizes. b) Simulated optical absorption of Au NRs with various ARs and inset: represents the linear relationship between different ARs and LSPR λ_{max} . (adopted from Ref. 27 & 28 © American Chemical Society)

As the refractive index of the surrounding medium is increased surface plasmon band of Au NPs red-shifts. The refractive index sensitivity order for Au NPs with different shapes is bipyramid > nanorod > sphere. Recently a detailed study of refractive index sensitivity vs. Au NPs shape has been conducted in water-glycerol mixture.³⁰

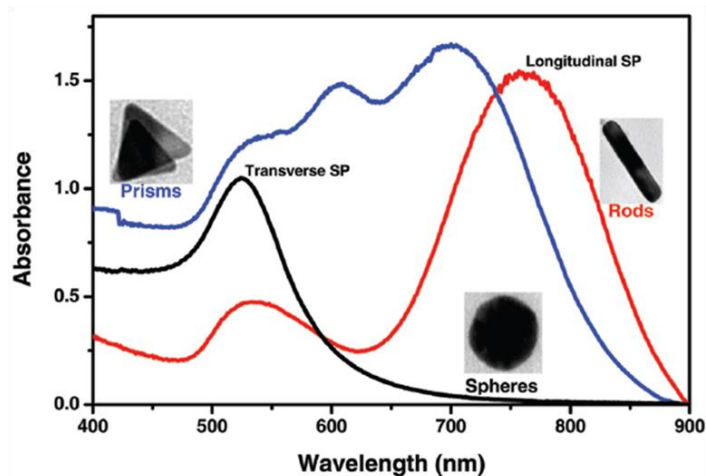


Figure 1.6: UV-vis spectra of Au NPs with different shapes. (adopted from Ref. 29 © The Royal Society of Chemistry)

The stabilizing agent also influences the surface plasmon band of metal nanoparticles. There are various kinds of capping agents used for nanoparticle synthesis. The extent to which the ligand or capping agent influences the electronic structure of metal depends on how strongly the ligand is bound to the surface of nanoparticles. Also, charge and packing density of capping agent affect the plasmon property of metal nanoparticles.¹

In addition to the influence of size and shape of Au NPs on its surface plasmon resonance, self-assembly of these NPs also has significant effect.³¹⁻³³ Thomas et al. extensively studied the controlled self-assembly of Au NRs (end to end) induced by various thiol molecules; by varying the concentration of thiols in Au NRs solution different kinds of self-assembly was achieved.³⁴⁻³⁶

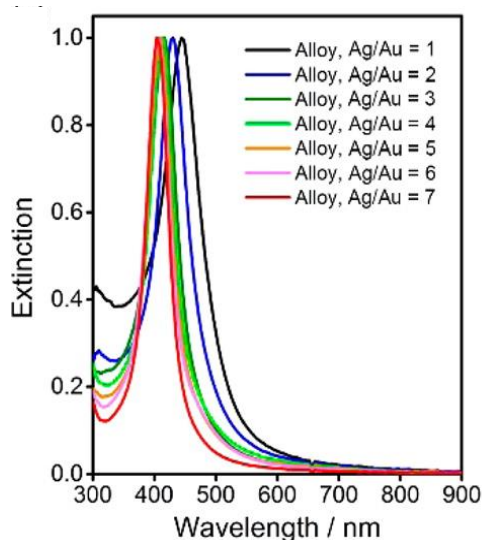


Figure 1.7: UV-vis spectra of Au-Ag alloy nanoparticles synthesized with different composition. (adopted from Ref. 39 © American Chemical Society)

Distinct properties can be achieved upon combining two or more elements in a single metal nanoparticle. For example, synergetic effect has been observed in catalysis and optical properties when Ag and Au were incorporated together in a nanoparticle.^{37,38} It is well known fact that Ag NPs possess prominent optical properties as compared to Au NPs. However, when it comes to its usage as drug delivery vehicle and substrate for SERS applications, its susceptibility towards oxidation hampers its effectiveness. However, introducing Au into Ag NPs (alloy) not only improves its resistance to oxidation but also renders tunability of the SPR band with the variation of composition (**Figure 1.7**).³⁹

1.4 Anisotropic Au NPs

Anisotropic or non-spherical Au NPs such as rods (NRs), octahedral, cubes, etc. are being explored in many important applications ranging from optics to sensing to catalysis.^{8,40,41} Thus, synthesis has become a very important field of research to access tailor-made nanostructures with uniform size and shape. To date, significant amount of advancement has been achieved regarding the development of milder synthetic protocols and successful execution of these NPs into various applications. The synthetic methods developed over the years can be categorized based on the solvents used; aqueous and organic phases. Organic phase synthesis requires high temperature and also results in poor tunability of size and shape. In contrast, aqueous phase synthesis is more versatile offering precise tuning of shape and size depending on applied experimental conditions. Furthermore, aqueous phase method can be sub-divided into two: i) seed mediated^{42,43} and ii) seedless syntheses.⁴⁴ The vast majority of reported syntheses of shape controlled Au NPs employed seed-mediated growth method.⁴⁵ This method involves two steps: synthesis of seeds (2-4 nm sized NPs) followed by, addition of seeds to the growth solution (whereas seedless method excludes the seed synthesis). It was developed by Murphy and co-worker for the synthesis of Ag NRs and nanowires (NWs). In the first step, Ag NPs seeds of 3 nm were synthesized by reducing AgNO₃ with NaBH₄ in presence of Na₃Ct and subsequently added to the growth solution containing AgNO₃, Cetyltrimethylammonium bromide (CTAB), ascorbic acid and NaOH.⁴³ Though the same method was also applied for the successful synthesis of Au NRs with different aspect ratios, poor yield (~30%) was encountered (**Figure 1.8g**).⁴⁶ The method for the Au NRs had not been popularized until El-Sayed and co-workers proposed the up-gradation of the same method which led to almost 100% yield of Au NRs by simply replacing the citrate capping agent with CTAB during the synthesis of seed (**Figure 1.8a-f**).⁴⁷

Later on, this method paved the way for the synthesis of different nanostructures such as cubes, octahedral, trigonal prism, bipyramid, star, etc..^{40,48-50} The versatility/flexibility of this method motivated the nanoscience community to investigate the mechanism of growth by understanding the role of various factors such as concentration of reagents, temperature, and pH of the growth solution etc.. Although, there are plenty of research articles regarding the synthesis and applications of various gold nanostructures, few reports merely focused on mechanism of

nanostructures formation.^{51,52} The Au NRs is the only structure for which formation mechanism has been extensively studied as compared to other Au nanostructures. In the following sections, it has been broadly discussed that the role of various factors which influence the growth mechanism of Au NRs. Such understanding is also very useful for the development of new synthetic protocols (most of this thesis work) for other anisotropic Au nanostructures.

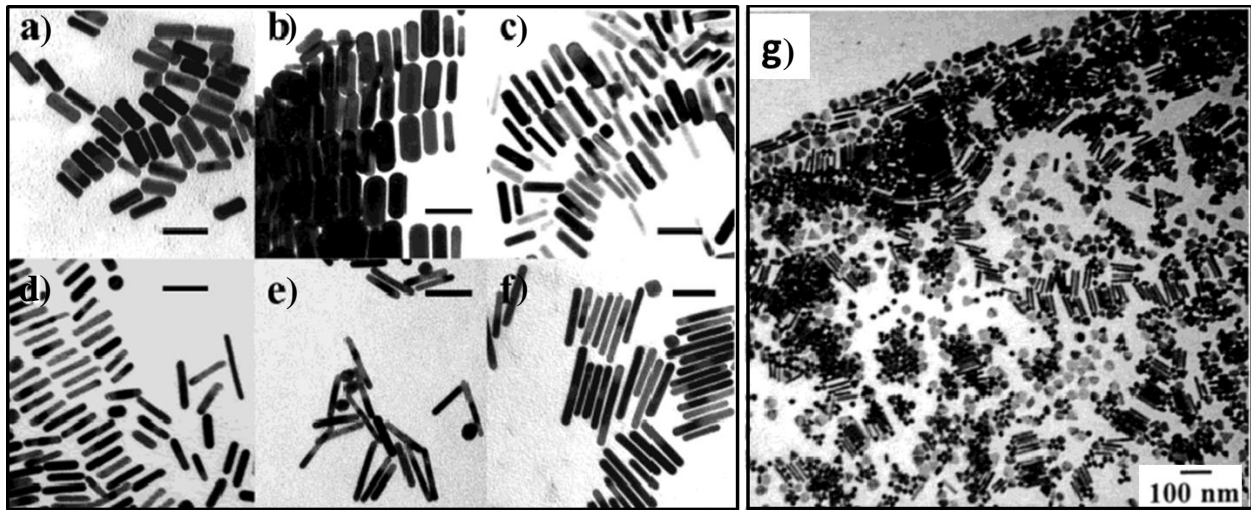


Figure 1.8: a-f) TEM images of Au NRs of different aspect ratio, synthesized by El-sayed method. g) TEM image of Au NRs (~30%) synthesized by Murphy method. (adopted from Ref. 47 & 46 © American Chemical Society)

1.4.1 Morphology and Age of the Seed

As described in the previous section, the yield and size uniformity of Au NRs was significantly improved just by changing the capping agent from Na_3Ct to CTAB during the synthesis of Au NPs seed. To explain this, Guyot-Sionnest and coworkers⁵³ have made thorough analysis of transmission electron microscope (TEM) (**Figure 1.9**) for the aforementioned seeds and thereby concluded that the actual cause of enhancement in yield was due to the difference in seed crystallinity rather than capping agent itself, i.e. citrate capped seed (Ct-Au NPs) solution consists of a mixture of various multiply twinned (singly, doubly, penta) crystalline nanostructures (**Figure 1.9b**) whereas in case of CTAB capped seeds (CTAB-Au NPs) all are associated with single crystallinity (**Figure 1.9a**). Furthermore, Ct-Au NPs seeds are almost enclosed with (111) planes while CTAB-Au NPs seeds are enclosed with (100) and (111).

It must be noted that just the use of CTAB-Au NPs seeds may not yield mono-dispersed Au NRs unless the seed (as synthesized) is introduced into the growth solution before its certain age. It has been shown that Au NRs yield decreases as the age of seed (t_{age}) increases ($>1\text{hr}$). To explain this, John et al. studied the impact of seed age on Au NRs quality by using microfluidic reaction

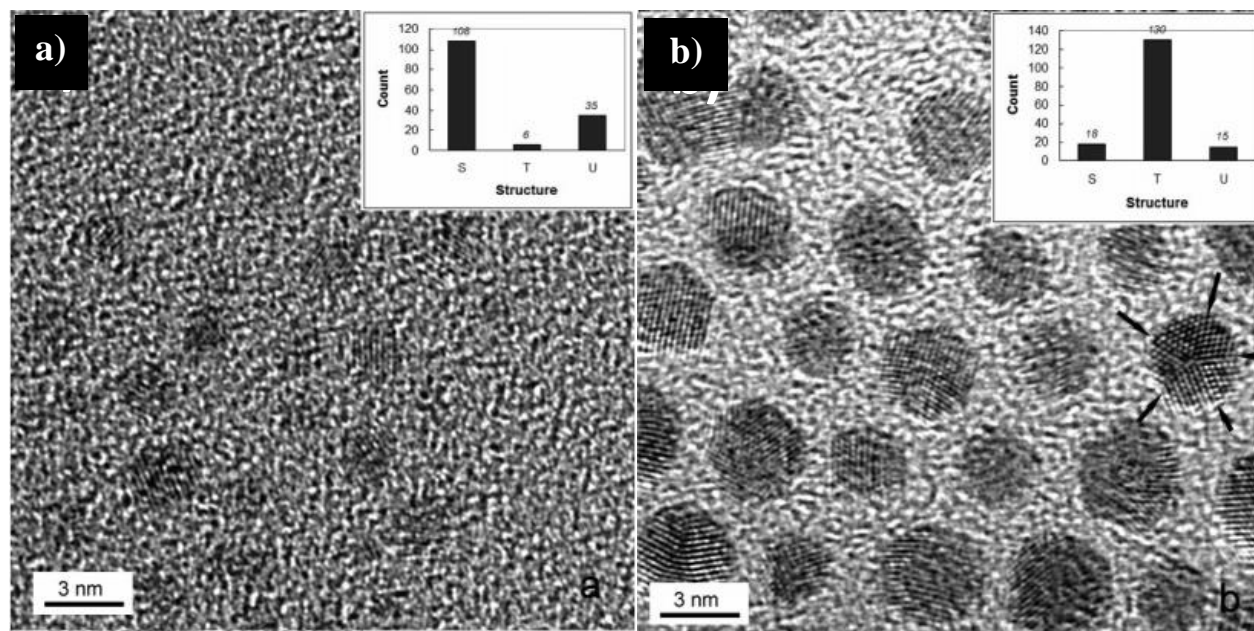


Figure 1.9: a) High-Resolution TEM image of CTAB-Au NPs seeds. b) High-Resolution TEM image of Ct-Au NPs seeds; the arrow marks in the right side are indicating the twinning in nanoparticle. Inset: histograms represent the relative portions of single (S), twinned (T) and unidentified (U) crystalline nanoparticles. (adopted from Ref. 53 © American Chemical Society)

apparatus through which real-time investigation of evolution of nanorods is initiated by continuous injection of freshly prepared seed into the growth solution and monitored in-line with UV-vis-NIR spectroscopy.⁵⁴ At age of seed is zero, most of the particles attains the diameter of between 1 nm to 2 nm which are catalytically more active and critical for the higher yield formation of Au NRs. It was also observed that as the seed ages their sizes and size distribution increased which is attributed to Oswald ripening, a phenomenon in which smaller particles get dissolved and deposited on bigger particles. Another group, Park et al. proposed that presence of gold nanoclusters ($<1\text{ nm}$) along with nanoparticles ($\sim 2\text{ nm}$) in the seed solution ($t_{\text{age}} = 0$) are actually responsible for the formation of Au NRs with less polydispersity.⁵⁵ And as the seed age increases, the portion of the multiply twinned nanostructures (icosahedrons and decahedron)

increases due to the coalescence between clusters and nanoparticles and results in thicker Au NRs (Figure 1.10).⁵⁵

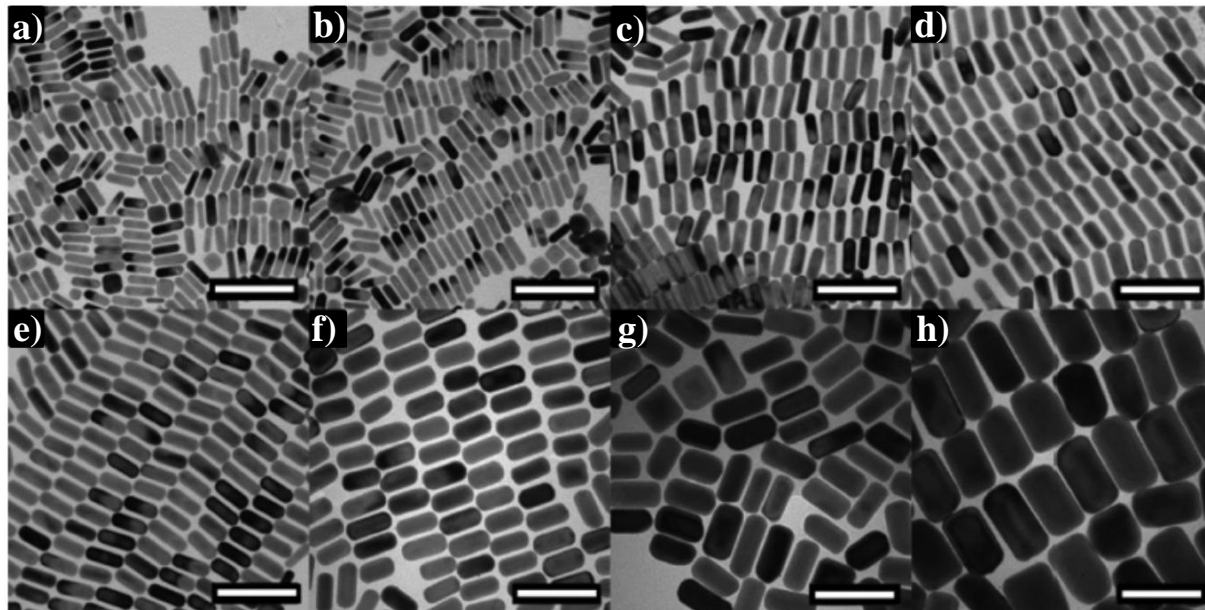


Figure 1.10: (a–h) TEM images of Au NRs grown from seeds with increasing aging time 10 s, 30 s, 1 min, 2 min, 10 min, 1 h, 12 h, and 2 day, respectively. The scale bar is 100 nm. (adopted from Ref. 55 © American Chemical Society)

Two other groups Jiang et al. and Liu et al. also examined the impact of seed age on Au NRs formation and observed similar results.^{56,57} Murphy et al. further elaborated the study of impact of seed nature on Au NRs yield by synthesizing the seeds in presence of various capping agents and analyzed the yield and size distribution of Au NRs.⁵⁸

1.4.2 Role of Surfactant

The presence of surfactant is indispensable in the growth solution for the synthesis of any anisotropic Au NCs. The widely used amphiphilic surfactants in seed-mediated growth method are CTAB, cetyltrimethylammonium chloride (CTAC), benzyldimethylhexadecylammonium chloride (BDAC), didodecyldimethylammonium bromide (DDAB), dodecyltrimethylammonium chloride (DTAC) and cetylpyridinium chloride (CPC) (please see the acronym section). Generally, amphiphilic surfactants are well-known for generating different kind of micelles (spherical, bilayer, cylindrical and lamellar) in water. It is believed that CTAB in growth media

is acting as a soft template during the growth of Au NR. Thus, Murphy et al. proposed the “zipping” mechanism for the growth of Au NRs. In this mechanism, inner-part of the bilayer cylindrical micelle of CTAB acts as template and promotes the 1D deposition of newly generated Au⁰ on seed particle (**Figure 1.11**).⁵⁹

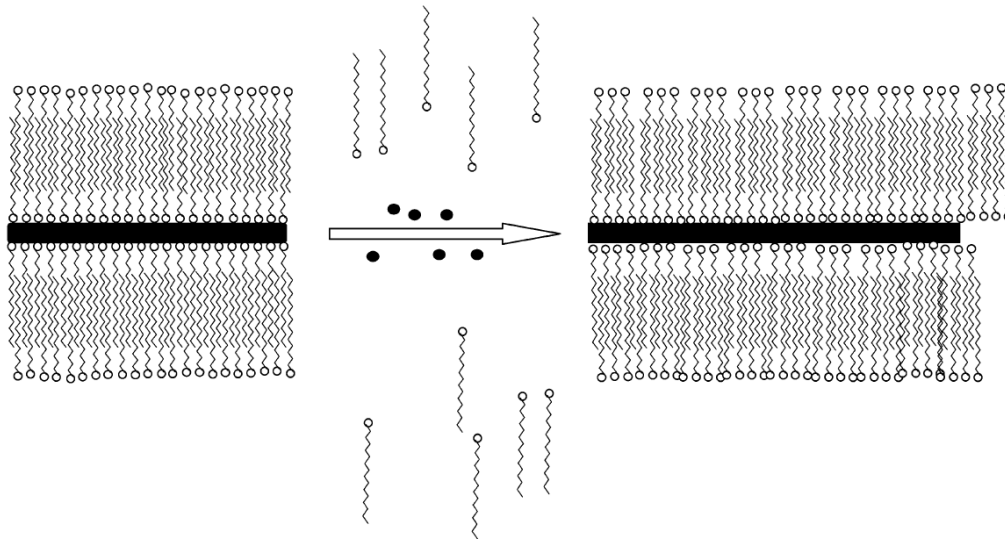


Figure 1.11: Cartoon illustrating “zipping”: the formation of the bilayer of C_n TAB(squiggles) on the nanorod (black rectangle) surface may assist nanorod formation as more gold ions (black dots) are introduced. (adopted from Ref. 59 © American Chemical Society)

The investigation was further extended to find out the impact of surfactant chain length, counter ion and head group on Au NRs yield and aspect ratio. A gradual increase in aspect ratio and yield of Au NRs was noticed as the chain length of surfactant (C_n TAB) was increased from $n=10$ to 18; it is attributed to increment in Van der Waal interaction between adjacent chains which in turn provide more stability to the micelle and hence favour the rod formation. Binary mixture of CTAB and BDAC resulted in even more increase in aspect ratio of Au NRs which is ascribed to decrease in repulsion between adjacent CTAB head groups due to the presence of BDAC which has a relatively bigger head group.⁴⁷ Under similar experimental conditions when CTAB was replaced with CTAC, ill-defined Au NCs were formed.

1.4.3 Role of Halides

Halides play a fundamentally essential role in the synthesis of anisotropic metal nanostructures. These ions have a tendency to selectively adsorb on certain faces of metal nanoparticles and thus,

act as shape directing agent during the evolution of metal nanostructures in the growth solution. HAuCl_4 is a readily commercially available gold salt which is used for the synthesis various Au NCs.

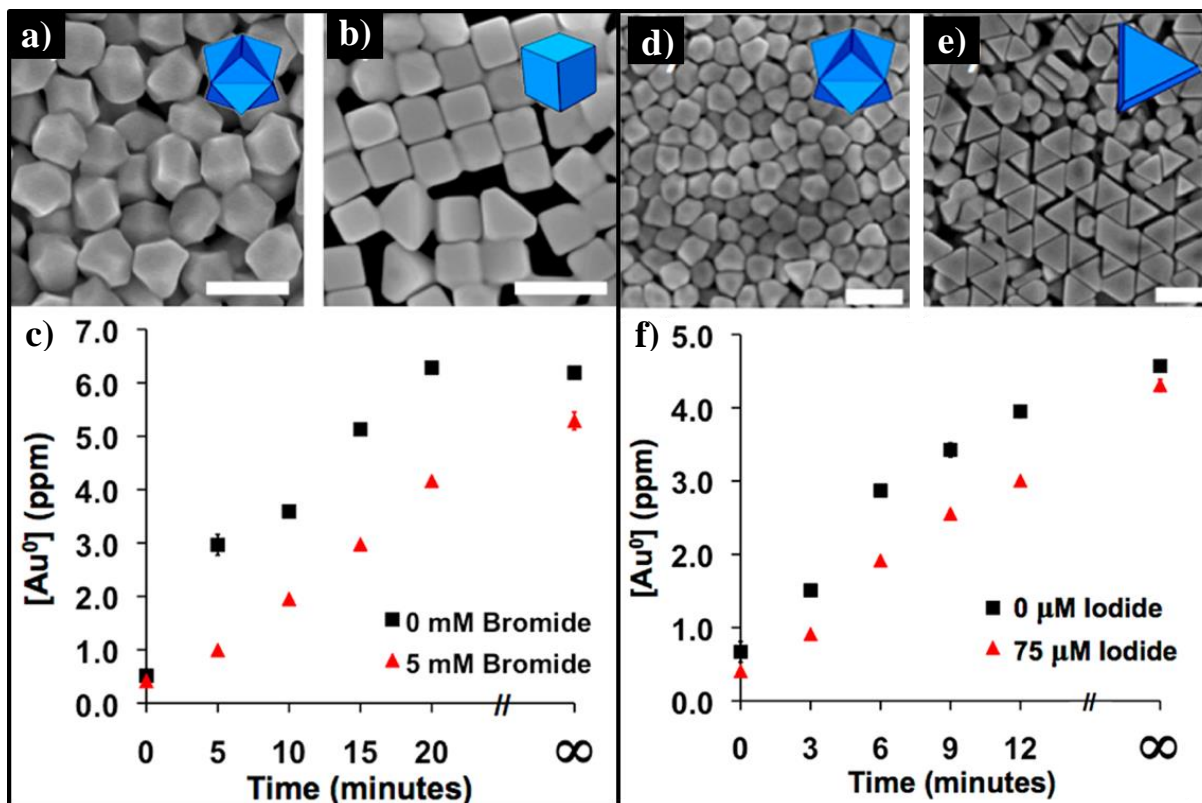


Figure 1.12: (a, b) SEM images of reaction products from growth solutions containing 50 mM CTAC and (a) 0.0 and (b) 5.0 mM NaBr, resulting in the formation of high-index faceted trisoctahedra and (100)-faceted cubes, respectively. Scale bars: 200 nm. (c) ICP-AES kinetics data of the reactions containing 0.0 mM (black squares) and 5.0 mM (red triangles) NaBr. (d–e) SEM images of reaction products from growth solutions containing 50 mM CTAC and (d) 0.0 and (e) 75.0 μM NaI, resulting in the formation of high-index faceted trisoctahedra and (100)-faceted truncated bitetrahedra, respectively. Scale bars: 200 nm. (f) ICP-AES kinetics data of the reactions containing 0.0 μM (black squares) and 75.0 μM (red triangles) NaI. (adopted from Ref. 60 © American Chemical Society)

According to the HSAB (hard and soft acids and bases) principle, the binding strength order of halides with Au (III) ions on metallic gold surface is $\text{Cl}^- < \text{Br}^- < \text{I}^-$. Therefore, Br^- or I^- can easily replace the Cl^- ions in the AuCl_4^- and thereby decrease the reduction potential of Au^{+3} in the

complex, i.e. $\text{AuCl}_4^- > \text{AuBr}_4^- > \text{AuI}_4^-$.⁶⁰ Therefore, introduction of Br^- or I^- into growth solution, not only lower the reduction potential of Au^{+3} ions, but also retard the growth rate of nanoparticle formation by strongly binding to the nanoparticle surface. As mentioned in the previous section, Ct-Au NPs seed consists of many multiply twinned nanostructures which give rise to a broad spectrum of anisotropic nanoparticles. The role of halides comes into play at this juncture as shown by Joseph et al. that I^- anions can effectively suppress the growth of nanorods thereby yielding nanoprisms.⁶¹ Mirkin and co-workers have shown that upon individual addition of Br^- and I^- into the growth solution (optimized for trisoctahedron synthesis) surprisingly resulted in the formation of cubes (**Figure 1.12b**) and truncated bitetrahedra (**Figure 1.12e**) (planar twinned analogue of the single crystalline octahedra) respectively. This is attributed to the factors: i) retardation of growth rate and ii) selective passivation of (100) and (111) facets by Br^- and I^- respectively (**Figure 1.12**).⁶⁰ The consumption rate of Au^+ precursor was tackled by measuring inductively coupled plasma atomic emission spectroscopy (ICP-AES) of aliquots collected every 5 min interval during the growth of Au NPs (**Figure 1.12**). The plot of 'production of Au^0 vs. time' depicts that in presence of halides (Br^- ; **Figure 1.12c**), (I^- ; **Figure 1.12f**) growth rate has been retarded. It was also observed that halide ions also have a significant effect on UPD deposited Ag layer on evolving Au NPs surface. This subject will be dealt with in the subsequent section.

1.4.4 Role of Silver

It has been shown in many articles that presence of AgNO_3 is indispensable during growth of Au NRs in the solution to achieve shape/size uniformity and precise tunability of aspect ratio and thereby optical properties. Such a paramount job done by Ag in Au NRs synthesis had excited the scientific community to pinpoint its role. Initially it was thought that silver forms AgBr_2^- complex that is selectively passivating certain facets of growing nanoparticle and thus promoting the Au NR growth. But as compared to AgBr_2^- complex Br^- ions strongly bind to the gold surface. In addition to this, the concentration of Br^- ion (from CTAB) in the growth solution is much higher (~1000 times) than Ag^+ ions. Furthermore, pH of the growth solution was maintained at 3 at which ascorbic acid cannot reduce Ag^+ to Ag^0 , since its reduction potential is 0.3V greater than that of it exhibit at pH = 8. All these considerations suggested that Ag must be operating through different mechanism. Mingzhao et al. introduced a new mechanism called

‘Underpotential deposition (UPD) of silver’ on gold nanoparticle surface during its growth.⁵³ The UPD is defined as “the deposition of a metal sub-monolayer or monolayer onto a different metal surface at a potential significantly less negative than for bulk deposition”.⁶² Theoretical calculation has shown that underpotential shift is proportional to the work function difference between adsorbate and adsorbent. Moreover, work function of adsorbate must be less than that of adsorbent.⁶³ The work function of Ag is less than that of Au by more than 0.5 V and thus underpotential deposition of silver readily takes place on gold surface. In general, work function of any metal is also depends on plane. The work function difference between gold and silver between planes (111), (100) and (110) are 0.57, 0.83 and 0.85 respectively. Therefore, the tendency order for UPD of silver to occur on aforementioned gold surfaces is (110) > (100) > (111) and hence the same order is followed for the binding strength of Ag on these gold surfaces. This can also be explained based on the number of nearest neighbouring gold atoms accessible for Ag atom to be bound on these planes (111), (100) and (110) as 3, 4 and 5 respectively (Figure 1.13).⁵³

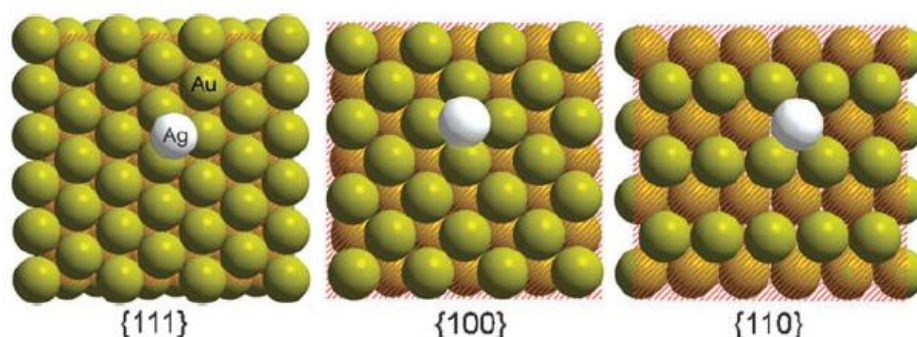


Figure 1.13: Schematic illustration of how silver atom(white) binds on (111), (100) and (110) planes of gold surface (adopted from Ref. 53 © American Chemical Society)

Sanchez et al. calculated the UPD shifts for the Au/Ag⁺ system, which corresponds to a compact monolayer of Ag on Au (111), Au (100) and Au (110), to be 0.12, 0.17 and 0.28 V respectively.⁶⁴ Thus, silver preferentially deposits on Au (110) surface of nanorods during its growth, though experimental conditions (pH = 3, 25 °C) do not favour the bulk silver deposition. Silver also plays a crucial role in symmetry breaking of seeds at its initial stage of growth and promote the anisotropic growth (nanorods).

The mechanism of Au NRs is still remains a matter of debate. Murphy et al. proposed that surfactant is acting as a soft-template for the growth of Au NRs from spherical seeds.⁵⁹

Mulvaney et al. proposed the electric field directed growth mechanism which is based on the charge gradient on seed particle at embryonic stage (after spherical seed become into spheroid); the higher curvature at the tip of spheroid Au NPs seed cause the loose packing of surfactant bilayer (CTAB) as compared to lateral portions and thereby facilitate the deposition of Au on the tips.⁶⁵ But none of the aforementioned mechanisms explained what driving forces triggered the initially isotropic seed to start growing anisotropically, i.e. how the symmetry breaking is taking place. Michael et al. have done rigorous TEM analysis to find out the origin of symmetry breaking at the initial stage of seed growth.⁶⁶ The shape of the CTAB-Au NPs seed⁴⁷ is cuboctahedron which enclosed with (111) and (100) planes; it is the minimum energy structure for FCC metal such as gold. The schematic diagram of cuboctahedron has been shown in the (Figure 1.14).⁶⁶

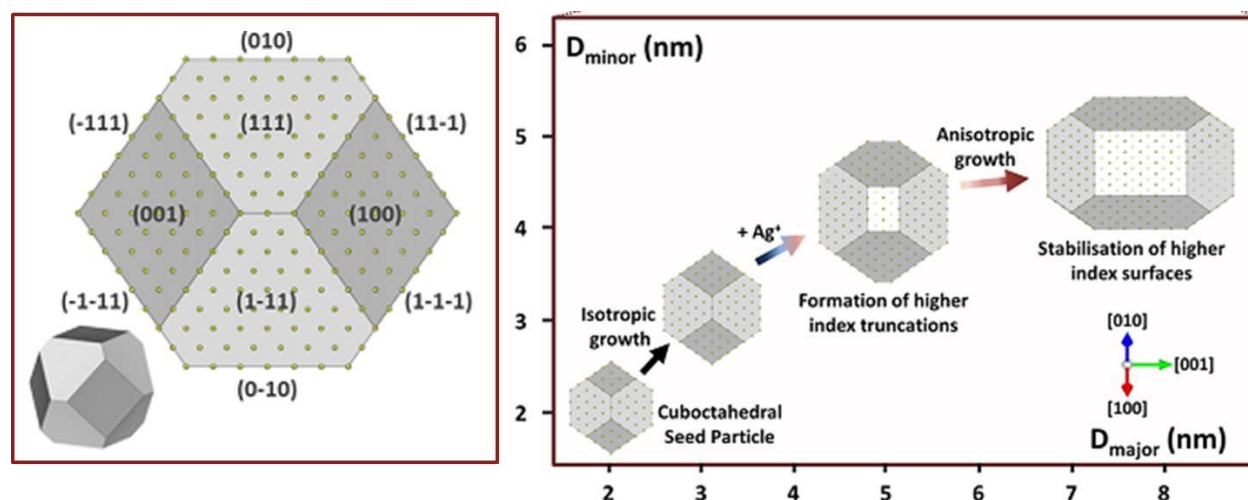


Figure 1.14: Left panel: Schematic model for the cuboctahedron and its projection in (110) direction. Right panel: Schematic for the gradual evolution of cuboctahedron in to nanorods. (adopted from Ref. 66 © American Chemical Society)

The size of the seed particle at which symmetry breaking occurs has been found to be in the range of 4-6 nm as confirmed by TEM technique. **Figure 1.14** on the right panel demonstrates the process of symmetry breaking where the initial cuboctahedron shape is transformed into the final nanorod shape via various intermediate stages. There is first, an isotropic growth of seed from its initial size of 2-3 nm till about 4 nm. At this point, small truncating surfaces (110) consisting of few atoms appear non-uniformly across the intersection of (111) facets. These truncating surfaces (110) by virtue of having relatively more open atomic arrangement are

therefore the preferred facets for silver underpotential deposition to take place. This in a way stabilizes the (110) facets and retards the deposition of gold, resulting in them becoming the side/lateral facets of the final nanorod structure. Furthermore, when the same experiment was performed without silver, no symmetry breaking was observed, i.e. Seeds were grown isotropically.

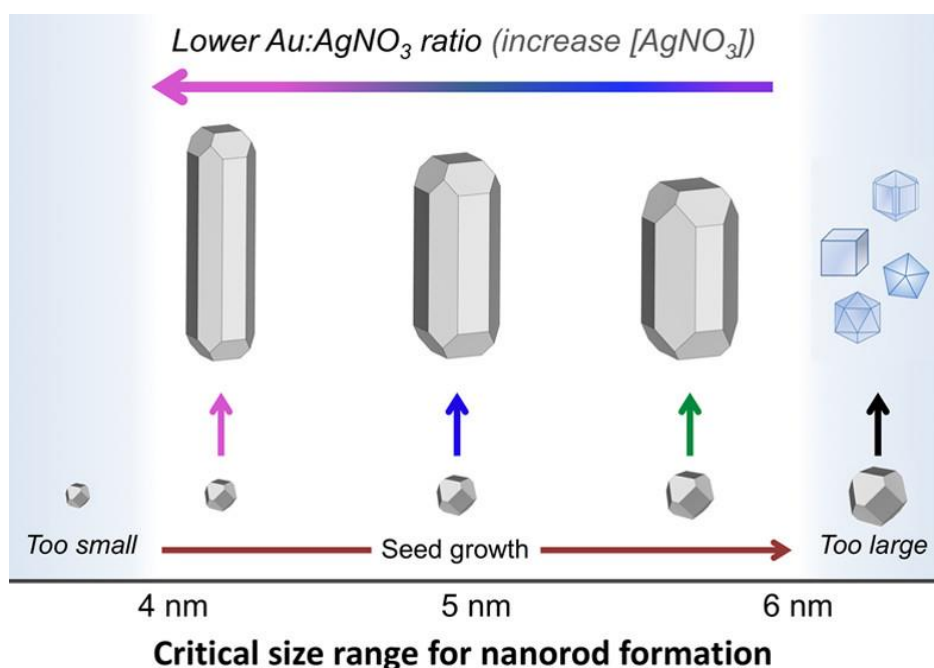


Figure 1.15: Schematic representation of how the quantity of AgNO₃ effect the critical size of seed at which symmetry breaking take place and subsequently aspect ratio of final Au NRs. (adopted from Ref. 67 © American Chemical Society)

So far it has been discussed that the factors which influence the nanorods growth from the isotropic seed particles. However, it has not been addressed properly that how the amount of silver in the growth solution determine the aspect ratio of fully grown Au NRs. Aspect ratio of the Au NRs increases with the amount of silver in the growth solution. Recently, Wenming et al. systematically studied the effect of silver quantity in the growth solution and its addition time on final Au NRs aspect ratio.⁶⁷

Though the symmetry breaking of seed takes place in the critical size range of 4 to 6 nm, it is also worthwhile to consider that exactly at which size it is occurring, since, fully grown Au NRs

have a higher aspect ratio when the symmetry breaking is taking place at the sizes close to 4 nm than that at 6 nm. Therefore, increasing the concentration of silver in the growth solution facilitate the symmetry breaking to occur at the lower size of seed and thereby yield higher aspect ratio Au NRs (**Figure 1.15**). Silver was not only successfully utilized for nanorods synthesis, but also for other nanostructures.⁶⁸

1.5 High-Index Faceted Metal Nanoparticles

Despite having made considerable progress in dimension-controlled synthesis, surfaces of the majority of such NCs, were enclosed with (111), (100) and (110) facets – so called low-index facets.⁴⁹ Metal NCs with high-index facets (represented by a set of Miller indices having at least one index greater than unity) exhibit high surface energy due to the presence of inadequately coordinated surface atoms at steps, edges and kinks (**Figure 1.16**; Left panel bottom).⁶⁹ High-index facet nanocrystals on sideline of the triangle can be geometrically viewed as integration of two low-index facet nanocrystals locating at both ends of its side-line. For example, tetrahexahedron structure is geometrical integration of rhombic dodecahedron and cube (**Figure 1.16**).⁷⁰

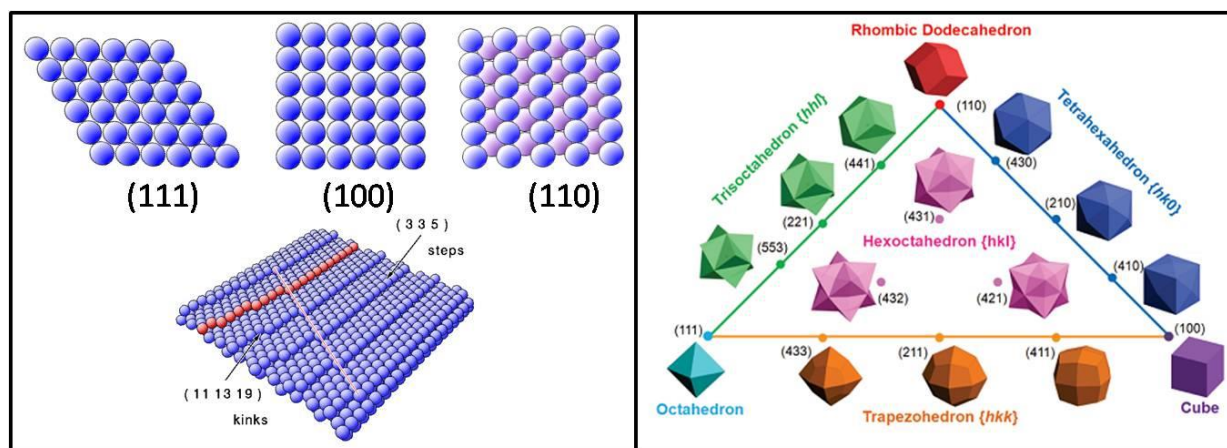


Figure 1.16: Left panel: Schematic representation of low-index (upper row) and high-index (bottom) planes. Right panel: Triangular diagram of low-index (vertices) and high-index faceted fcc metal nanocrystals (adopted from Ref. 70 © American Chemical Society).

These features are, on one hand, boosting their applications in heterogeneous catalysis,⁷¹ and on other hand, making synthetic approaches challenging. During the growth of nanocrystal high-index facets appear and are preferentially eliminated in order to minimize the total surface

energy of nanocrystal. High-index (730) faceted Pt NCs were prepared for the first time in 2007 via an electrochemical method ⁷² and later on, this method was applied to synthesis of other noble nanostructures with high-index facets. ⁷³ Though electrochemical method permitted to synthesize few noble high-index facet nanocrystals, precise tunability of size and large scale synthesis remained drawbacks of this method. Many wet-chemical methods were developed to synthesize various shaped noble metal nanocrystals enclosed with high-index facets.^{31,33,74-78}




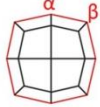

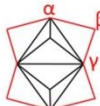

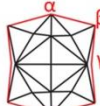
Structure	High-indexed polyhedron	Zone	Surface facets	Miller index (n≥2)	Microfacet notation	Projection direction	Projection image	Projection angle/degree
	Tetrahedron (THH)	[001]	{hk0} ₂₄ (h>k>0)	(n, n-1, 0) (n, 1, 0)	n(110)x(100) n(100)x(110)	[001]		$\alpha = 2\arctan\left(\frac{h}{k}\right)$ $\beta = 270 - \alpha$
	Trapezohedron (TPH)	[011̄]	{hkk} ₂₄ (h>k>0)	(n+1, n-1, n-1) (2n-1, 1, 1)	n(111)x(100) n(100)x(111)	[001]		$\alpha = 2\arctan\left(\frac{h}{k}\right)$ $\beta = 270 - \alpha$
	Trisoctahedron (TOH)	[110̄]	{hhl} ₂₄ (h>l>0)	(n+1, n+1, n-1) (2n-1, 2n-1, 1)	n(111)x(110) n(110)x(111)	[110]		$\alpha = 2\arctan\left(\frac{\sqrt{2}h}{h-l}\right)$ $\beta = 90 - \left(\frac{\alpha}{2}\right) + \left(\frac{\gamma}{2}\right)$ $\gamma = 2\arctan\left(\frac{\sqrt{2}h}{l}\right)$
	Hexoctahedron (HOH)		{hkl} ₄₈ (h>k>l>0)			[110]		$\alpha = 2\arctan\left(\frac{\sqrt{2}h}{h-l}\right)$ $\beta = 90 - \left(\frac{\alpha}{2}\right) + \left(\frac{\gamma}{2}\right)$ $\gamma = 2\arctan\left(\frac{k+l}{\sqrt{2}l}\right)$

Table 1.1: Crystallographic details of four types of HIF NCs and the Projection Method to determine their Miller indices. (adopted from Ref. 69 © American Chemical Society)

As it is shown in the triangle diagram, the HIF NCs are geometrically derived from the low index facet nanocrystals. So there exists a correlation between the geometric structure of the nanoparticle and the facets it is enclosed with. When such geometric structures enclosed with low index facets (cube, octahedral and rhombic dodecahedra) are manipulated so that the facets are ‘pushed in’ or ‘pulled out’ of their centers, they give rise to various exotic structures which are bound by high-index facets. Projection method has been formulated to determine the Miller indices of the HIF NCs, based on which four equations have been derived for the four different HIF NCs (**Table 1.1**).⁶⁹ The microfacet notation makes it easy to obtain the appropriate microfacet expression for a given high-index facet. This notation has a general form n(h_tk_tl_t)x(h_sk_sl_s), meaning ‘n’ atomic width of (h_tk_tl_t) terraces separated by mono atomic (h_sk_sl_s)

steps. For example, (410) facets of tetrahedra (THH) can be indicated as a stepped surface composed of a terrace in four atomic width of (100) symmetry separated by a mono atomic step of (110) symmetry denoted as 4(100)x(110). Technically, an accurate identification of surface planes exposed on high-indexed polyhedral is still a challenge. As one approach, the surface atomic arrangement obtained from a high-resolution transmission electron microscopy (HR-TEM) image in conjunction with a microfacet illustration, can be used to determine Miller indices of high-index facets (Figure 1.17).^{79,80}

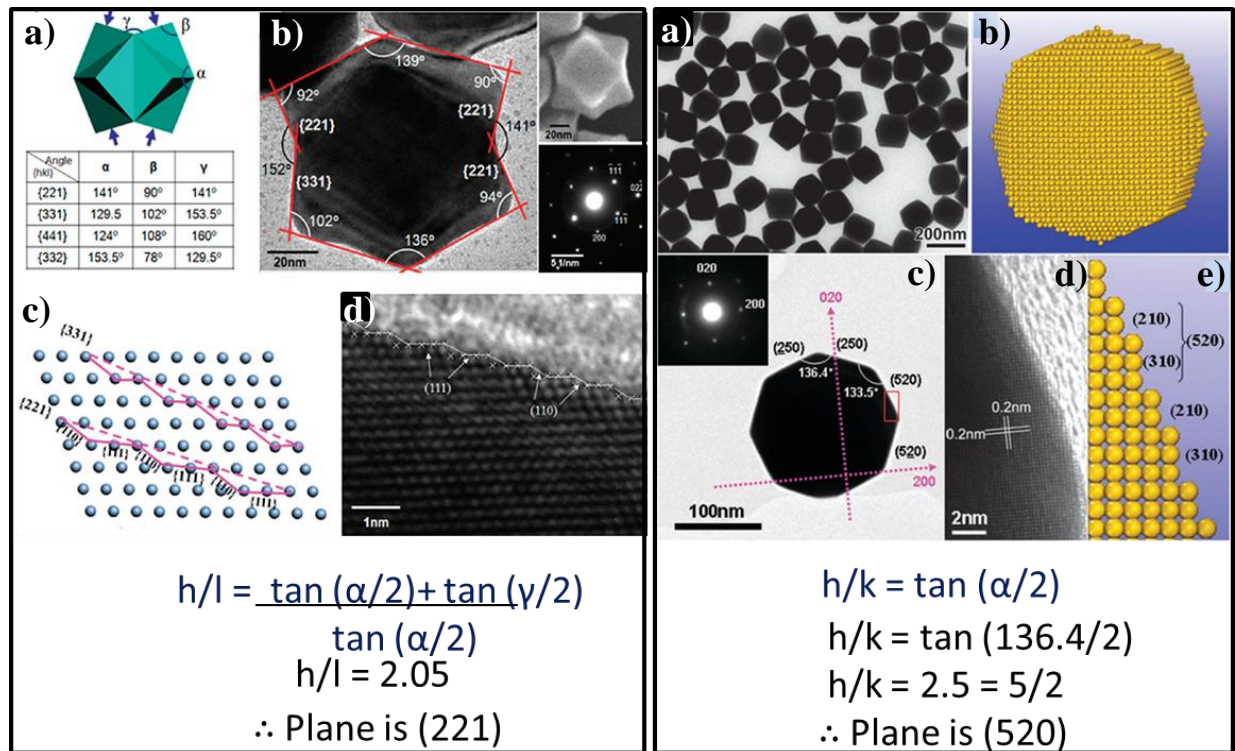


Figure 1.17: Left panel: a) Model of trisoctahedron (TOH), b) TEM image of TOH projected in to [110] direction, c) Schematic representation of high-index planes (221) and (331), d) HR-TEM image captured at one of the edge of TOH shown in (b) and calculation (below) made for the determination of facet using equation given in the Table 1. Right panel: a) TEM image of THH Au NCs, b) Schematic representation for THH, c) TEM image of THH Au NC projected in to [100] direction, d) HR-TEM image captured at the portion indicated with red box in (c), e) Schematic structure of atomic arrangements found in (d), and the calculation made below is to estimate the facet of TOH using the equation given in Table 1.1.(adopted from Ref. 79© American Chemical Society and Ref. 80 @ The Royal Society of Chemistry).

1.6 Metal Nanowires (NWs)

One dimensional (1D) Au NWs are of great interest due to their high aspect ratio as well as the large anisotropy which is the highest among other Au nanostructures. This lends them their unusual optical, electrical and chemical properties which have potential applications in nanoelectronics, photonics, sensors, mechanical energy storage, flexible electrode with high transparency and conductivity, and in SERS.^{81,82} Owing to the great promises that Au NWs hold, significant approaches have been made to synthesize them to tap into their potentials. Template (hard and soft) syntheses were one of the earliest and most effective approaches⁸³⁻⁸⁵ followed by slow reduction of gold salt (HAuCl_4) using oleylamine or combined chemicals (ascorbic acid, oleic acid, nitric acid etc).^{82,83,86-93} Ravishankar and co-workers demonstrated a multistep strategy to obtain Au NWs in toluene using a mixture of oleic acid, oleylamine and ascorbic acid.⁹⁴ Here Au NWs were produced via an oriented attachment of Au NPs (**Figure 1.18**).

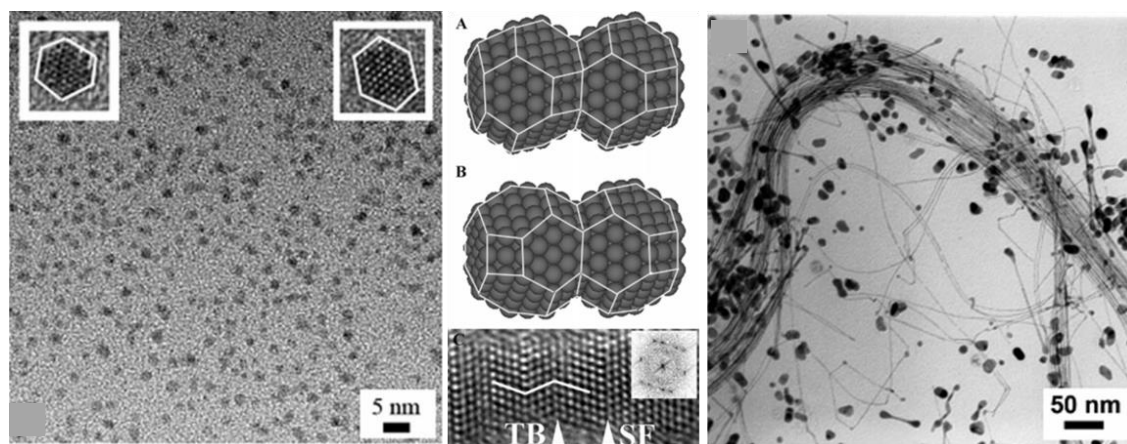


Figure 1.18: *Left:* Bright-field TEM microscopy image of gold nanoparticles formed in the solution phase. The insets show that the particles are faceted with (111) and (100) facets. *Middle:* A schematic illustration of the attachment of two faceted nanoparticles in A) perfectly matching orientation and B) twinned orientation. Twin defects are frequently seen in the nanowires owing to the low twin boundary energy for gold. C) A high-resolution image illustrating a twin boundary (TB) and a stacking fault (SF) in the nanowires. The fast Fourier transform (FFT) from the twinned region clearly depicts the twin relationship. *Right:* Bundles of nanowires formed in the solution phase on ageing after the addition of ascorbic acid. (adopted from Ref. 94@ Wiley-VCH)

Zhong and co-workers reported a novel synthesis of ultra-long and highly monodispersed and surfactant free Au NWs synthesized by a galvanic replacement reaction of Tellurium NWs as sacrificial template.⁹⁵ Xiangyang and co-workers proposed a facile hydrothermal approach in the presence of dendrimers, wherein the dendrimers were used to reprise the role played by oleylamine thereby minimizing the environmental hazard that comes with the use of organic solvents.⁹⁶ Other synthetic routes such as seed mediated growth;^{81,87,97} electrochemical deposition and particle assembly have also been reported.⁹⁸

1.7 Bimetallic nanoparticles

As is mentioned in the previous section, bringing the size of a metal to nanoscale domain will render them to exhibit distinct and intriguing optical and electronic properties as compared to its bulk counterparts. In this size regime all properties become very sensitive regarding minute variations in their dimensions.⁹⁹ Despite the change in shape and size, properties can also be tuned by incorporating two or more metals in a single nanoparticle (alloy nanoparticles) and changing the composition. Alloy nanoparticles possess very different physical and chemical properties with respect to the monometallic nanoparticles of individual components.¹⁰⁰

Some properties such as magnetic, optical and catalytic are specific for certain elemental nanoparticles. For example, Pt, Pd, Ru and Rh are used for catalysis; Au, Ag and Cu are used for their optical properties; and Fe, Co and Ni are used for their magnetic properties. Hence, the alloy nanoparticle of two elements (with distinct properties) would simultaneously exhibit both the properties of individual components. In some cases, it has been observed that the properties of one component of the alloy is significantly enhanced due to the presence of minute amount of another element in the same nanoparticle; Catalytic activity of Pt NPs and air stability of Ag NPs are increased significantly upon incorporating Au into them. Therefore, these nanoparticles afford novel applications in various fields such as catalysis, sensors and biological applications. Among all bimetallic systems, Au-Ag has been widely studied owing to their attention-grabbing optical and electrochemical properties. In particular, the plasmon resonance of Au-Ag NPs can be precisely tuned with composition over the range of 380 nm to 520 nm, i.e. from SPR of pure Ag NPs to Au NPs (**Figure 1.7**). Such a precise tunability of SPR and catalytic activity of Au-Ag NPs relies on the degree of homogeneous distribution of components in the nanoparticle.³⁹

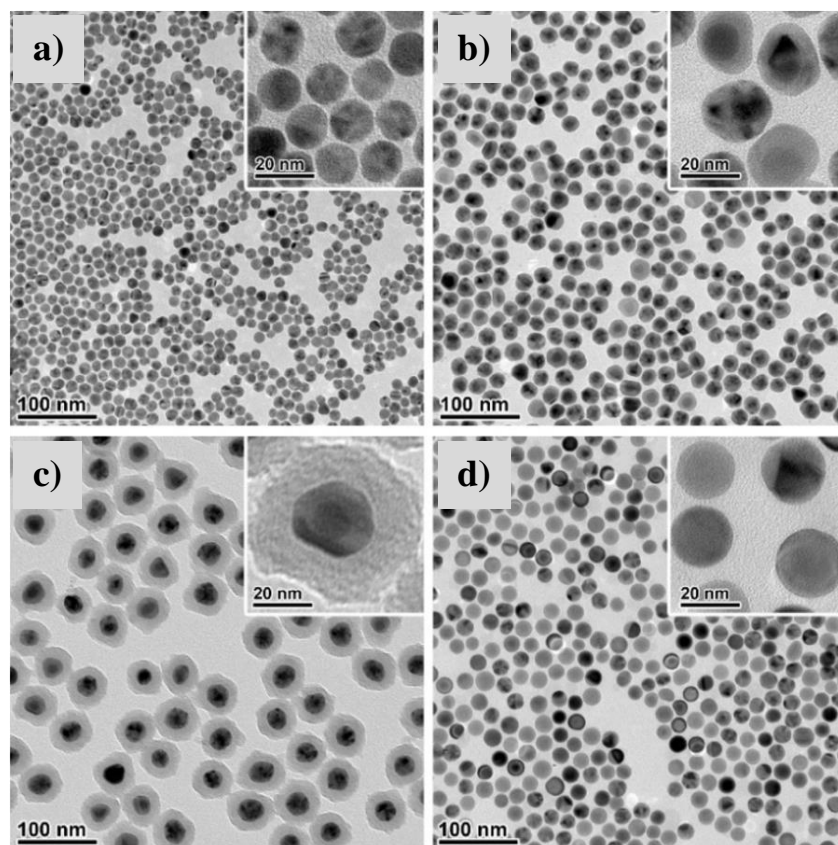


Figure 1.19: TEM images of a) Au NPs, b) Au@Ag NPs, c) Au@Ag@SiO₂ and d) Au-Ag alloy NPs. (adopted from Ref. 39 © American Chemical Society)

Types of alloy NPs based on atomic structure are 1) core-shell, 2) inhomogeneous and 3) homogeneous (intermetallic). Among these, synthesis of homogeneous alloy NPs is relatively challenging. There have been few rules proposed by some research groups^{101,102} which can predict the atomic structure of alloy NPs –so called ‘segregation rules’. According to these rules, homogeneous alloy of Au-Ag NPs is possible. Few methods attempted to synthesis such alloy NPs of gold and silver include citrate reduction,¹⁰³ borohydride reduction,¹⁰⁴ photocatalytic reduction,¹⁰⁵ radiolytic reduction,¹⁰⁶ laser ablation,¹⁰⁷ solvent extraction-reduction,¹⁰⁸ and water-in-oil microemulsion method.¹⁰⁹ Most of the methodologies followed the co-reduction of commonly available metal salts HAuCl₄ and AgNO₃ in presence of various capping agents.¹¹⁰⁻¹¹³ However, none of the above methods could synthesize homogeneous Au-Ag alloy NPs due to the unavoidable problem of AgCl precipitation (upon mixing of HAuCl₄ and AgNO₃) which in turn cannot be reduced to Ag⁰ and hence the synthesis of Au-Ag NPs became difficult.

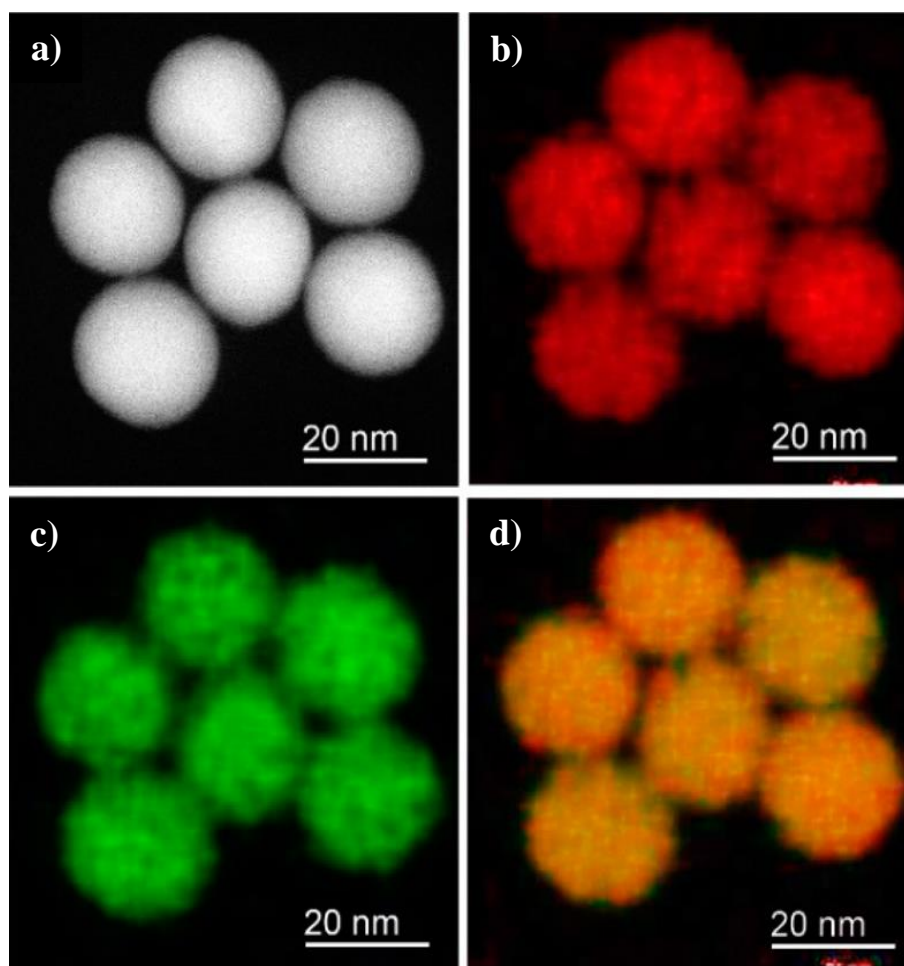


Figure 1.20: Elemental analysis of the Ag/Au alloy nanospheres (Ag/Au = 5): (a) DF-STEM image; (b, c) EDX elemental maps of Au and Ag, respectively; (d) merged image of (b) and (c). (adopted from Ref. 39 © American Chemical Society)

Recently, Chuanbo et al. devised a method in which core-shell Au-Ag NPs are synthesized in the first step followed by SiO₂ coating (Au@Ag@SiO₂) and annealed at 1000⁰C for 6hrs. Then, SiO₂ shell was removed in presence of polyvinylpyrrolidone (PVP) and re-dispersed into aqueous medium (**Figure 1.19**).³⁹ EDX elemental map as synthesized Au-Ag alloy NPs clearly shows the homogeneous distribution of Au and Ag (**Figure 1.20**). This method has been found to be novel but it involved multi-steps. Also control of composition seems to be obscure and not robust. In the year 2002, Murphy et al. could synthesize Au-Ag alloy NPs as per the feeding moles of precursors at very lower concentration (5 μM) i.e. below the solubility product of AgCl (K_{sp} = 1.8x10⁻¹⁰). However, such lower concentration hindered its processing in applications.

1.8 References

- (1) Ghosh, S. K.; Pal, T. Interparticle Coupling Effect on the Surface Plasmon Resonance of Gold Nanoparticles: From Theory to Applications. *Chem. Rev.* **2007**, *107*, 4797.
- (2) Halas, N. J.; Lal, S.; Chang, W. S.; Link, S.; Nordlander, P. Plasmons in strongly coupled metallic nanostructures. *Chem. Rev.* **2011**, *111*, 3913.
- (3) Moores, A.; Goettmann, F. d. r. The plasmon band in noble metal nanoparticles: an introduction to theory and applications. *New J. Chem.* **2006**, *30*, 1121.
- (4) Stratakis, M.; Garcia, H. Catalysis by supported gold nanoparticles: beyond aerobic oxidative processes. *Chem. Rev.* **2012**, *112*, 4469.
- (5) Akiyama, T.; Nishida, T.; Matsumoto, T.; Sakaguchi, H.; Suzuki, A.; Oku, T. Effect of gold nanoparticle in hole-transport layer on inverted organic thin-film solar cell performance. *Phys. Status Solidi A* **2014**, *211*, 1645.
- (6) Saha, K.; Agasti, S. S.; Kim, C.; Li, X.; Rotello, V. M. Gold nanoparticles in chemical and biological sensing. *Chem. Rev.* **2012**, *112*, 2739.
- (7) Daniel, M.-C.; Astruc, D. Gold Nanoparticles: Assembly, Supramolecular Chemistry, Quantum-Size-Related Properties, and Applications toward Biology, Catalysis, and Nanotechnology. *Chem. Rev.* **2004**, *104*, 293.
- (8) Dreaden, E. C.; Alkilany, A. M.; Huang, X.; Murphy, C. J.; El-Sayed, M. A. The golden age: gold nanoparticles for biomedicine. *Chem. Soc. Rev.* **2012**, *41*, 2740.
- (9) Jain, P. K.; Huang, X.; El-Sayed, I. H.; El-Sayed, M. A. Noble Metals on the Nanoscale: Optical and Photothermal Properties and Some Applications in Imaging, Sensing, Biology, and Medicine. *Acc. Chem. Res.* **2008**, *41*, 1578.
- (10) Kelly, K. L.; Coronado, E.; Zhao, L. L.; Schatz, G. C. The Optical Properties of Metal Nanoparticles: The Influence of Size, Shape, and Dielectric Environment. *J. Phys. Chem. B* **2003**, *107*, 668.
- (11) Eustis, S.; El-Sayed, M. A. Why gold nanoparticles are more precious than pretty gold: Noble metal surface plasmon resonance and its enhancement of the radiative and nonradiative properties of nanocrystals of different shapes. *Chem. Soc. Rev.* **2006**, *35*, 209.

- (12) Zhang, J.; Worley, J.; Dénonnée, S.; Kingston, C.; Jakubek, Z. J.; Deslandes, Y.; Post, M.; Simard, B.; Braidy, N.; Botton, G. A. Synthesis of Metal Alloy Nanoparticles in Solution by Laser Irradiation of a Metal Powder Suspension. *J. phys. Chem. B* **2003**, *107*, 6920.
- (13) Morgan S. Sibbald, G. C., and Therese M. Cotton Reduction of Cytochrome c by Halide-Modified, Laser-Ablated Silver Colloids. *J. Phys. Chem.* **1996**, *100*, 4672.
- (14) Wang, Y.; Xia, Y. Bottom-Up and Top-Down Approaches to the Synthesis of Monodispersed Spherical Colloids of Low Melting-Point Metals. *Nano Lett.* **2004**, *4*, 2047.
- (15) Sau, T. K.; Rogach, A. L. Nonspherical Noble Metal Nanoparticles: Colloid-Chemical Synthesis and Morphology Control. *Adv. Mater.* **2010**, *22*, 1781.
- (16) Kimling, J.; Maier, M.; Okenve, B.; Kotaidis, V.; Ballot, H.; Plech, A. Turkevich Method for Gold Nanoparticle Synthesis Revisited. *J. Phys. Chem. B* **2006**, *110*, 15700.
- (17) Irvani, S. Green synthesis of metal nanoparticles using plants. *Green Chem.* **2011**, *13*, 2638.
- (18) Prasad, B.; Stoeva, S. I.; Sorensen, C. M.; Klabunde, K. J. Digestive-ripening agents for gold nanoparticles: alternatives to thiols. *Chem. Mater.* **2003**, *15*, 935.
- (19) Sahu, P.; Prasad, B. L. V. Effect of digestive ripening agent on nanoparticle size in the digestive ripening process. *Chem. Phys. Lett.* **2012**, *525-526*, 101.
- (20) Sahu, P.; Prasad, B. L. V. Fine control of nanoparticle sizes and size distributions: temperature and ligand effects on the digestive ripening process. *Nanoscale* **2013**, *5*, 1768.
- (21) Sahu, P.; Prasad, B. L. V. Time and Temperature Effects on the Digestive Ripening of Gold Nanoparticles: Is There a Crossover from Digestive Ripening to Ostwald Ripening? *Langmuir* **2014**, *30*, 10143.
- (22) MER, V. K. L. Nucleation in Phase Transitions. *Ind. Eng. Chem. Res.* **1952**, *44*, 1270.
- (23) Polte, J.; Ahner, T. T.; Delissen, F.; Sokolov, S.; Emmerling, F.; Thünemann, A. F.; Kraehnert, R. Mechanism of Gold Nanoparticle Formation in the Classical Citrate Synthesis Method Derived from Coupled In Situ XANES and SAXS Evaluation. *J. Am. Chem. Soc.* **2010**, *132*, 1296.
- (24) Loh, N. D.; Sen, S.; Bosman, M.; Tan, S. F.; Zhong, J.; Nijhuis, C. A.; Král, P.; Matsudaira, P.; Mirsaidov, U. Multistep nucleation of nanocrystals in aqueous solution. *Nat. Chem.* **2017**, *9*, 77.
- (25) J. Israelachvili. *Intermolecular & Surface Forces*, Academic Press, London, **1997**.

- (26) Zhang, H.; Wang, D. Controlling the Growth of Charged-Nanoparticle Chains through Interparticle Electrostatic Repulsion. *Angew. Chem., Int. Ed.* **2008**, *47*, 3984.
- (27) El-Sayed, S. L. a. M. A. Size and Temperature Dependence of the Plasmon Absorption of Colloidal Gold Nanoparticles. *J. phys. Chem. B* **1999**, *103*, 4212.
- (28) Link, S.; Mohamed, M. B.; El-Sayed, M. A. Simulation of the Optical Absorption Spectra of Gold Nanorods as a Function of Their Aspect Ratio and the Effect of the Medium Dielectric Constant. *J. Phys. Chem. B* **1999**, *103*, 3073.
- (29) Attia, Y. A.; Buceta, D.; Requejo, F. G.; Giovanetti, L. J.; López-Quintela, M. A. Photostability of gold nanoparticles with different shapes: the role of Ag clusters. *Nanoscale* **2015**, *7*, 11273.
- (30) Chen, H.; Kou, X.; Yang, Z.; Ni, W.; Wang, J. Shape- and Size-Dependent Refractive Index Sensitivity of Gold Nanoparticles. *Langmuir* **2008**, *24*, 5233.
- (31) Walker, D. A.; Leitsch, E. K.; Nap, R. J.; Szleifer, I.; Grzybowski, B. A. Geometric curvature controls the chemical patchiness and self-assembly of nanoparticles. *Nat. Nanotech.* **2013**, *8*, 676.
- (32) Xu, L.; Kuang, H.; Wang, L.; Xu, C. Gold nanorod ensembles as artificial molecules for applications in sensors. *J. Mater. Chem.* **2011**, *21*, 16759.
- (33) Sun, Z.; Ni, W.; Yang, Z.; Kou, X.; Li, L.; Wang, J. pH-Controlled reversible assembly and disassembly of gold nanorods. *Small* **2008**, *4*, 1287.
- (34) S. T. Shibu Joseph, B. I. I., P. Pramod, and K. George Thomas Gold Nanorods to Nanochains: Mechanistic Investigations on Their Longitudinal Assembly Using α,ω -Alkanedithiols and Interplasmon Coupling. *J. Phys. Chem. B* **2006**, *110*, 150.
- (35) P. Pramod, S. T. S. J., and K. George Thomas Preferential End Functionalization of Au Nanorods through Electrostatic Interactions. *J. Am. Chem. Soc.* **2007**, *129*, 6712.
- (36) K. George Thomas, S. B., Binil Itty Ipe, S. T. Shibu Joseph, and Prashant V. Kamat Uniaxial Plasmon Coupling through Longitudinal Self-Assembly of Gold Nanorods. *J. Phys. Chem. B* **2004**, *108*, 13066.
- (37) Zhang, H. J.; Haba, M.; Okumura, M.; Akita, T.; Hashimoto, S.; Toshima, N. Novel Formation of Ag/Au Bimetallic Nanoparticles by Physical Mixture of Monometallic Nanoparticles in Dispersions and Their Application to Catalysts for Aerobic Glucose Oxidation. *Langmuir* **2013**, *29*, 10330.

- (38) Liu, J.-H.; Wang, A.-Q.; Chi, Y.-S.; Lin, H.-P.; Mou, C.-Y. Synergistic Effect in an Au–Ag Alloy Nanocatalyst: CO Oxidation. *J. Phys. Chem. B* **2005**, *109*, 40.
- (39) Gao, C.; Hu, Y.; Wang, M.; Chi, M.; Yin, Y. Fully Alloyed Ag/Au Nanospheres: Combining the Plasmonic Property of Ag with the Stability of Au. *J. Am. Chem. Soc.* **2014**, *136*, 7474.
- (40) Grzelczak, M.; Perez-Juste, J.; Mulvaney, P.; Liz-Marzan, L. M. Shape control in gold nanoparticle synthesis. *Chem. Soc. Rev.* **2008**, *37*, 1783.
- (41) Burda, C.; Chen, X.; Narayanan, R.; El-Sayed, M. A. Chemistry and Properties of Nanocrystals of Different Shapes. *Chem. Rev.* **2005**, *105*, 1025.
- (42) Johnson, C. J.; Dujardin, E.; Davis, S. A.; Murphy, C. J.; Mann, S. Growth and form of gold nanorods prepared by seed-mediated, surfactant-directed synthesis. *J. Mater. Chem.* **2002**, *12*, 1765.
- (43) Jana, N. R.; Gearheart, L.; Murphy, C. J. Wet chemical synthesis of silver nanorods and nanowires of controllable aspect ratio. *Chem. Commun.* **2001**, 617.
- (44) Liu, K.; Bu, Y.; Zheng, Y.; Jiang, X.; Yu, A.; Wang, H. Seedless Synthesis of Monodispersed Gold Nanorods with Remarkably High Yield: Synergistic Effect of Template Modification and Growth Kinetics Regulation. *Chem. Eur. J.* **2017**, *23*, 3291.
- (45) Sau, T. K.; Murphy, C. J. Room temperature, high-yield synthesis of multiple shapes of gold nanoparticles in aqueous solution. *J. Am. Chem. Soc.* **2004**, *126*, 8648.
- (46) Jana, N. R.; Gearheart, L.; Murphy, C. J. Wet chemical synthesis of high aspect ratio cylindrical gold nanorods. *J. Phys. Chem. B* **2001**, *105*, 4065.
- (47) Nikoobakht, B.; El-Sayed, M. A. Preparation and growth mechanism of gold nanorods (NRs) using seed-mediated growth method. *Chem. Mater.* **2003**, *15*, 1957.
- (48) Lee, J.-H.; Gibson, K. J.; Chen, G.; Weizmann, Y. Bipyramid-templated synthesis of monodisperse anisotropic gold nanocrystals. *Nat. Commun.* **2015**, *6*, 7571.
- (49) Niu, W.; Zheng, S.; Wang, D.; Liu, X.; Li, H.; Han, S.; Chen, J.; Tang, Z.; Xu, G. Selective Synthesis of Single-Crystalline Rhombic Dodecahedral, Octahedral, and Cubic Gold Nanocrystals. *J. Am. Chem. Soc.* **2009**, *131*, 697.
- (50) Gómez-Graña, S.; Fernández-López, C.; Polavarapu, L.; Salmon, J.-B.; Leng, J.; Pastoriza-Santos, I.; Pérez-Juste, J. Gold Nanooctahedra with Tunable Size and Microfluidic-Induced 3D Assembly for Highly Uniform SERS-Active Supercrystals. *Chem. Mater.* **2015**, *27*, 8310.

- (51) Park, K.; Drummy, L. F.; Wadams, R. C.; Koerner, H.; Nepal, D.; Fabris, L.; Vaia, R. A. Growth Mechanism of Gold Nanorods. *Chem. Mater.* **2013**, *25*, 555.
- (52) Edgar, J. A.; McDonagh, A. M.; Cortie, M. B. Formation of Gold Nanorods by a Stochastic “Popcorn” Mechanism. *ACS Nano* **2012**, *6*, 1116.
- (53) Liu; Guyot-Sionnest, P. Mechanism of Silver(I)-Assisted Growth of Gold Nanorods and Bipyramids. *J. Phys. Chem. B* **2005**, *109*, 22192.
- (54) Watt, J.; Hance, B. G.; Anderson, R. S.; Huber, D. L. Effect of Seed Age on Gold Nanorod Formation: A Microfluidic, Real-Time Investigation. *Chem. Mater.* **2015**, *27*, 6442.
- (55) Park, K.; Hsiao, M.-S.; Koerner, H.; Jawaid, A.; Che, J.; Vaia, R. A. Optimizing Seed Aging for Single Crystal Gold Nanorod Growth: The Critical Role of Gold Nanocluster Crystal Structure. *J. Phys. Chem. C* **2016**, *120*, 28235.
- (56) Liu, J.; Duggan, J. N.; Morgan, J.; Roberts, C. B. Seed-mediated growth and manipulation of Au nanorods via size-controlled synthesis of Au seeds. *J Nanopart Res* **2012**, *14*, 1289.
- (57) Jiang, X. C.; Pileni, M. P. Gold nanorods: Influence of various parameters as seeds, solvent, surfactant on shape control. *Colloids and Surfaces A: Physicochemical and Engineering Aspects* **2007**, *295*, 228.
- (58) Murphy, A. G. a. C. J. Seed-Mediated Synthesis of Gold Nanorods: Role of the Size and Nature of the Seed. *Chem. Mater.* **2004**, *16*, 3633.
- (59) Jinxin Gao, C. M. B., and Catherine J. Murphy Dependence of the Gold Nanorod Aspect Ratio on the Nature of the Directing Surfactant in Aqueous Solution. *Langmuir* **2003**, *19*, 9065.
- (60) Langille, M. R.; Personick, M. L.; Zhang, J.; Mirkin, C. A. Defining Rules for the Shape Evolution of Gold Nanoparticles. *J. Am. Chem. Soc.* **2012**, *134*, 14542.
- (61) DuChene, J. S.; Niu, W.; Abendroth, J. M.; Sun, Q.; Zhao, W.; Huo, F.; Wei, W. D. Halide Anions as Shape-Directing Agents for Obtaining High-Quality Anisotropic Gold Nanostructures. *Chem. Mater.* **2013**, *25*, 1392.
- (62) Herrero, E.; Buller, L. J.; Abruña, H. D. Underpotential Deposition at Single Crystal Surfaces of Au, Pt, Ag and Other Materials. *Chem. Rev.* **2001**, *101*, 1897.
- (63) Kolb, D. M.; Przasnyski, M.; Gerischer, H. Underpotential deposition of metals and work function differences. *J. Electroanal. Chem.* **1974**, *54*, 25.
- (64) Sánchez, C. G.; Del Pópolo, M. G.; Leiva, E. P. M. An embedded atom approach to underpotential deposition phenomena. *Surf. Sci.* **1999**, *421*, 59.

- (65) Pérez-Juste, J.; Liz-Marzán, L. M.; Carnie, S.; Chan, D. Y. C.; Mulvaney, P. Electric-Field-Directed Growth of Gold Nanorods in Aqueous Surfactant Solutions. *Adv. Funct. Mater.* **2004**, *14*, 571.
- (66) Walsh, M. J.; Barrow, S. J.; Tong, W.; Funston, A. M.; Etheridge, J. Symmetry Breaking and Silver in Gold Nanorod Growth. *ACS Nano* **2015**, *9*, 715.
- (67) Tong, W.; Walsh, M. J.; Mulvaney, P.; Etheridge, J.; Funston, A. M. Control of Symmetry Breaking Size and Aspect Ratio in Gold Nanorods: Underlying Role of Silver Nitrate. *J. Phys. Chem. C* **2017**, *121*, 3549.
- (68) Langille, M. R.; Personick, M. L.; Zhang, J.; Mirkin, C. A. Defining rules for the shape evolution of gold nanoparticles. *J. Am. Chem. Soc.* **2012**, *134*, 14542.
- (69) Quan, Z.; Wang, Y.; Fang, J. High-index faceted noble metal nanocrystals. *Acc. Chem. Res.* **2012**, *46*, 191.
- (70) Yu, Y.; Zhang, Q.; Liu, B.; Lee, J. Y. Synthesis of nanocrystals with variable high-index Pd facets through the controlled heteroepitaxial growth of trisoctahedral Au templates. *J. Am. Chem. Soc.* **2010**, *132*, 18258.
- (71) Qian, Z.; Park, S.-J. Silver Seeds and Aromatic Surfactants Facilitate the Growth of Anisotropic Metal Nanoparticles: Gold Triangular Nanoprisms and Ultrathin Nanowires. *Chem. Mater.* **2014**, *26*, 6172.
- (72) Tian, N.; Zhou, Z.-Y.; Sun, S.-G.; Ding, Y.; Wang, Z. L. Synthesis of tetrahexahedral platinum nanocrystals with high-index facets and high electro-oxidation activity. *science* **2007**, *316*, 732.
- (73) Yu, N. F.; Tian, N.; Zhou, Z. Y.; Huang, L.; Xiao, J.; Wen, Y. H.; Sun, S. G. Electrochemical synthesis of tetrahexahedral rhodium nanocrystals with extraordinarily high surface energy and high electrocatalytic activity. *Angew. Chem., Int. Ed.* **2014**, *53*, 5097.
- (74) Yu, S.; Li, N.; Wharton, J.; Martin, C. R. Nano Wheat Fields Prepared by Plasma-Etching Gold Nanowire-Containing Membranes. *Nano Letters* **2003**, *3*, 815.
- (75) Li, L.; Peng, Y.; Yue, Y.; Hu, Y.; Liang, X.; Yin, P.; Guo, L. Synthesis of concave gold nanocuboids with high-index facets and their enhanced catalytic activity. *Chem. Commun.* **2015**, *51*, 11591.
- (76) Jana, J.; Ganguly, M.; Pal, T. Enlightening surface plasmon resonance effect of metal nanoparticles for practical spectroscopic application. *RSC Advances* **2016**, *6*, 86174.

- (77) Jing, H.; Zhang, Q.; Large, N.; Yu, C.; Blom, D. A.; Nordlander, P.; Wang, H. Tunable plasmonic nanoparticles with catalytically active high-index facets. *Nano Lett.* **2014**, *14*, 3674.
- (78) Zhang, Q.; Zhou, Y.; Villarreal, E.; Lin, Y.; Zou, S.; Wang, H. Faceted Gold Nanorods: Nanocuboids, Convex Nanocuboids, and Concave Nanocuboids. *Nano Lett.* **2015**, *15*, 4161.
- (79) Yu, Y.; Zhang, Q.; Lu, X.; Lee, J. Y. Seed-mediated synthesis of monodisperse concave trisoctahedral gold nanocrystals with controllable sizes. *J. Phys. Chem. C* **2010**, *114*, 11119.
- (80) Li, J.; Wang, L.; Liu, L.; Guo, L.; Han, X.; Zhang, Z. Synthesis of tetrahedral Au nanocrystals with exposed high-index surfaces. *Chemical communications* **2010**, *46*, 5109.
- (81) Xu, F.; Hou, H.; Gao, Z. Synthesis and Crystal Structures of Gold Nanowires with Gemini Surfactants as Directing Agents. *ChemPhysChem* **2014**, *15*, 3979.
- (82) Takahata, R.; Yamazoe, S.; Koyasu, K.; Tsukuda, T. Surface Plasmon Resonance in Gold Ultrathin Nanorods and Nanowires. *J. Am. Chem. Soc.* **2014**, *136*, 8489.
- (83) Hong, X.; Wang, D.; Li, Y. Kinked gold nanowires and their SPR/SERS properties. *Chem. Commun.* **2011**, *47*, 9909.
- (84) Gao, X.; Lu, F.; Dong, B.; Liu, Y.; Gao, Y.; Zheng, L. Facile synthesis of gold and gold-based alloy nanowire networks using wormlike micelles as soft templates. *Chem. Commun.* **2015**, *51*, 843.
- (85) Bai, H.; Xu, K.; Xu, Y.; Matsui, H. Fabrication of Au nanowires of uniform length and diameter using a monodisperse and rigid biomolecular template: collagen-like triple helix. *Angew. Chem., Int. Ed.* **2007**, *46*, 3319.
- (86) Zhou, M.; Lin, M.; Wang, Y.; Guo, X.; Guo, X.; Peng, L.; Ding, W. Organic-free synthesis of ultrathin gold nanowires as effective SERS substrates. *Chem. Commun.* **2015**, *51*, 11841.
- (87) Wang, Y.-N.; Wei, W.-T.; Yang, C.-W.; Huang, M. H. Seed-Mediated Growth of Ultralong Gold Nanorods and Nanowires with a Wide Range of Length Tunability. *Langmuir* **2013**, *29*, 10491.
- (88) Wang, C.; Sun, S. Facile synthesis of ultrathin and single-crystalline Au nanowires. *Chem. Asian. J.* **2009**, *4*, 1028.
- (89) Huo, Z.; Tsung, C.-k.; Huang, W.; Zhang, X.; Yang, P. Sub-Two Nanometer Single Crystal Au Nanowires. *Nano Lett.* **2008**, *8*, 2041.

- (90) Feng, H.; Yang, Y.; You, Y.; Li, G.; Guo, J.; Yu, T.; Shen, Z.; Wu, T.; Xing, B. Simple and rapid synthesis of ultrathin gold nanowires, their self-assembly and application in surface-enhanced Raman scattering. *Chem. Commun.* **2009**, 1984.
- (91) Ju, J.-J.; Lu, C.-X.; Jan, J.-S. Synthesis of Gold Nanowire Networks and Nanoparticles by Tyrosine Reduction of Chloroaurate. *J. Nanosci. Nanotechnol.* **2012**, *12*, 2802.
- (92) Kim, F.; Sohn, K.; Wu, J.; Huang, J. Chemical Synthesis of Gold Nanowires in Acidic Solutions. *J. Am. Chem. Soc.* **2008**, *130*, 14442.
- (93) Vasilev, K.; Zhu, T.; Wilms, M.; Gillies, G.; Lieberwirth, I.; Mittler, S.; Knoll, W.; Kreiter, M. Simple, One-Step Synthesis of Gold Nanowires in Aqueous Solution. *Langmuir* **2005**, *21*, 12399.
- (94) Halder, A.; Ravishankar, N. Ultrafine Single-Crystalline Gold Nanowire Arrays by Oriented Attachment. *Adv. Mater.* **2007**, *19*, 1854.
- (95) Guo, T.; Yu, G.; Zhang, Y.; Xiang, H.; Chang, F.; Zhong, C.-J. Synthesis of Ultralong, Monodispersed, and Surfactant-Free Gold Nanowire Catalysts: Growth Mechanism and Electrocatalytic Properties for Methanol Oxidation Reaction. *J. Phys. Chem. C* **2017**, *121*, 3108.
- (96) Liu, H.; Cao, X.; Yang, J.; Gong, X.-Q.; Shi, X. Dendrimer-mediated hydrothermal synthesis of ultrathin gold nanowires. *Sci. Rep.* **2013**, *3*, 3181.
- (97) Imura, C.-M.; Mori, T.; Imura, Y.; Kawai, T. Dendritic gold nanowires supported on SiO₂ nanoparticles fabricated by a seed growth method. *New J. Chem.* **2016**, *40*, 7048.
- (98) Li, C. C.; Chen, L. B.; Li, Q. H.; Wang, T. H. Seed-free, aqueous synthesis of gold nanowires. *CrystEngComm* **2012**, *14*, 7549.
- (99) Shin, K. S.; Kim, J. H.; Kim, I. H.; Kim, K. Novel fabrication and catalytic application of poly(ethylenimine)-stabilized gold–silver alloy nanoparticles. *J. Nanopart. Res.* **2012**, *14*.
- (100) Zhang, Q.; Lee, J. Y.; Yang, J.; Boothroyd, C.; Zhang, J. Size and composition tunable Ag–Au alloy nanoparticles by replacement reactions. *Nanotechnology* **2007**, *18*, 245605.
- (101) Guisbiers, G.; Mendoza-Cruz, R.; Bazán-Díaz, L.; Velázquez-Salazar, J. J.; Mendoza-Perez, R.; Robledo-Torres, J. A.; Rodríguez-Lopez, J.-L.; Montejano-Carrizales, J. M.; Whetten, R. L.; José-Yacamán, M. Electrum, the Gold–Silver Alloy, from the Bulk Scale to the Nanoscale: Synthesis, Properties, and Segregation Rules. *ACS Nano* **2016**, *10*, 188.
- (102) Guisbiers, G.; Mendoza-Cruz, R.; Bazán-Díaz, L.; Velázquez-Salazar, J. J.; Mendoza-Perez, R.; Robledo-Torres, J. A.; Rodríguez-López, J.-L.; Montejano-Carrizales, J. M.; Whetten,

R. L.; José-Yacamán, M. Response to “Comment on ‘Electrum, the Gold–Silver Alloy, from the Bulk Scale to the Nanoscale: Synthesis, Properties, and Segregation Rules’”. *ACS Nano* **2016**, *10*, 10620.

(103) Link, S.; Wang, Z. L.; El-Sayed, M. A. Alloy Formation of Gold–Silver Nanoparticles and the Dependence of the Plasmon Absorption on Their Composition. *J. Phys. Chem. B* **1999**, *103*, 3529.

(104) Liz-Marzan, L. M.; Philipse, A. P. Stable hydrosols of metallic and bimetallic nanoparticles immobilized on imogolite fibers. *J. Phys. Chem.* **1995**, *99*, 15120.

(105) Sato, T.; Kuroda, S.; Takami, A.; Yonezawa, Y.; Hada, H. Photochemical formation of silver-gold (Ag–Au) composite colloids in solutions containing sodium alginate. *Appl. Organomet. Chem.* **1991**, *5*, 261.

(106) Mulvaney, P.; Giersig, M.; Henglein, A. Electrochemistry of multilayer colloids: preparation and absorption spectrum of gold-coated silver particles. *J. Phys. Chem.* **1993**, *97*, 7061.

(107) Hodak, J. H.; Henglein, A.; Giersig, M.; Hartland, G. V. Laser-Induced Inter-Diffusion in AuAg Core–Shell Nanoparticles. *J. Phys. Chem. B* **2000**, *104*, 11708.

(108) Esumi, K.; Shiratori, M.; Ishizuka, H.; Tano, T.; Torigoe, K.; Meguro, K. Preparation of bimetallic palladium-platinum colloids in organic solvent by solvent extraction-reduction. *Langmuir* **1991**, *7*, 457.

(109) Chen, D.-H.; Chen, C.-J. Formation and characterization of Au–Ag bimetallic nanoparticles in water-in-oil microemulsions. *J. Mater. Chem.* **2002**, *12*, 1557.

(110) Mallin, M. P.; Murphy, C. J. Solution-Phase Synthesis of Sub-10 nm Au–Ag Alloy Nanoparticles. *Nano Lett.* **2002**, *2*, 1235.

(111) Raveendran, P.; Fu, J.; Wallen, S. L. A simple and “green” method for the synthesis of Au, Ag, and Au–Ag alloy nanoparticles. *Green Chem.* **2006**, *8*, 34.

(112) Pal, A.; Shah, S.; Devi, S. Synthesis of Au, Ag and Au–Ag alloy nanoparticles in aqueous polymer solution. *Colloids Surf. A* **2007**, *302*, 51.

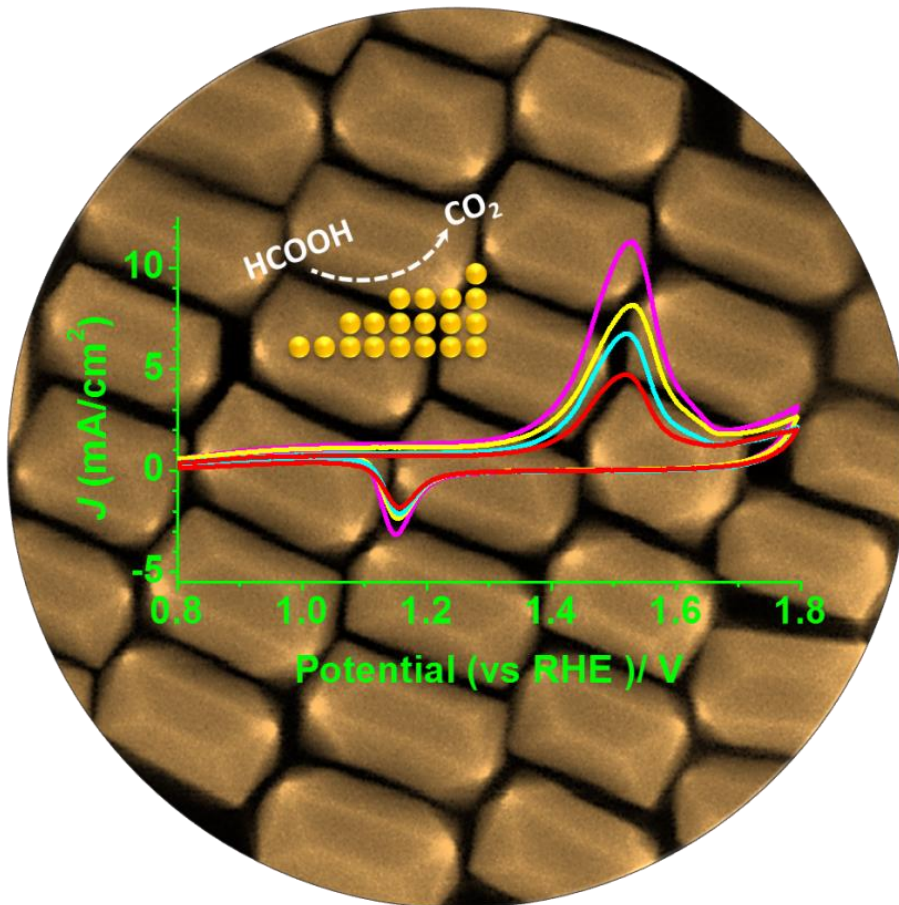
(113) Huang, J.; Vongehr, S.; Tang, S.; Lu, H.; Shen, J.; Meng, X. Ag dendrite-based Au/Ag bimetallic nanostructures with strongly enhanced catalytic activity. *Langmuir* **2009**, *25*, 11890.

Chapter-2

High-Index Faceted Gold Nanocrystals (Au NCs)

Part-A

Synthesis and Applications of Convex Au NCs



2A.1 Introduction

Chapter 1 has dealt with the clear differences in low- and high-index faceted nanocrystals. Numerous articles are available regarding the size and shape controlled synthesis of low-index faceted nanocrystals. However, high-index faceted nanocrystals are much less explored owing to their high energy surface (associated with presence of inadequately coordinated atoms at steps, edges and kinks) making them difficult to be synthesized.¹⁻³ In addition, the aqueous synthetic methodologies mostly used ascorbic acid as mild reducing agent, which is highly sensitive towards pH and temperature of the growth solution. This warranted investigating some new reducing agents which are relatively less active than ascorbic acid, so that the control over growth of nanoparticles would be enhanced. Here, we introduced tannic acid (TA) as a mild reducing agent for the first time for the synthesis of high-index faceted elongated tetrahedra (ETHH) Au NCs with high degree of size and shape controllability.

2A.2 Materials/Methods

Tannic acid (TA), gold (III) chloride trihydrate ($\text{HAuCl}_4 \cdot 3\text{H}_2\text{O}$), silver nitrate (AgNO_3), cetyltrimethylammonium bromide (CTAB), cetyltrimethylammonium chloride (CTAC), cetylpyridinium chloride (CPC), sodium borohydride (NaBH_4) and ascorbic acid were purchased from Sigma-Aldrich. Sodium hydroxide (NaOH) (analytical reagent) was bought from Rankem. Sulfuric (H_2SO_4) and formic acid (HCOOH) were purchased from Thomas Baker. All chemical were used as such. Milli-Q water (18.2 M Ω) was used for all experiments.

A typical synthesis of ETHH Au NCs is as follows: rapid addition of NaBH_4 (75 μL , 20 mM) to a mixture of Millipore water H_2O (1 mL), CTAB (1.25 mL, 0.2 M) and HAuCl_4 (0.156 mL, 4 mM) resulted in a brownish colour solution, which indicated the formation of seeds. The growth solution was made by sequential addition of an appropriate amount of water (in order to make a total volume of 2 mL), NaOH (20 μL , 0.1 M), HAuCl_4 (0.25 mL, 4 mM), CTAB (1 mL, 0.2 M) and AgNO_3 (varied, 4 mM). Subsequent introduction of TA (10 μL , 100 mM) turned the color of the solution from dark yellow to pale yellow in 10 min due to $\text{Au(III)} \rightarrow \text{Au(I)}$ reduction. The pH of the growth solution before and after addition of TA was observed to be ~ 5.2 and ~ 3.3 , respectively. Finally, to the growth solution, seed solution (3 μL , varied concentration) was added and allowed the NCs to grow for 12 h (and beyond upon decreasing the amount of seed) at

room-temperature. The resultant concentrations of reagents in the growth solution are HAuCl₄ (0.5 mM), CTAB (0.1 M), NaOH (1 mM), AgNO₃ (0.1 mM for 50 μL) and TA (0.5 mM).

Synthesis of 34 nm octahedral Au NCs was done by following the reported method with minor modifications.⁴ Aqueous solution (1.25 mL) of H₂Cl₄ (0.25 mM) and CTAB (75 mM) was made. Subsequent treatment of this solution with NaBH₄ (37 μL, 20 mM) led to the formation of seed particles. This solution was 100 times diluted with water and then used as seed. The growth solution was made by addition of HAuCl₄ (50 μL, 4mM), CTAB (0.4 mM, 0.2 M) and AA (0.3 mL, 100 mM). To this solution 60 μL seed was added and then left the reaction mixture undisturbed at room temperature for 8 h. Finally, the purple-red color of the solution indicated the formation of octahedral Au NCs.

Octahedral Au NCs with 164 nm size was synthesized according to the reported protocol with minor modifications.⁵ This procedure involves multiple steps to finally realize the octahedral Au NCs. Seed nanoparticles were synthesized as per the protocol used for the ETHH Au NCs. For the synthesis of Au NRs 2.4 μL of seed solution was mixed with growth solution that contains HAuCl₄ (0.25 mL, 4 mM), CTAB (1mL, 0.2 M), AgNO₃ (30 μL, 4 mM) and AA (16 μL, 100 mM) and then allowed the growth at 30 °C for 2h. Then as formed Au NRs were washed twice through centrifugation (12,000 rpm, 10 min) and re-dispersed in 1.15 mL CTAB (10 mM) solution. Subsequently, this solution was treated with the solution of 0.194 mL HAuCl₄ (4 mM) and 0.3 mL AA (100 mM) in order to overgrow the Au NRs at 40 °C for 1 hr. Later this solution was centrifuged (10,000 rpm, 8 min) and removed the supernatant followed by re-dispersed in milli-Q water. Repeated the same and re-dispersed in 1.5 mL CTAB (10 mM) solution. Afterward treated with 75 μL HAuCl₄ (4 mM) solution and kept undisturbed at 40 °C for 12 h. The solution was then washed three times with CPC (100 mM) with alternate centrifugation (10,000 rpm, 8 min) and dissolution and finally re-dispersed in 1.575 mL CPC (100 mM) solution and used as a seed in the growth solution for the fabrication of octahedral Au NCs. The seed (20 μL) mixed with the growth solution which was made by addition of aqueous solutions of 0.25 mL HAuCl₄ (4 mM), 13 μL AA (100 mM) and 2.5 mL CPC (0.2 M) in to 2.35 mL of Milli-Q water and allowed to react for 2 h. Subsequently, excess precursors were removed by centrifugation (5000 rpm, 7 min) and preserved.

UV-vis spectra were recorded from Chemito SPECTRASCAN UV 2600. FE-SEM and TEM images were captured through ZEISS Ultra Plus and TECHNAI T30 respectively. Electrocatalytic studies were carried out by Biologic SP-300 potentiostat. Raman spectra were recorded by Horiba JY Labram HR800 micro Raman spectrometer with laser wavelength of 632.8nm, Helium-Neon laser, 20 mW power.

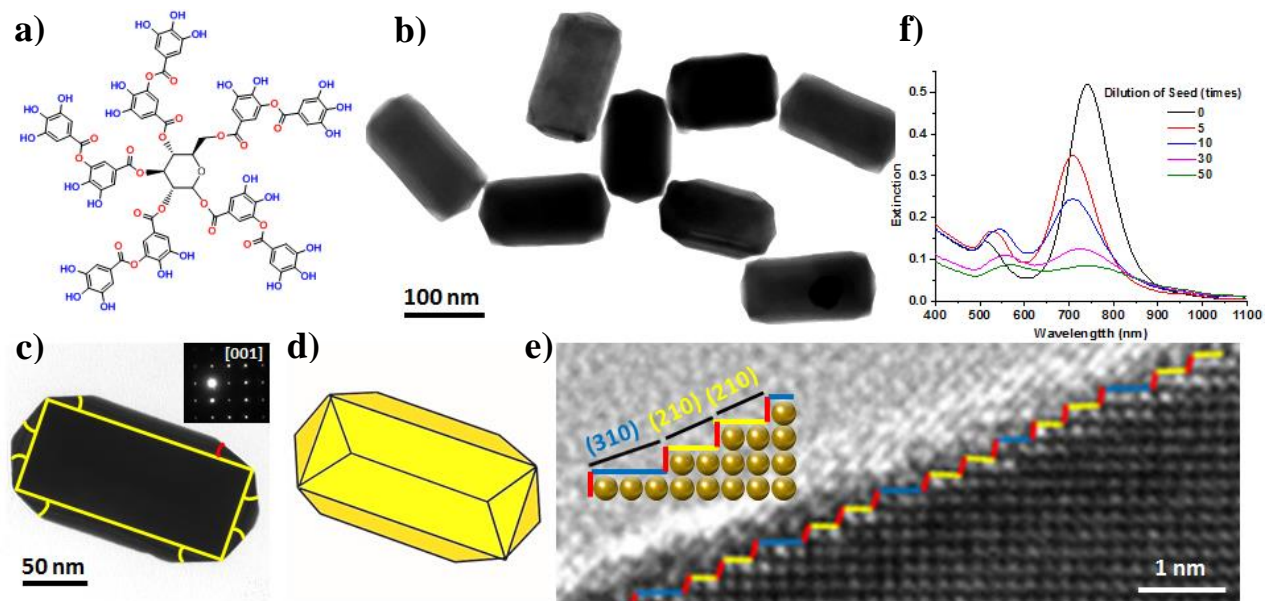


Figure 2A.1: a) Schematic of TA. b) TEM image for the as synthesized ETHH Au NCs. c) TEM image of ETHH Au NC (yellow box) oriented at the [001] zone axis; inset: SAED pattern for the same particle. d) Schematic illustration of the ETHH Au NC in. e) HR-TEM image showing the atomic resolution steps in ETHH Au NC. f) UV-vis spectra recorded for the ETHH Au NCs synthesized with varying the amount of seed (diluted original seed) in the growth solution.

2A.3 Results and discussion

High-index facets of ETHH Au NCs were characterized by transmission electron microscopy (TEM) analysis. **Figure 2A.1b** displays randomly oriented ETHH Au NCs synthesized with 10 times the dilution of the original seed solution and 50 μL AgNO_3 . To define the facets, the ETHH Au NC was chosen in such a way that its orientation is in the [001] direction which was determined by the SAED pattern (**Figure 2A.1c**). The angles between the bevel and the base of the ETHH Au NCs were measured to be 23.2, 24.8, 27.5, 22.3, 25.7, 21.5, 24.6, and 22.0 (starting clockwise from the marked red coloured angle in **Figure 2A.1c**). The average value of

all these angles was estimated to be $\sim 23.9^\circ$ and thereby suggesting that our as synthesized ETHH Au NCs were enclosed with (730) planes (schematically shown in **Figure 2A.1d**).¹ A high-resolution (HR) TEM image clearly shows the arrangements of single-atomic step terraces with the size of two and three atoms (**Figure 2A.1e**). The repeating unit of sub-planes ‘(310)(210)(210)’ is representing (730) planes corroborating the consistent mathematical analysis in **Figure 1.1c (Table 1.1)**. Note also that apart from ETHH, this method also allowed us to size controlled fabrication of concave cube Au NCs with high-index facets by replacing the CTAB with CTAC (**Figure 2A.2**).^{6,7} Notably, we observed the elongation of THH NCs whereas concave nanocubes were not elongated. Earlier, it has been demonstrated that the nature of the surfactant (counter ions) and its concentration played crucial roles in determining the shape of NCs.⁸⁻¹⁰ At a concentration of 100 mM, the feasibility of the formation of cylindrical-micelle templates is much higher for CTAB than CTAC.⁹ Thus, the formation of elongated nanostructures (quasi-one-dimensional) can be easily directed by CTAB while CTAC directed more isotropic nanostructures; specifically at higher concentrations, likewise in the present study. By replacing CTAB with dodecyldimethyl-ammonium bromide (DDAB) THH Au NCs were generated perhaps due to the presence of two long aliphatic chains restricting the formation of cylindrical-micelle templates.¹⁰ Also, an extensive study by Mirkin and co-workers proposed a ‘locks in’ mechanism which is operational in the case of CTAC prohibiting the elongation at an early stage of growth and thereby leading to the formation of isotropic NCs (concave cubes).⁸ In our field-emission electron microscopy (FE-SEM) studies (**Figure 2A.3**), as synthesized ETHH Au NCs exhibit well-defined shapes and sizes with visible vertices and lateral facets. Precise control over the dimensions of ETHH Au NCs was achieved by simply varying the quantity of seed (0, 5, 10, 30 and 50 times dilution of the original solution) in the growth solution while keeping the AgNO_3 quantity fixed at 50 μL . Upon decreasing the seed quantity, the length and width (as shown schematically in **Figure 2A.3a**) of the ETHH Au NCs increased while the average aspect ratio reduced (**Figure 2A.3b–f**).

These results are consistent with the UV-vis spectra (**Figure 2A.1f**), where it has been observed that the transverse surface plasmon resonance (TSPR) peak gradually red-shifted from 513 nm to 565 nm whereas the longitudinal surface plasmon resonance (LSPR) peak first became blue-shifted from 740 nm to 706 nm and then red-shifted to 743 nm. Note also that the absorbance of

both TSPR and LSPR were suppressed with increasing the dimensions of ETHH Au NCs, which could be due to the dominance of scattering.¹¹

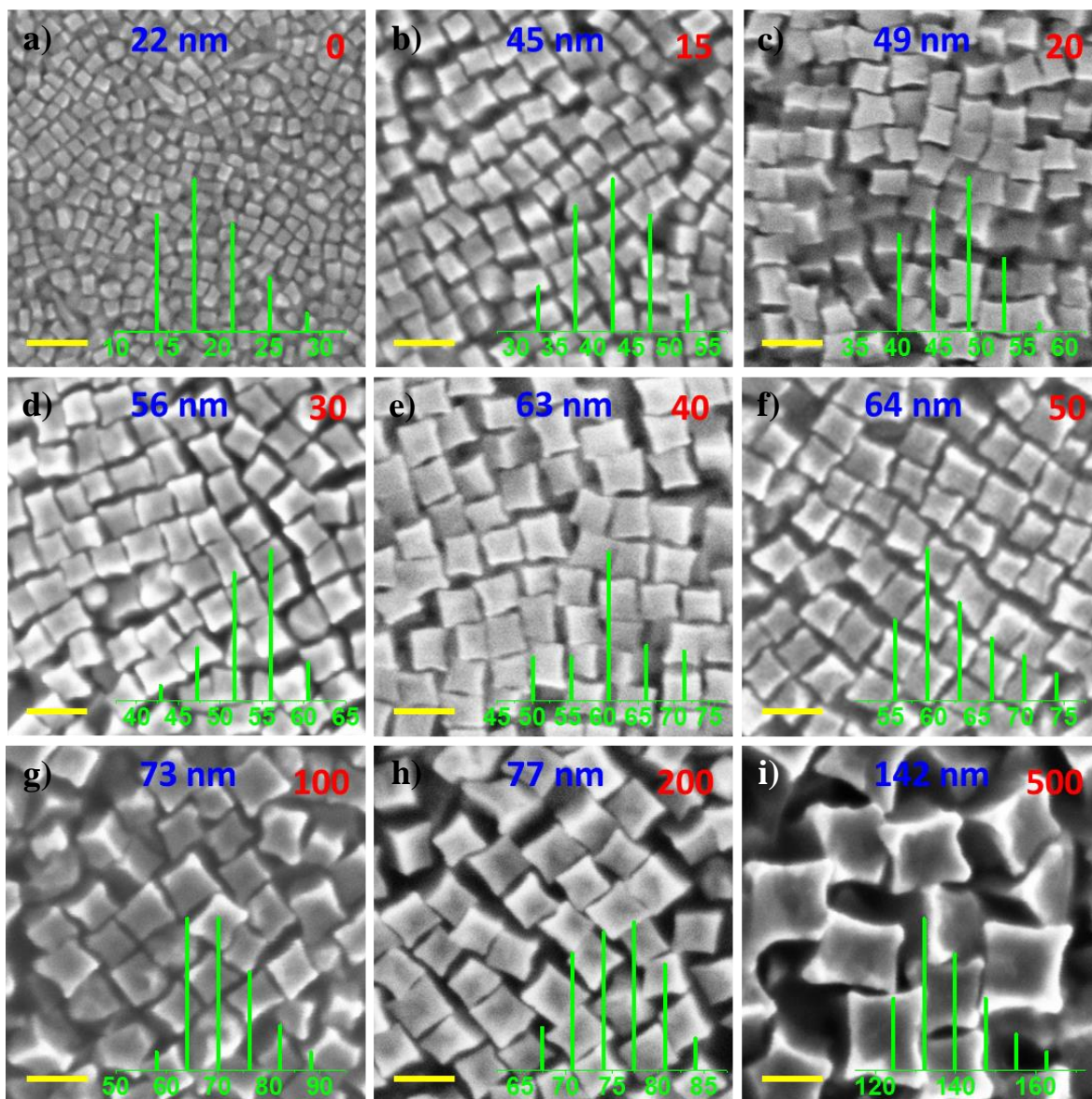


Figure 2A.2: (a-i) FE-SEM images of concave cubic Au NCs synthesized by using 0, 15, 20, 30, 40, 50, 100, 200 and 500 times (labelled with red) dilution of original seed into the growth solution respectively. Concave cubic Au NCs synthesized by the same procedure used for the ETHH Au NCs, but the CTAC was used instead of CTAB; scale bar is 100 nm for all. Average lengths of edges are labelled with blue colour. Histogram was drawn for each sample (green colour) by surveying above 50 number of particles; scale bar is stand for edge length (nm).

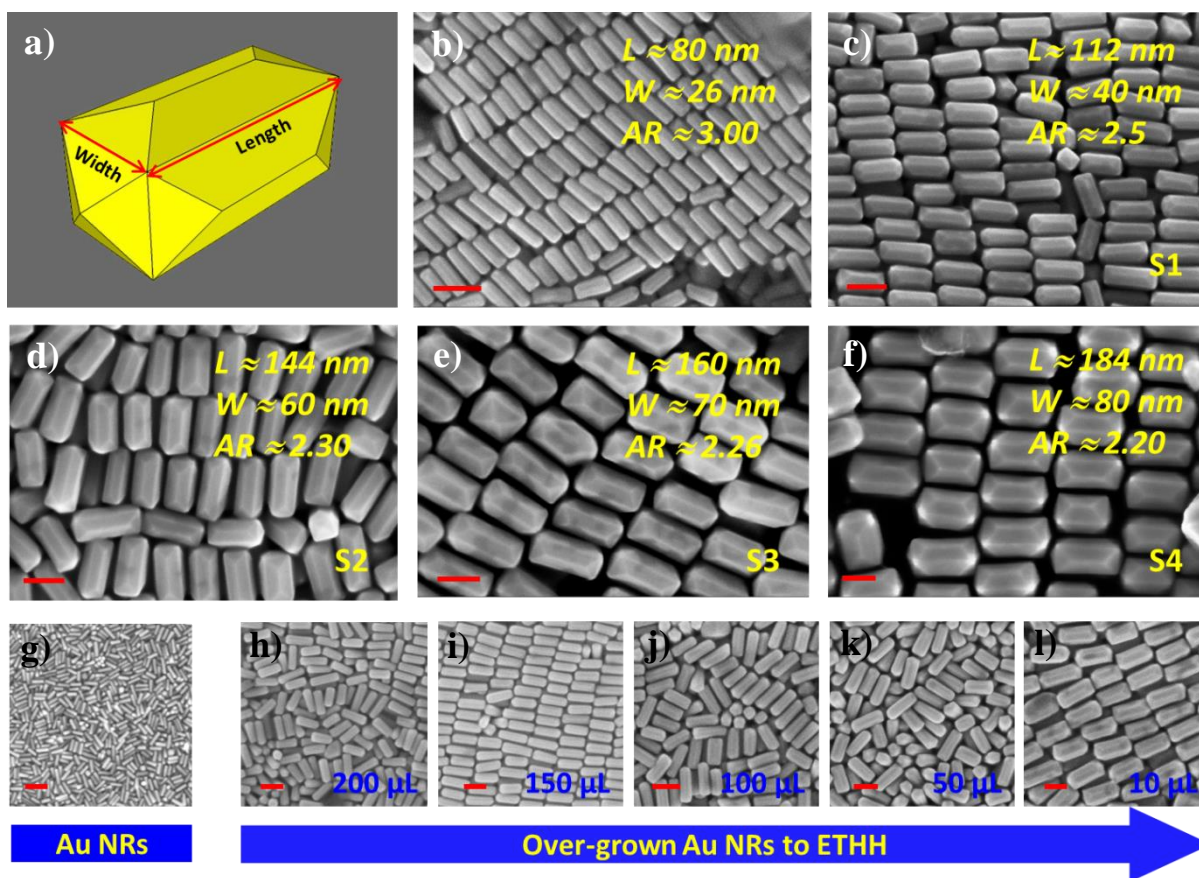


Figure 2A.3: a) Schematic representation of the ETHH Au NC. b –f) FE-SEM images of ETHH Au NCs synthesized by using 0, 5, 10, 30 and 50 times dilution of the original seed solution, respectively. The yellow labels on the images, L , W and AR stand for average length, width and aspect ratio (sum of the individual values divided by the number of particles), respectively; S1, S2, S3 and S4 (c–f) are the sample names. g) FE-SEM image (colored) of Au NRs. h–l) FE-SEM images (colored) of ETHH Au NCs synthesized by over-growing the Au NRs (the amount of Au NR solution used is labelled in yellow). All scale bars represent a length of 100 nm in the respective images.

The following sheds some light on the mechanistic aspects of the formation of ETHH Au NCs, which were not well-discussed in earlier reports.^{12,13} These significant observations imply that ETHH Au NCs perhaps evolved via Au NRs as an intermediate. To justify our proposal, we have studied the over-growth of Au NRs (Figure 2A.3g), under similar experimental conditions as for the ETHH Au NC synthesis (Figure 2A.3b–f). Despite varying the amount of seed (Au NRs) from 200 μL to 10 μL , all of them resulted in ETHH Au NCs; specifically, upon decreasing the

amount of seed, a gradual increase in the dimensions accompanied by pronounced facets was observed (**Figure 2A.3h–i**). Moreover, to enhance our understanding regarding the mechanism, the same experiment was performed with well characterized cylindrical Au NRs (synthesized by using ascorbic acid) which also resulted in ETHH Au NCs. Thus, we can conclude that ETHH Au NCs were grown via NRs.¹⁴ In addition to this we have investigated the evolution of ETHH Au NCs by taking out the during the growth of ETHH Au NCs (S2); aliquot from the growth solution has been taken out at time points of 2, 4, 8 and 24 h as seed introduced. After 2 h and 4h of seed addition, ill-defined nanocrystals (no shape uniformity) were observed. However, at 8 h uniformly shaped ETHH Au NCs were observed and further progression growth till 24 h given rise to completely grown NCs were noticed (**Figure 2A.4**).

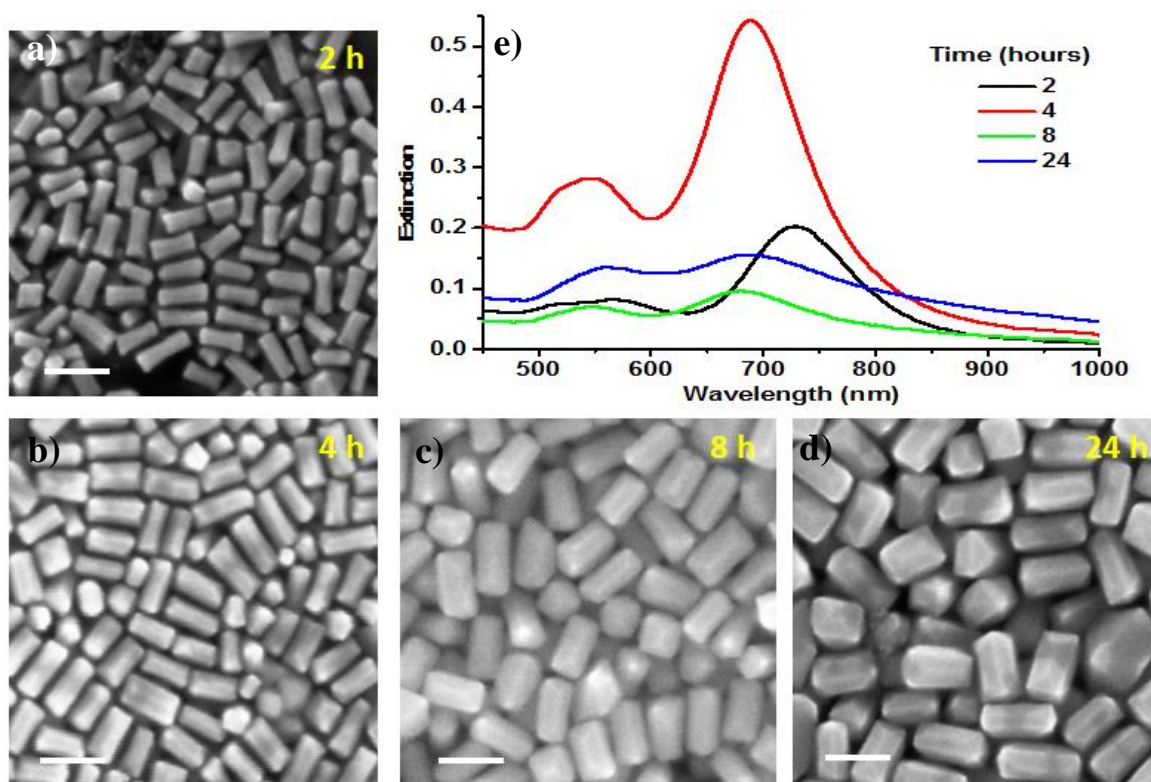


Figure 2A.4: FE-SEM images were captured at a) 2, b) 4, c) 8 and d) 24 h (from introduction of seed into the growth solution) during the evolution of ETHH Au NCs. UV-vis spectra for corresponding FE-SEM images. Scale bar is 100 nm for all.

In order to tune the surface plasmons of ETHH Au NCs, we have simply varied the AgNO_3 amount from 30 to 100 μL while keeping the seed quantity fixed (3 μL) in each sample preparation. With increasing concentration of AgNO_3 , a gradual red-shift of the LSPR peak from

715 nm to 815 nm and a negligible blue-shift of the TSPR peak from 517 to 513 nm is clearly visible in the UV-vis spectra (**Figure 2A.5a**) which is ascribed to gradual rise in the aspect ratio of the NCs.⁴ Recently, Wang *et al.* have elegantly shown that the geometry-controlled overgrowth of Au NRs involved distinctive pathways: Ag under-potential deposition and Au–Ag electro-less co-deposition. Such pathways were demonstrated to be switchable upon varying the experimental parameters (mainly concentration of AgNO₃, surfactants, and reducing agents)¹⁵ – so called kinetically versus thermodynamically controlled products. We believe that our adopted synthetic procedure enabled the formation of thermodynamically controlled^{16,17} Au NCs since TA is a much milder reducing agent and the growth of Au NCs took a considerably longer time via Ag under-potential deposition. The FE-SEM images of the Au NCs synthesized in the presence of 30, 60 and 90 μL of AgNO₃ (**Figure 2A.5b**) display the preservation of ETHH morphology with high structural purity. Absence of other characteristic features in the UV-vis spectra corroborated the FE-SEM observations on the high-structural purity. To our knowledge, such a precise and gradual tuning of the surface plasmons of high-index faceted Au NCs across a wavelength of 100 nm is reported here for the first time.

This experiment was performed as follows, ETHH Au NCs washed twice with water by centrifugation and then loaded the amount of 85 μg on glassy carbon electrode; this electrode used as working electrode. Graphite rod and Hg/HgSO₄ were used as counter and reference electrodes respectively. Electrocatalysis of formic acid (0, 0.25, 0.5, 0.75 and 1M) was performed in H₂SO₄ (0.5 M) solution by applying the voltage scan rate of 50 mVs⁻¹. Nitrogen gas purging was allowed throughout the experiment. The first two cycles of measurements were discarded in order to avoid the interference of absorbed gases in the solution. These measurements were done for the samples S1, S2, S3, S4 (**Figure 2A.3**) and octahedral Au NCs (**Figure 2A.6**). Electrochemically active surface area was calculated for the samples S3 and Oh2 (**Figure 2A.6b**) based on oxide stripping results.

The electro-catalytic performance of our ETHH Au NCs with well-defined dimensions (S1 to S4 in **Figure 2A.3**) was evaluated by cyclic-voltammetry (CV). Note that CV can also be used to assess the various surface structures of metal nanoparticles; specifically, recent studies showed characteristic CV traces for the high-index faceted Au NCs.^{7,12}

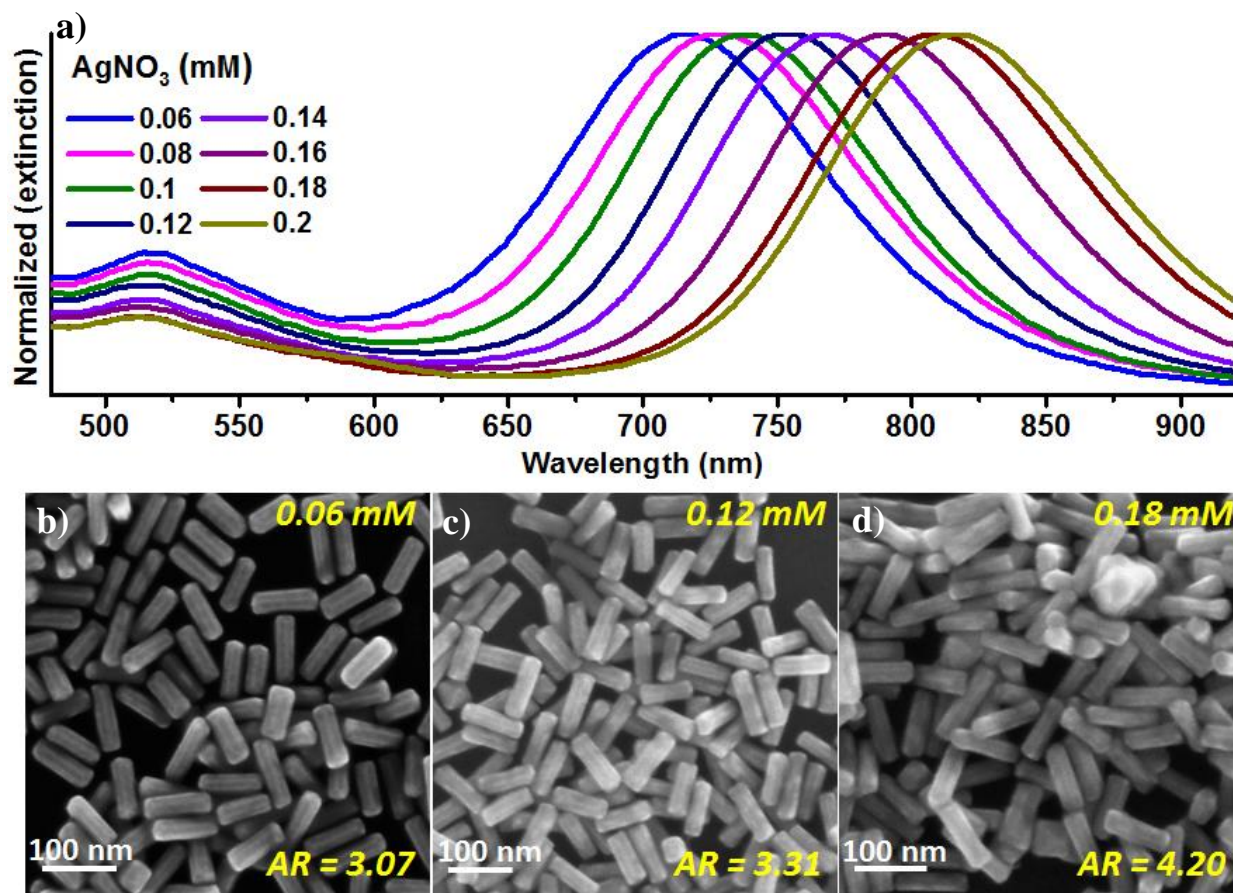


Figure 2A.5: a) UV-vis spectra recorded for the ETHH Au NCs synthesized by varying the concentration of AgNO_3 while keeping the amount of seed constant ($3\mu\text{L}$; original). b – d) FE-SEM images of ETHH Au NCs corresponding to 0.06, 0.12 and 0.18 mM of AgNO_3 , respectively. The average aspect ratio is labelled in yellow (sum of the individual values divided by the number of particles). All scale bars represent a length of 100 nm in the respective images.

CV traces of ETHH Au NCs with different sizes (sample S1, S2, S3 and S4) exhibited an oxidation peak around 1.4 V and the current density value decreased with increasing the size (Figure 2A.7a). For comparison, we have tested the electrochemical performance of low-index faceted octahedral (Oh) Au NCs (see Figure 2A.7a) with sizes of 34 nm (Oh1) and 164 nm (Oh2) (Figure 2A.6); size is the distance between opposite vertices of the Oh. Notable observations in Figure 2A.7a are (i) occurrence of the oxidation peak of Oh NCs (for both sizes) at 1.6 V, which is 0.2 V (0.17 V in an earlier report¹²) larger than that of ETHH NCs (1.4 V) irrespective of their dimensions; (ii) the current density value for Oh NCs (164 nm) is much lower than that of ETHH NCs of similar size (160 nm).

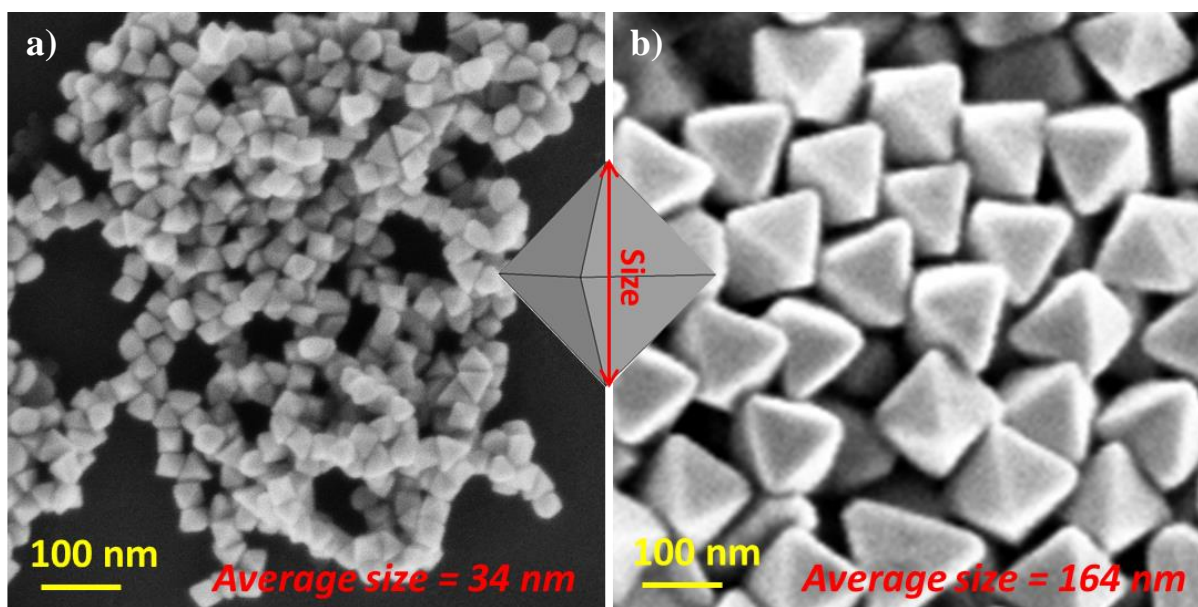


Figure 2A.6: FE-SEM images of octahedral Au NCs. a) Synthesized according to reported procedure.⁴ b) Produced by following the existing report;⁵ in the final step 20 μL of CPC capped seed solution was added to the growth solution.

We have studied the electro-catalytic oxidation of HCOOH (FA) (to CO_2 and H_2O) with different concentrations (0.25 M, 0.5 M, 0.75 M and 1 M) for each set of the ETHH Au NCs (S1, S2, S3 and S4 in **Figure 2A.3**; **Figure 2A.8**). An aqueous solution of 0.5 M H_2SO_4 was used as the electrolyte and the scan rate was fixed at 50 mVs^{-1} . **Figure 2A.7b** shows CV traces recorded during the oxidation of 1 M HCOOH employing ETHH (S3) and Oh (Oh2) Au NCs as catalysts and it is discernible that HCOOH oxidation occurred at $1.3 < V < 1.7$, which is consistent with the earlier report that oxidation takes place via single formate as the active intermediate.¹⁸ The observed lower oxidation potential value and higher peak current density clearly suggested that our as synthesized ETHH Au NCs are superior candidates compared to Oh Au NCs for such reactions ($\sim 150\%$ better).

In fact, with respect to the oxidation of HCOOH, the electro-chemically active surface area (ECAS) value for the S3 sample was found to be higher than that of the Oh2 sample; and also the mass activity and specific activity values for the S3 sample were estimated to be consistently higher than those of the Oh2 sample (**Table 2A.1**).

Table 2A.1: Quantitative analysis of HCOOH oxidation CV recorded (**Figure 2A.7**) for the Au NCs

Au NCs	Mass activity (A mg ⁻¹)	ECSA (cm ² mg ⁻¹)	Specific activity (mA cm ⁻²)
S3	15.64X10 ⁻³	76.95	2.02X10 ⁻²
Oh2	10.03X10 ⁻³	70.83	1.41X10 ⁻²

The degree of electro-oxidation of HCOOH could be fine-tuned upon varying the dimensions of the ETHH Au NCs ($S1 < S2 < S3 < S4$); the oxidation peak current density gradually reduced as the size was increased (**Figure 2A.7c**). A gradual decrease in the value of the peak current density with respect to either the length or the width of the ETHH NCs was realized (**Figure 2A.4d**).

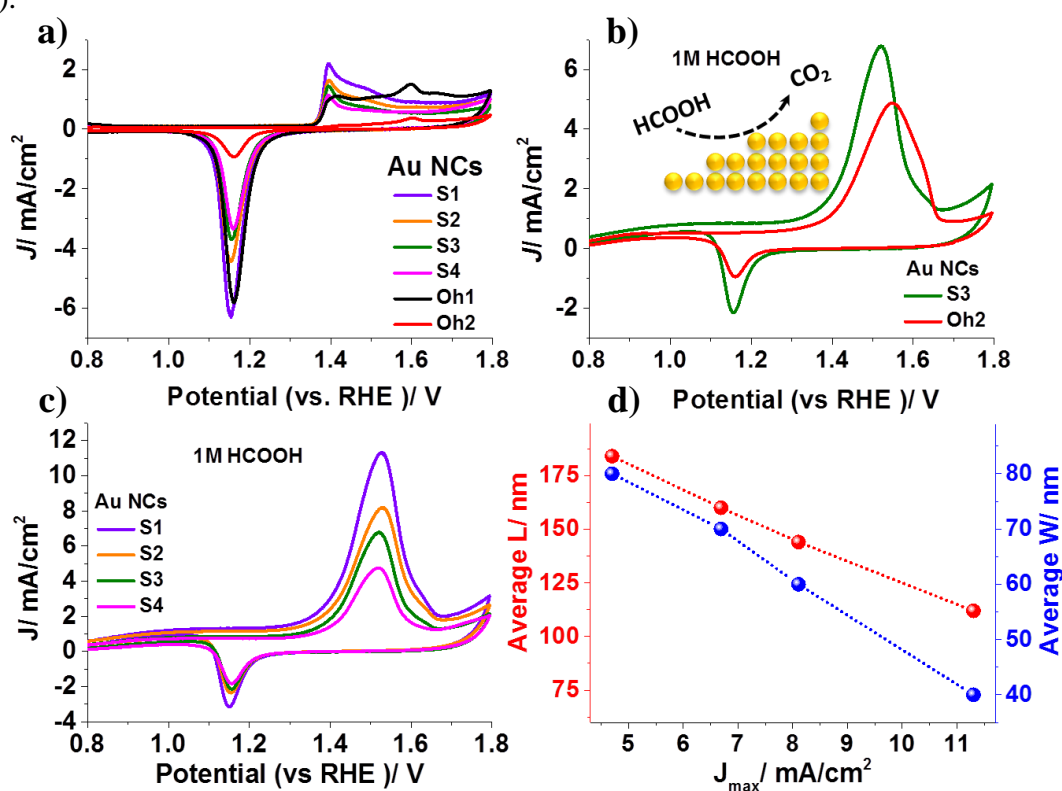


Figure 2A.7: a) CV traces recorded for the samples S1, S2, S3, and S4 (see **Figure 2A.2**), and octahedral Au NCs (Oh1 and Oh2) in the presence of 0.5 M H₂SO₄. b) CVs of 1 M HCOOH oxidation were recorded for the S3 (green) and Oh2 (red) Au NCs. c) CVs were recorded for the oxidation of 1 M HCOOH by S1, S2, S3 and S4. d) Plot of average length (L) and width (W) vs. oxidation peak current density in (c) for S1, S2, S3 and S4.

We have recorded CV traces with other concentrations of HCOOH (0.25 M, 0.5 M and 0.75 M) employing four sets of ETHH Au NCs and in each case, the peak current density value was

gradually increasing with increasing concentration and tending to a saturation value which could be due to complete coverage of the ECAS at higher concentrations (**Figure 2A.8a**). Furthermore, for the first time, we have performed a durability test on the ETHH Au NCs (S3) at 1 M HCOOH up to 550 cycles of continued operation (**Figure 2A.8b**).

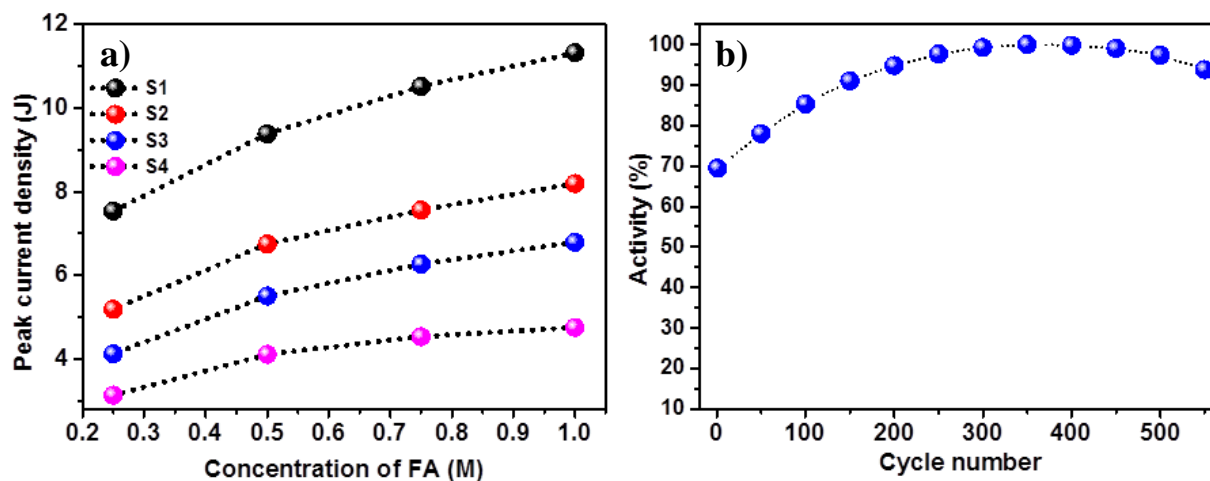


Figure 2A.8: a) Plot of oxidation peak current densities (during the FA oxidation) obtained for ETHH Au NCs versus different concentrations of FA used in the electrolyte solution. b) Electrocatalytic durability test was performed for the sample S3 in HCOOH (1M) + H₂SO₄ (0.5 M) electrolyte solution.

Overall, the efficiency gradually increased (initial access of the electrolytes to the NCs was limited due to a high scan rate of 50 mVs⁻¹) until it attained 100% at 300 cycles and subsequently sustained up to 550 cycles. To investigate the role of surface convexity and concavity, we have performed electro-oxidation of HCOOH by using ETHH Au NCs (S1 and S3; **Figure 2A.3**) and compared the results with those of CC Au NCs having similar sizes (CC1 and CC3; **Figure 2A.2**). Remarkably, irrespective of surface convexity or concavity, the Au NCs with high-index facets synthesized by using TA as the reducing agent exhibited electro-chemical performances that are very much alike. Such a controlled electro-oxidation of HCOOH not only reveals the effectiveness of our adopted synthetic method but also appears useful for the development of direct-formic acid fuel cells.

Raman measurement was carried out through the following way. As synthesized ETHH Au NCs (S2 and S4; **Figure 2A.3**) solutions of 1mL were centrifuged at 6000 rpm for 7 min and removed the supernatant and subsequently the precipitate re-dispersed into the 1mL MQ-water. These

solutions were centrifuged again with the same parameters and re-dispersed the precipitate into 50 μL MQ-water with sonication (after discarding the supernatant). Subsequently these solutions were treated with 50 μL of benzenethiol (BT) (10 μM , in ethanol) and kept for incubation for 12 h (the resultant concentration of BT (C_{SERS}) is 5 μM). After drop-casting these sample on glass slide, dried under the incandescent lamp (200 W) for 20 min. Raman spectra were recorded for these samples along with neat BT (its concentration (C_{RS}) calculated to be 9.676 M) at 2 mW with acquisition time of 5s by using 632.8 nm lasers as source. The intensity of the peak calculated from origin software. Lorentzian (function) fit of the corresponding (peak) curve provided the area under the curve i.e. intensity of that peak (I_{SERS} or I_{RS}). Thus, analytical enhancement factors (AEF) for the peaks at 1070 and 1570 cm^{-1} were calculated (see the **Table 2A.2&3**).

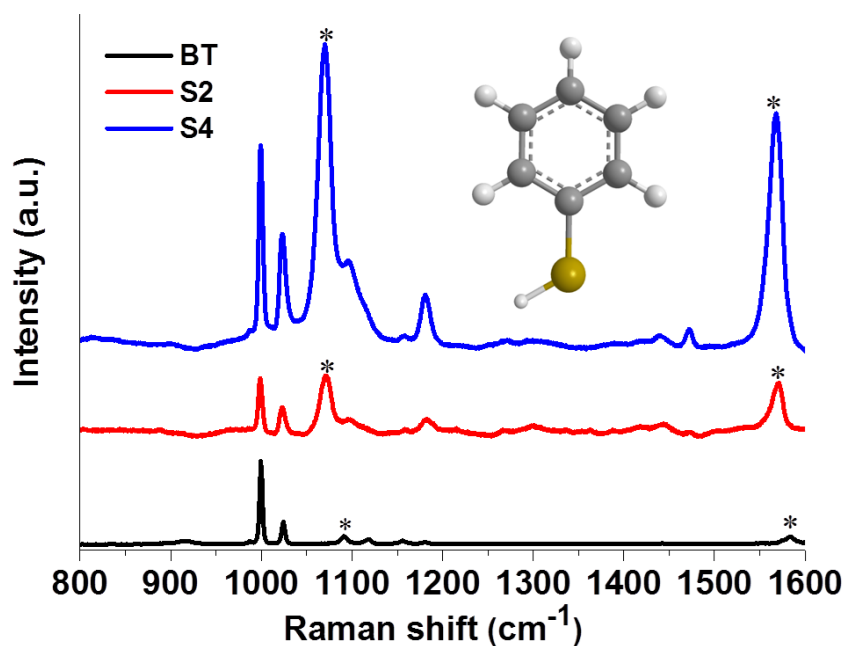


Figure 2A.9: Raman spectra of neat BT (black) and of BT on S2 (red) and S4 (blue) ETHH Au NCs. Enhancement factors were calculated with respect to peaks (1070 cm^{-1} and 1570 cm^{-1} ; **Table 2A.2 and 3**). Inset: Molecular scheme of BT.

We have carried out surface-enhanced Raman scattering (SERS) experiments with benzenethiol (BT) as a probe molecule (**Figure 2A.9**). Remarkably, analytical enhancement factors (AEF) of BT on the S2 and S4 samples were estimated to be $\approx (1-5) \times 10^8$ and $\approx (3-8) \times 10^7$, respectively (**Table 2A.2a and b**).¹⁹⁻²²

Note that the AEF value was predominantly due to electromagnetic factors since BT is typically a non-resonant SERS reporter.¹⁹ In our system of ETHH Au NCs, the AEF was larger in S4 than that in S2, which is consistent with an earlier report on the increase of the enhancement factor upon increasing the particle size viz. the structural purity and uniform size distribution of our ETHH Au NCs perhaps reduced signal fluctuations.²³

Table 2A.2: Calculation of AEFs of the samples S2 and S4 for the SERS peaks at 1070 cm⁻¹.

ETHH Au NCs	I_{SERS} of 1070 cm ⁻¹	C_{SERS} (M)	I_{RS} (BT)	C_{RS} (M)	$I_{\text{SERS}}/I_{\text{RS}}$	AEF = $I_{\text{SERS}}/I_{\text{RS}} * C_{\text{RS}}/C_{\text{SERS}}$
S4	668642	5x10 ⁻⁶	7327	9.676	91.25	1.76x10 ⁸
S2	125486	5x10 ⁻⁶	7327	9.676	17.12	3.31x10 ⁷

Table 2A.3: Calculation of AEFs of the samples S2 and S4 for the SERS peaks at 1570 cm⁻¹.

ETHH Au NCs	I_{SERS} of 1570 cm ⁻¹	C_{SERS} (M)	I_{RS} (BT)	C_{RS} (M)	$I_{\text{SERS}}/I_{\text{RS}}$	AEF = $I_{\text{SERS}}/I_{\text{RS}} * C_{\text{RS}}/C_{\text{SERS}}$
S4	528136	5x10 ⁻⁶	10428	9.676	50.646	1.0x10 ⁸
S2	81730	5x10 ⁻⁶	10428	9.676	7.837	1.51x10 ⁷

Thus, our results on the electro-catalysis along with more than a million-fold in the AEF in SERS measurements by using high-index faceted ETHH Au NCs appear as a significant addition to earlier findings.²⁴

2A.4 Summary and Conclusions

In summary, we have successfully employed tannic acid as a mild reducing agent in the seed-mediated growth method for the fabrication of ETHH and CC Au NCs enclosed with high-index facets. Simply, by changing the concentration of seed solution, the dimensions of ETHH Au NCs could be precisely controlled, which directly impacted their electro-catalytic performances. Electro-oxidation of HCOOH by ETHH (and CC) Au NCs was observed to be ~150% higher than that of low-index faceted Au NCs (Oh) of similar sizes. Also, durability test revealed a significant retention of the electro-catalytic efficiency (up to 550 cycles). By tuning the amount of AgNO₃, surface plasmons (spanning over 100 nm) of ETHH Au NCs could be fine-tuned.

NRs were proposed to be the intermediate for the generation of the ETHH structure. The ETHH Au NCs were found to be SERS-active and a remarkable AEF in the range of 10^7 – 10^8 was estimated for the benzenethiol molecule. We anticipate our findings to be useful in the development of various high-index faceted NCs with well-defined structure–property relationships; specifically, bringing nanoelectro-catalysis and nanoplasmonics together on one platform.

2A.5 References

- (1) Quan, Z. W.; Wang, Y. X.; Fang, J. Y. High-Index Faceted Noble Metal Nanocrystals. *Accounts Chem Res* **2013**, *46*, 191.
- (2) Zhou, Z. Y.; Tian, N.; Li, J. T.; Broadwell, I.; Sun, S. G. Nanomaterials of high surface energy with exceptional properties in catalysis and energy storage. *Chem Soc Rev* **2011**, *40*, 4167.
- (3) Tian, N.; Zhou, Z. Y.; Sun, S. G.; Ding, Y.; Wang, Z. L. Synthesis of tetrahexahedral platinum nanocrystals with high-index facets and high electro-oxidation activity. *Science* **2007**, *316*, 732.
- (4) Fan, F. R.; Liu, D. Y.; Wu, Y. F.; Duan, S.; Xie, Z. X.; Jiang, Z. Y.; Tian, Z. Q. Epitaxial growth of heterogeneous metal nanocrystals: from gold nano-octahedra to palladium and silver nanocubes. *J. Am. Chem. Soc.* **2008**, *130*, 6949.
- (5) Niu, W.; Zheng, S.; Wang, D.; Liu, X.; Li, H.; Han, S.; Chen, J.; Tang, Z.; Xu, G. Selective synthesis of single-crystalline rhombic dodecahedral, octahedral, and cubic gold nanocrystals. *J Am Chem Soc* **2009**, *131*, 697.
- (6) Zhang, H.; Jin, M. S.; Xia, Y. N. Noble-Metal Nanocrystals with Concave Surfaces: Synthesis and Applications. *Angew Chem Int Edit* **2012**, *51*, 7656.
- (7) Zhang, J. A.; Langille, M. R.; Personick, M. L.; Zhang, K.; Li, S. Y.; Mirkin, C. A. Concave Cubic Gold Nanocrystals with High-Index Facets. *J Am Chem Soc* **2010**, *132*, 14012.
- (8) Langille, M. R.; Personick, M. L.; Zhang, J.; Mirkin, C. A. Defining Rules for the Shape Evolution of Gold Nanoparticles. *J Am Chem Soc* **2012**, *134*, 14542.
- (9) Gao, J.; Bender, C. M.; Murphy, C. J. Dependence of the Gold Nanorod Aspect Ratio on the Nature of the Directing Surfactant in Aqueous Solution. *Langmuir* **2003**, *19*, 9065.

- (10) Li, J.; Wang, L. H.; Liu, L.; Guo, L.; Han, X. D.; Zhang, Z. Synthesis of tetrahedral Au nanocrystals with exposed high-index surfaces. *Chem Commun* **2010**, *46*, 5109.
- (11) Xie, S.; Choi, S.-I.; Xia, X.; Xia, Y. Catalysis on faceted noble-metal nanocrystals: both shape and size matter. *Current Opinion in Chemical Engineering* **2013**, *2*, 142.
- (12) Ming, T.; Feng, W.; Tang, Q.; Wang, F.; Sun, L. D.; Wang, J. F.; Yan, C. H. Growth of Tetrahedral Gold Nanocrystals with High-index Facets. *J Am Chem Soc* **2009**, *131*, 16350.
- (13) Li, J.; Chang, M. M.; Peng, H.; Zhou, X. M.; Li, D. P.; Li, Y. X. Growth of elongated tetrahedral gold nanoparticles with high-index facets and their enhanced electrocatalytic properties. *Mater Lett* **2014**, *120*, 216.
- (14) Zhang, Q.; Wang, H. Facet-Dependent Catalytic Activities of Au Nanoparticles Enclosed by High-Index Facets. *Acs Catal* **2014**, *4*, 4027.
- (15) Zhang, Q.; Jing, H.; Li, G. G.; Lin, Y.; Blom, D. A.; Wang, H. Intertwining Roles of Silver Ions, Surfactants, and Reducing Agents in Gold Nanorod Overgrowth: Pathway Switch between Silver Underpotential Deposition and Gold–Silver Codeposition. *Chem. Mater.* **2016**, *28*, 2728.
- (16) Langille, M. R.; Personick, M. L.; Zhang, J.; Mirkin, C. A. Defining Rules for the Shape Evolution of Gold Nanoparticles. *J. Am. Chem. Soc.* **2012**, *134*, 14542.
- (17) Xia, Y.; Xia, X.; Peng, H. C. Shape-Controlled Synthesis of Colloidal Metal Nanocrystals: Thermodynamic versus Kinetic Products. *J Am Chem Soc* **2015**, *137*, 7947.
- (18) Li, N.; Zhao, P.; Astruc, D. Anisotropic gold nanoparticles: synthesis, properties, applications, and toxicity. *Angewandte Chemie* **2014**, *53*, 1756.
- (19) Sajanalal, P. R.; Sreepasad, T. S.; Samal, A. K.; Pradeep, T. Anisotropic nanomaterials: structure, growth, assembly, and functions. *Nano reviews* **2011**, *2*.
- (20) Vigderman, L.; Zubarev, E. R. High-Yield Synthesis of Gold Nanorods with Longitudinal SPR Peak Greater than 1200 nm Using Hydroquinone as a Reducing Agent. *Chem Mater* **2013**, *25*, 1450.
- (21) Chen, H. M.; Hsin, C. F.; Liu, R. S.; Lee, J. F.; Jang, L. Y. Synthesis and Characterization of Multi-Pod-Shaped Gold/Silver Nanostructures. *J. Phys. Chem. C* **2007**, *111*, 5909.
- (22) Chung, K. T.; Wong, T. Y.; Wei, C. I.; Huang, Y. W.; Lin, Y. Tannins and human health: a review. *Critical reviews in food science and nutrition* **1998**, *38*, 421.
- (23) Handler, P.; Baker, R. D. THE TOXICITY OF ORALLY ADMINISTERED TANNIC ACID. *Science* **1944**.

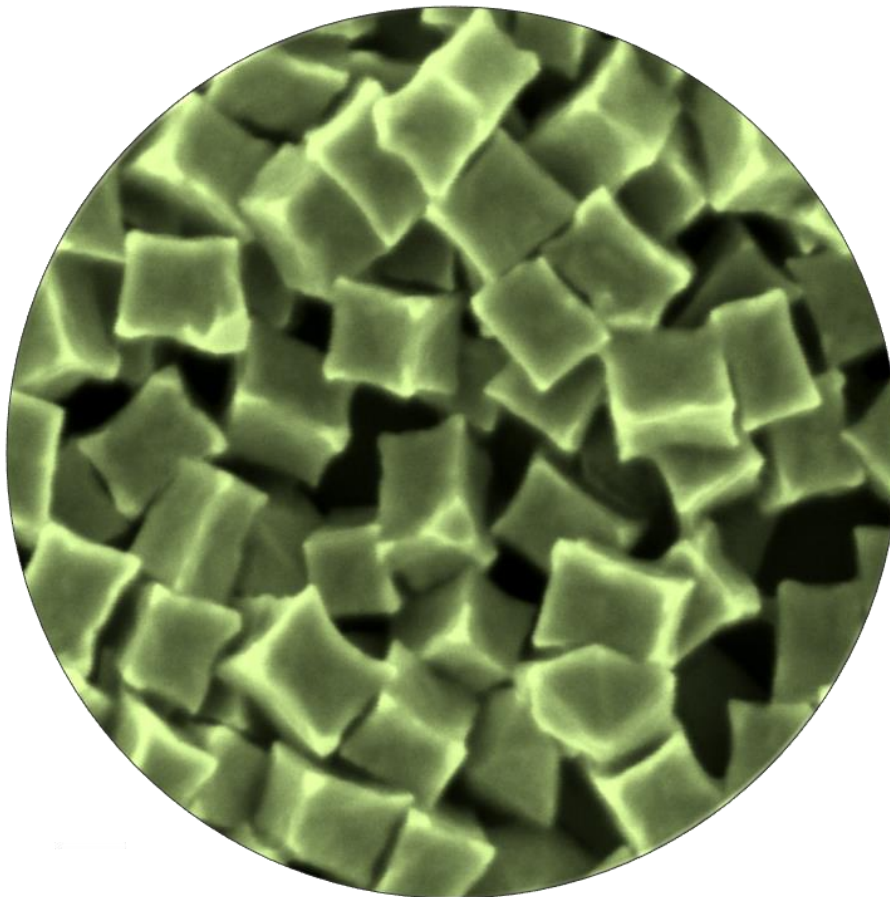
(24) Zhang, Q. F.; Zhou, Y. D.; Villarreal, E.; Lin, Y.; Zou, S. L.; Wang, H. Faceted Gold Nanorods: Nanocuboids, Convex Nanocuboids, and Concave Nanocuboids. *Nano Lett* **2015**, *15*, 4161.

Chapter-2

High-Index Faceted Gold Nanocrystals (Au NCs)

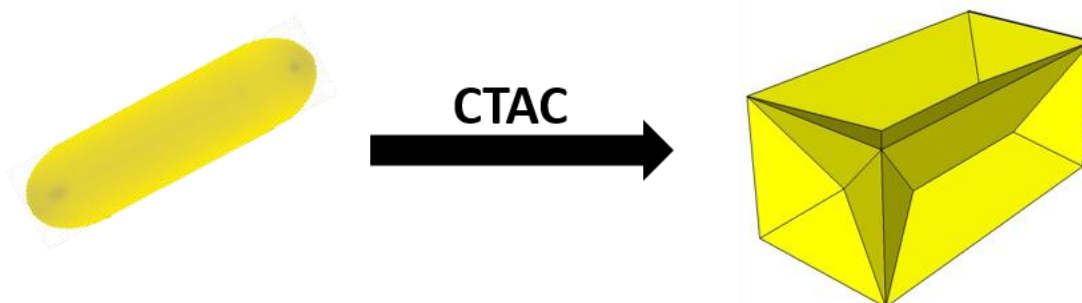
Part-B

Synthesis and Characterization of Concave Cuboid Au NCs



2B.1 Introduction

As shown in the previous section, we have successfully synthesized convex Au NCs (ETHH) with high-dimension tunability by using tannic acid (TA) as a mild reducing agent in the seed-mediated growth method. We have further extended the use of TA for the size controlled synthesis of concave cuboid (CCB) Au NCs i.e. depression on faces (inverse pyramid) of cuboid structure. Very few literatures are available regarding the synthesis of such nanocrystals. However, synthesis of CCB Au NCs with precisely controlled dimension accompanied by high yield has not been observed in the previous literatures.¹⁻⁶ Huang *et al.* pioneered the synthesis of CCB Au NCs with the seed mediated growth technique and investigated distinctive plasmonic property using finite element method.⁶ This was shortly followed by Zhang *et al.*, using the same method they could control the degree of concavity by varying the amount of AgNO_3 and found that these NCs are enclosed with high-index facets.² While former two methods used Au NRs as seed, Peng *et al.* not only used spherical seed but also introduced didodecylammonium bromide (DDAB) as a surfactant to successfully synthesize CCB Au NCs.⁷ Qingfeng *et al.* put forward Cu(II) as a shape directing agent in binary combination of CTAB/CTAC surfactants.³ Surprisingly, all the above mentioned methods used ascorbic acid as a mild reducing agent and a bromide ion containing surfactant (CTAB and DDAB). Mirkin *et al.* extensively investigated the role of Ag ion and counter anion of surfactant and claimed that bromide ions do not favor the formation of concave structure.⁸ In addition to this, ascorbic acid is generally found to be very sensitive with respect to pH and temperature of the growth solution, as also mentioned in the previous chapter. Herein, we have successfully used the tannic acid (TA) as the mild reducing agent to synthesize CCBs by tuning its size over a wide range (70 to 200 nm) with prominent concavity which was missing in the previous reports.



Schematic representation: over growth of Au NR to CCB Au NR in presence of CTAC.

2B.2 Materials and Methods

Tannic acid (TA), gold (III) chloride trihydrate ($\text{HAuCl}_4 \cdot 3\text{H}_2\text{O}$), silver nitrate (AgNO_3), cetyltrimethylammonium bromide (CTAB), cetyltrimethylammonium chloride (CTAC), cetylpyridinium chloride (CPC), and sodium borohydride (NaBH_4) were purchased from Sigma-Aldrich. Sodium hydroxide (analytical reagent) was bought from Rankem. All chemicals were used as such. Milli-Q water ($18.2 \text{ M}\Omega$) was used for all experiments.

A typical synthesis of Au NRs is as follows: rapid addition of NaBH_4 (75 μL , 20 mM) to a mixture of Millipore water H_2O (1 mL), CTAB (1.25 mL, 0.2 M) and HAuCl_4 (0.156 mL, 4 mM) resulted in a brownish color solution, which indicated the formation of seeds. The growth solution was made by sequential addition of an appropriate amount of water (in order to make a total volume of 2 mL), sodium hydroxide (NaOH) (20 μL , 0.1 M), HAuCl_4 (0.25 mL, 4 mM), CTAC (1 mL, 0.2 M) and AgNO_3 (varied, 4 mM). Subsequent introduction of TA (10 μL , 100 mM) turned the color of the solution from pale yellow to almost colourless in 10 min due to Au (III) \rightarrow Au (I) reduction. Finally, to the growth solution, seed solution of 50 μL was added and allowed the Au NRs to grow for 12 hat room temperature. Excess surfactant (CTAB) has been removed by performing centrifugation (9000 rpm, 7 min) twice with Milli-Q water. Subsequently, these Au NRs were used as seed in the growth solution same as above but CTAB is replaced with CTAC. By varying the amount of seed (Au NRs) and AgNO_3 in the growth solution, allowed to control over the dimension and degree of concavity of CCB NCs respectively.

UV-vis spectra were recorded from Chemito SPECTRASCAN UV 2600. FE-SEM and TEM images were captured through ZEISS Ultra Plus and TECHNAI T30 respectively.

2B.3 Results and Discussion

Dimension of CCBNCs has been controlled by varying the amount of seed (Au NRs). When the amount of seed introduced into the growth solution was systematically reduced from 200 μL to 5 μL , it was found that it lead to the formation of CCB NCs with increasing length and width, the latter being more prominent when the amount of seed was reduced below 100 μL . The overall result being the decrease in the aspect ratio of the CCB NCs from 2.2 to 1.5. Thus, just by playing with the amount of seed introduced into the growth solution, the dimension has been

tuned from about 70 nm to 200 nm. This is reflected in the absorption spectra which show a pronounced effect on the two TSPR and a subtle effect on the LSPR. In the earlier report,⁶ the origin of two TSPR peaks in UV-vis spectra has been clearly illustrated (**Figure 2B.1**) i.e the first and the second peaks are assigned as edge (T1) and hybrid (T2; edge + corner) plasmon oscillation modes respectively. It is clearly seen in the UV-vis spectra (**Figure 2B.1**) that T2 mode has significantly red-shifted from 612 to 740 nm on reducing the amount of seed (Au NRs) from 200 μL to 5 μL respectively. All SPR peaks are prominent till the seed (Au NRs) amount is 20 μL . Upon further decreasing the amount from 10 to 5 μL , T2 and LSPR got merged, resulting in one big broad shoulder. T1 on the other hand remained mostly unaffected with a minor red-shift from 530 to 580 nm on decreasing the seed amount.

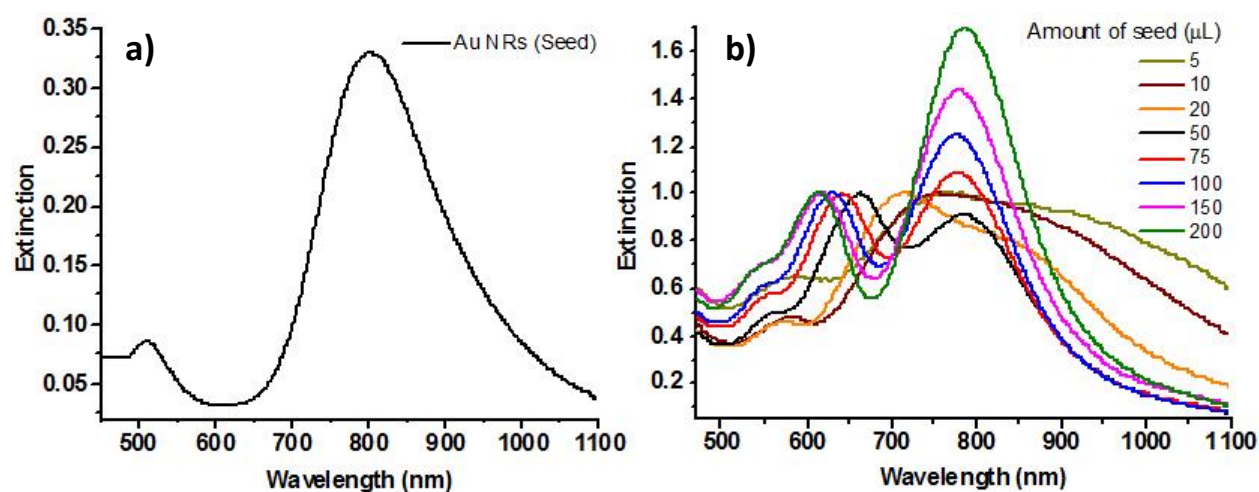


Figure 2B.1: a) UV-vis spectrum of Au NRs used as seed for the synthesis of concave cuboid Au NCs. b) UV-vis spectra of CCB Au NCs synthesized by varying the amount of seed in the growth solution in presence of 0.1 mM AgNO_3 (equivalent to 50 μL for the 2 mL of growth solution).

The corresponding FE-SEM (**Figure 2B.2**) images and dimension analysis revealed that aspect ratio remained almost constant from amount of seed 200 μL to 50 μL while average length and width gradually increased 79 to 107 nm and 35.6 to 52.7 nm respectively, whereas varying the seed between from 20 to 5 μL aspect ratio remained constant at 1.5 but the average length and width increased from 129 to 184 and 78 to 120 nm respectively. Such precise tuning of optical properties were absent in previous literatures. Our success in precise tuning over SPR is attributed to the usage of CTAC as capping and as well as shape directing agent. In an earlier report it has been shown that by varying the amount of AgNO_3 lead to the control over degree of

concavity of CCB Au NCs.² Mirkin et al. extensively studied the effect of AgNO_3 in the formation of concave cubic Au NCs in presence of CTAC and suggested that during the growth of concave cube structure, silver is acting through ‘lock in’ mechanism i.e. Ag strongly bind to the faces of cube and allow the deposition of Au^0 to occur selectively on edges which in turn results in protrusion of edges.

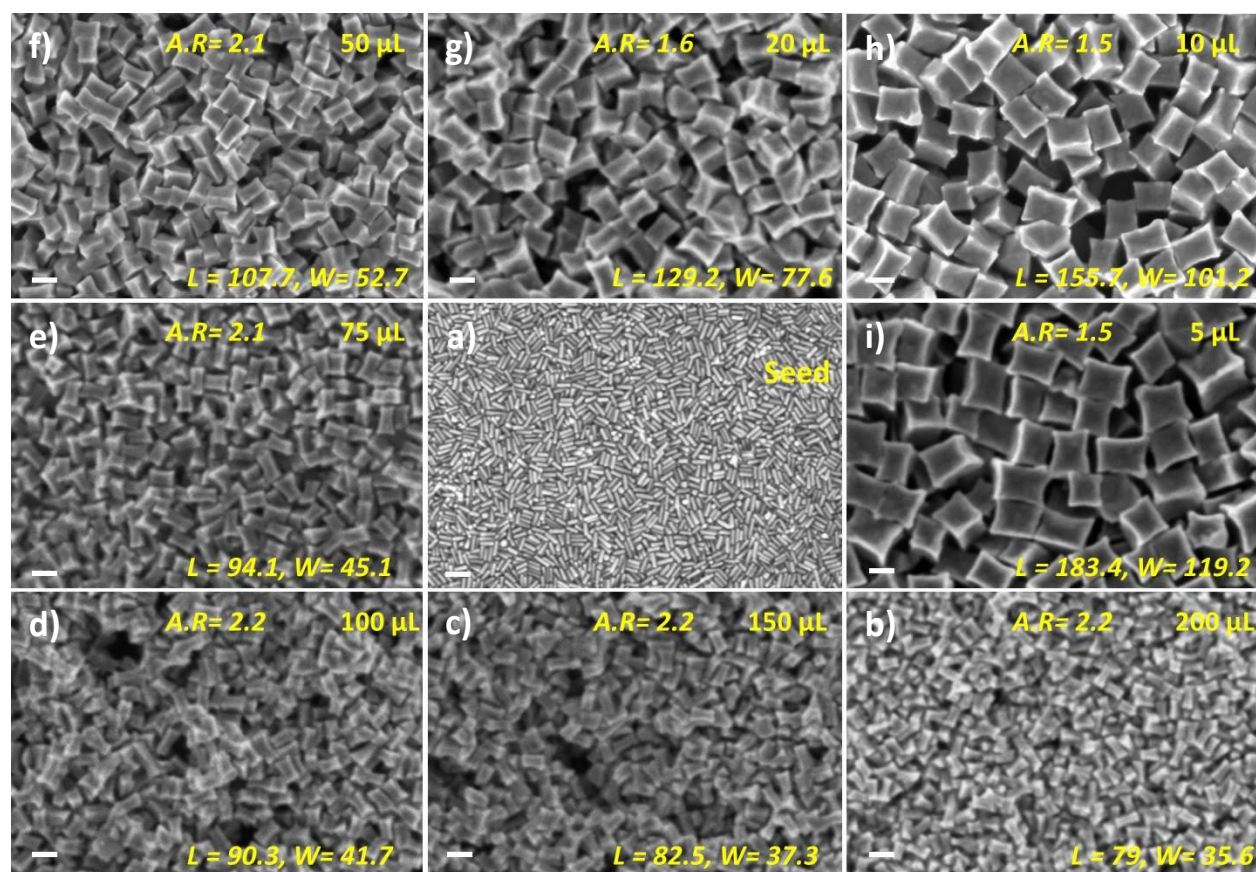


Figure 2B.2: a) FE-SEM image of Au NRs seed. b-i) Concave cuboid Au NCs were synthesized by varying the amount of seed in the growth solution as 200, 150, 100, 75, 50, 20, 10 and 5 μL (labeled on images); Labels L, W and A.R. stands for average length (nm), width (nm) and aspect ratio of CCB NCs in the FE-SEM images. Scale bar is 100 nm for all.

Keeping this in mind, we varied the amount of AgNO_3 from 10 to 100 μL when seed amount was maintained at 20 μL in the over-growth of Au NRs which resulted in the increase of protrusion of edges (**Figure 2B.3b-g**) and this observation is consistent with the earlier report.² In addition to increasing the yield of CCB Au NCs, Ag also plays a vital role in improving the quality CCB Au NCs (**Figure 2B.3b** to c).

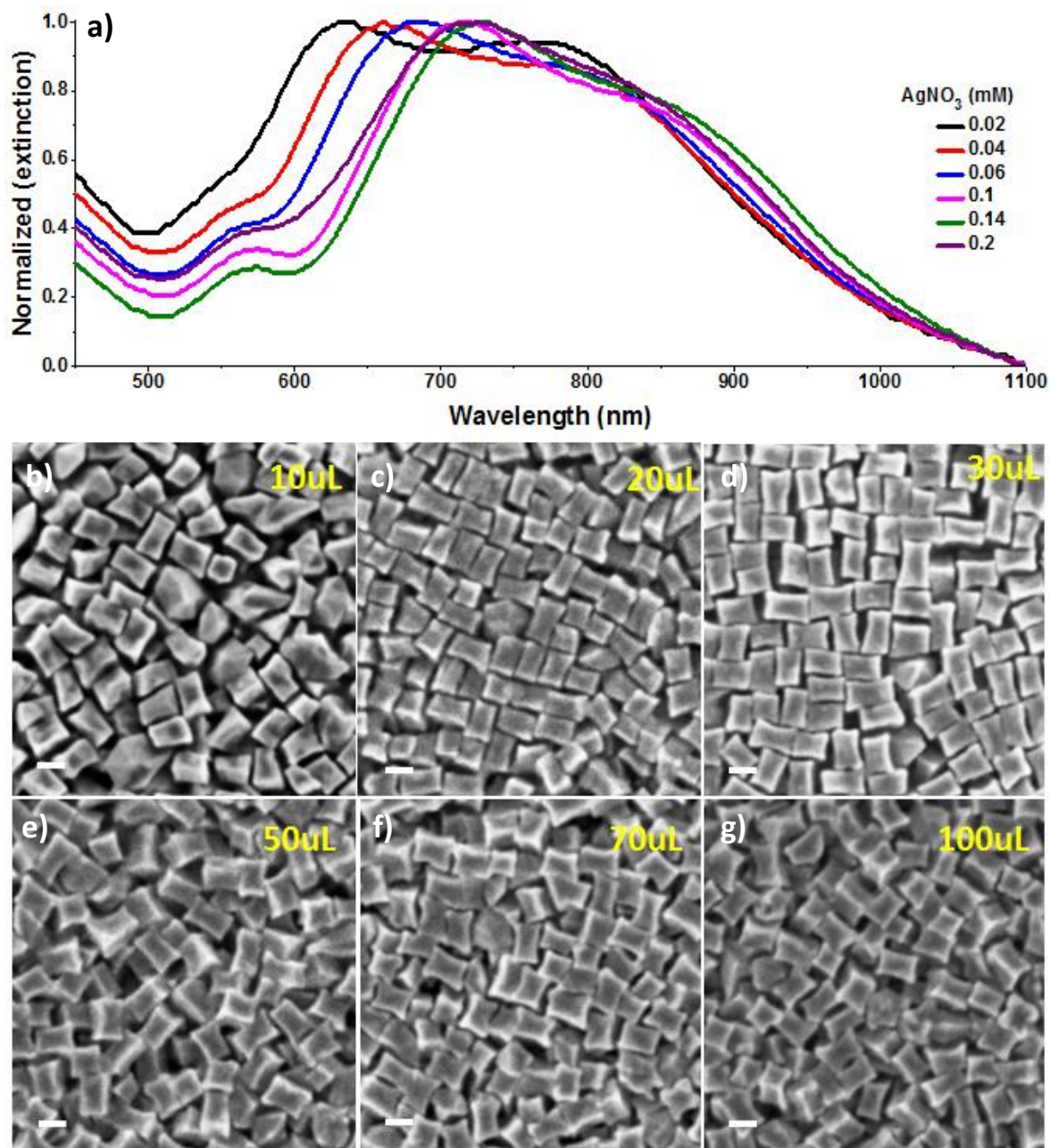


Figure 2B.3: a) UV-vis absorbance recorded for the CCB Au NCs synthesized with varying the concentration (values are equivalent to the amounts of 10, 20, 30, 50, 70 & 100 μL for the 2 mL total volume of the growth solution) of AgNO_3 while keeping the amount of seed (20 μL) constant. b-g) FE-SEM images were captured for the corresponding samples; labeled in yellow colour. Scale bar is 100 nm for all.

These observations are consistent with the UV-vis absorbance spectra where T2 peak red-shifted from 636 to 720 nm on increasing the quantity of AgNO_3 from 10 to 100 μL respectively which

suggest that edges are more protruded with the amount of AgNO_3 . This observation is consistent with the previous report by Zhang et al.²

Further characterization study has been done with TEM instrument. We have chosen CCB Au NCs synthesized with 50 μL of seed (FE-SEM image; **Figure 2B.4a**). TEM images show two regions differing in contrast. The light and dark portions correspond to the protruded edge (thin layer) and middle part (thick) of the CCB Au NCs respectively (**Figure 2B.4b-c**). To determine the facets of CCB Au NCs, HR-TEM image (**Figure 2B.4d**) was captured at the region marked with red box (**Figure 2B.4c**) on CCB Au NCs is projected in [100] direction with respect to the electron beam. This image shows the stepped kind of atomic arrangement at the edge marked with yellow lines drawn on terraces, which therefore determines that these nanocrystals are indeed enclosed with high index facets.

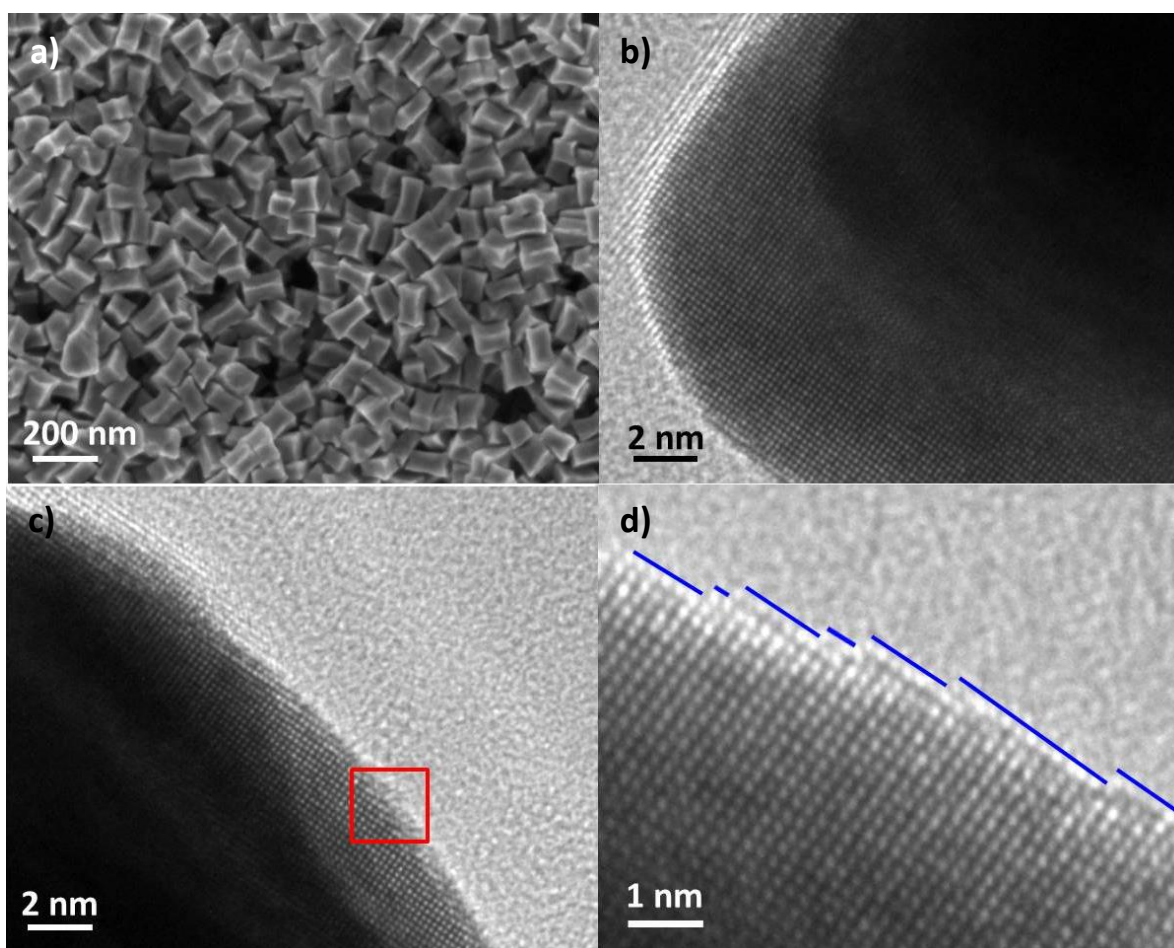


Figure 2B.4: a) FE-SEM image of CCB Au NCs synthesized with 50 μL of seed. b-c) TEM images of CCB Au NCs (a). d) HR-TEM image of the portion marked with red box in (c).

2B.4 Summary and Conclusions

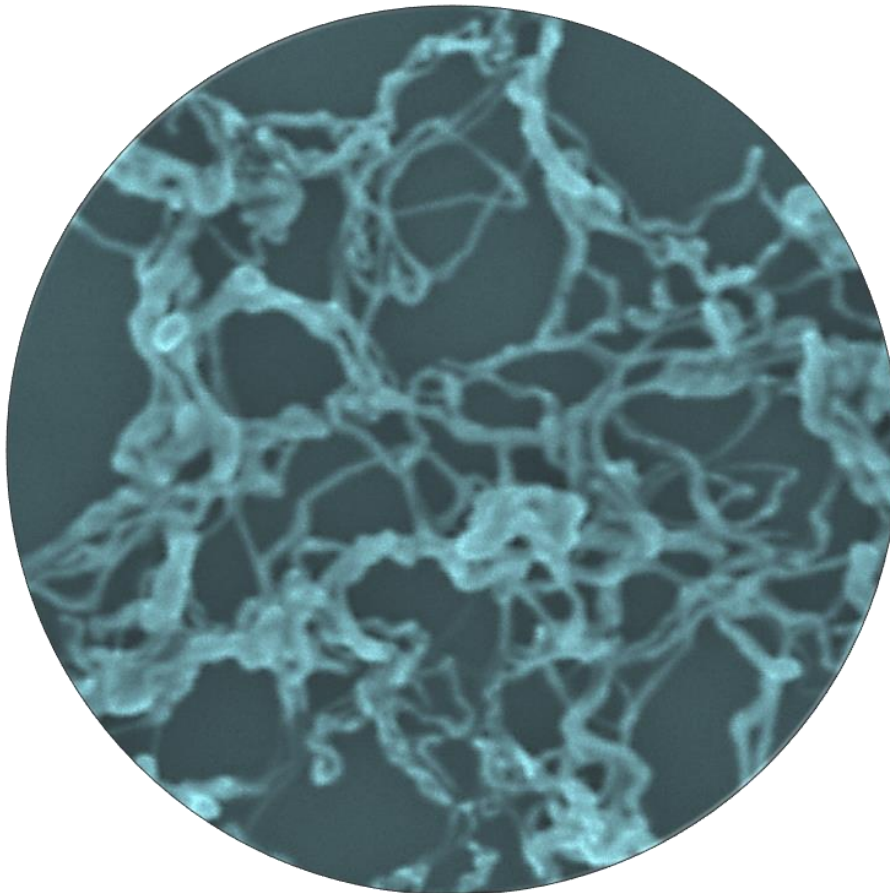
We have successfully synthesized the CCB Au NCs with precise tunability of the dimensions accompanied by optical properties which was absent in previously reported literature. Size and degree of concavity has been tuned by varying the amount of seed and AgNO₃ in the growth solution, respectively. HR-TEM characterization disclosed that as synthesized CCB Au NCs are enclosed with high-index facets. Our investigation reveals that CTAC is playing a decisive role in the fabrication of CCB Au NCs. Such NCs are very promising for SERS and catalytic applications. Tannic acid has proven again to be a good mild reducing agent and warrant the further investigation to access other metal nanostructures.

2B.5 References

- (1) Matteini, P.; de Angelis, M.; Ulivi, L.; Centi, S.; Pini, R. Concave gold nanocube assemblies as nanotraps for surface-enhanced Raman scattering-based detection of proteins. *Nanoscale* **2015**, *7*, 3474.
- (2) Zhang, L. F.; Zhang, C. Y. Controlled growth of concave gold nanobars with high surface-enhanced Raman-scattering and excellent catalytic activities. *Nanoscale* **2013**, *5*, 5794.
- (3) Zhang, Q.; Zhou, Y.; Villarreal, E.; Lin, Y.; Zou, S.; Wang, H. Faceted Gold Nanorods: Nanocuboids, Convex Nanocuboids, and Concave Nanocuboids. *Nano Lett.* **2015**, *15*, 4161.
- (4) Zhang, Q.; Jing, H.; Li, G. G.; Lin, Y.; Blom, D. A.; Wang, H. Intertwining Roles of Silver Ions, Surfactants, and Reducing Agents in Gold Nanorod Overgrowth: Pathway Switch between Silver Underpotential Deposition and Gold–Silver Codeposition. *Chem. Mater.* **2016**, *28*, 2728.
- (5) Romo-Herrera, J. M.; Gonzalez, A. L.; Guerrini, L.; Castiello, F. R.; Alonso-Nunez, G.; Contreras, O. E.; Alvarez-Puebla, R. A. A study of the depth and size of concave cube Au nanoparticles as highly sensitive SERS probes. *Nanoscale* **2016**, *8*, 7326.
- (6) Huang, Y.; Wu, L.; Chen, X.; Bai, P.; Kim, D.-H. Synthesis of Anisotropic Concave Gold Nanocuboids with Distinctive Plasmonic Properties. *Chem. Mater.* **2013**, *25*, 2470.
- (7) Li, L.; Peng, Y.; Yue, Y.; Hu, Y.; Liang, X.; Yin, P.; Guo, L. Synthesis of concave gold nanocuboids with high-index facets and their enhanced catalytic activity. *Chem. Commun.* **2015**, *51*, 11591.
- (8) Zhang, J.; Langille, M. R.; Personick, M. L.; Zhang, K.; Li, S.; Mirkin, C. A. Concave Cubic Gold Nanocrystals with High-Index Facets. *J. Am. Chem. Soc.* **2010**, *132*, 14012.

Chapter-3

Synthesis and Characterization of Gold Nanowires (Au NWs)



3.1 Introduction

In previous chapters it has been shown that tannic acid is very efficient and benign reagent for the synthesis of convex and concave Au NCs. In this chapter, we have extended its potency for the fabrication of gold nanowires (NWs). Since, 1D nanostructure, such as Au NWs have been receiving considerable attention from researchers due to their enthralling properties such as high electron and photon transfer ability rendering them to be used in transparent electrodes, optoelectronic devices, energy storage devices, fuel cells and catalysis.¹⁻⁶ To date, momentous progress has been realized on the subject of Au NWs synthesis and their execution in various aforementioned applications. Synthetic methodologies developed so far are based on either hard or soft templates.^{7,8} In hard template mediated growth process, solid porous materials are used whereas soft template method uses micelles, made from self-assembly of long-chain aliphatic molecules such as oleylamine, oleic acid, CTAB etc.⁹⁻¹² Despite the widespread use of soft template method, using toxic, expensive, scarcely available chemicals, involvement of multiple steps or the long synthetic procedure still remain major concerns.¹³⁻²¹ So, there is always a look out for new synthetic methodologies which can mitigate the above problems. Here we have devised a method which overcame the above mentioned obstacles: our procedure comprises of readily available less toxic chemical and completion of growth takes only few minutes.

3.2 Materials and Methods

Gold (III) chloride trihydrate ($\text{HAuCl}_4 \cdot 3\text{H}_2\text{O}$), silver nitrate (AgNO_3), sodium hydroxide (NaOH), benzylhexadecyldimethylammonium chloride (BDAC), cetyltrimethylammonium chloride (CTAC), cetylpyridinium chloride (CPC) and tannic acid (TA) were purchased from Sigma-Aldrich and used as such. All experiments were performed with Milli-Q water of 18.2 M Ω .

Synthesis of Au NWs is as follows: first aqueous solution of BDAC (0.1 M), HAuCl_4 (0.5 mM), AgNO_3 (0.1 mM) and NaOH (3 mM) was made in a glass vial of 15 mL. After addition of TA (0.5 mM) to this solution, the colour changed from pale yellow to light brownish. Subsequently, heating at 75^o C for 5 min turned the solution colour to dark brown, indicating the formation of Au NWs.

UV-vis spectra were recorded from Chemito SPECTRASCAN UV 2600. FE-SEM and TEM images were captured through ZEISS Ultra Plus and TECHNAI T30 respectively.

3.3 Results and Discussions

As shown in the previous chapter Au NRs exhibit two SPR bands in UV-vis spectrum corresponding to transverse (lower wavelength) and longitudinal (higher wavelength) surface plasmon resonance where the LSPR gets red-shifted significantly as the aspect ratio of Au NRs is increased. Au NWs although analogous to high aspect ratio Au NRs, they do not possess two distinctive SPR bands. The absorbance of LSPR band is spread over the range of 700 to 2000 nm and the TSPR is inconspicuous of its presence at 510 nm (**Figure 3.1a**) indicating the absence of spherical Au NPs impurities which is well correlated with FE-SEM image (**Figure 3.1b**).

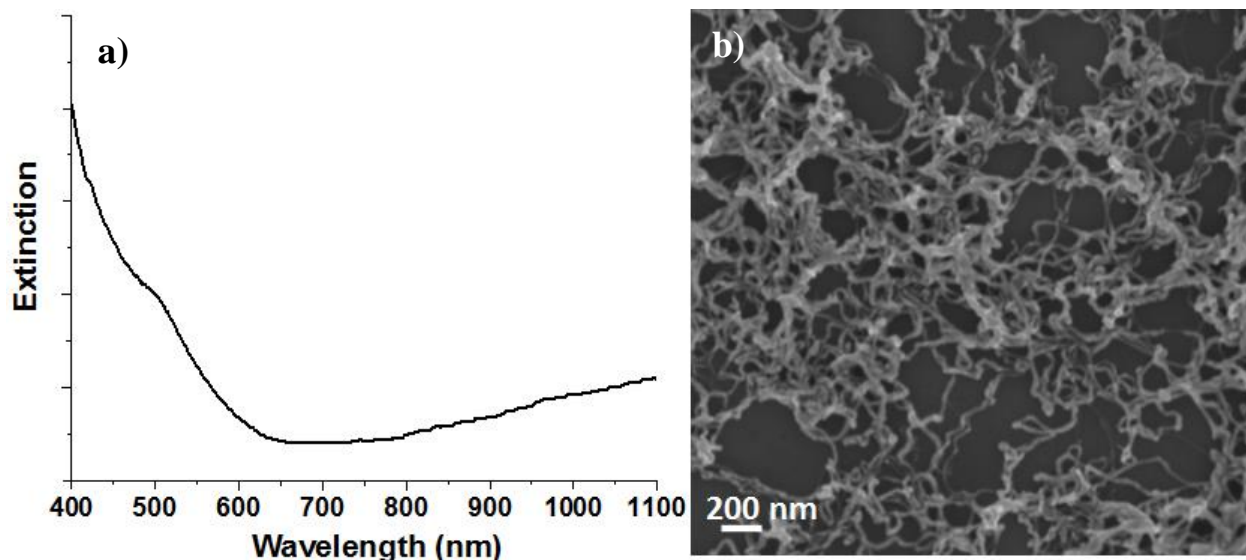


Figure 3.1: a) UV-vis absorbance spectrum recorded for as synthesized Au NWs. b) FE-SEM image of Au NWs.

Such high yield synthesis of Au NWs motivated us to investigate the role of each chemical species present in the growth solution which allowed us to understand the significance of each parameter. To know the importance of head group of BDAC surfactant, we have performed experiments with CTAC and CPC (both contain hexadecyl chain and chloride as counter anion; **Figure 3.2**) at different amount of NaOH in the growth solution. UV-vis spectral measurement revealed that irrespective of amount of NaOH used, CTAC and CPC resulted in almost spherical

Au NPs i.e. only one SPR band observed at ~ 520 nm whereas the band at higher wavelength completely disappeared (**Figure 3.2b and c**). In addition, BDAC also did not give rise to Au NWs unless the concentration of NaOH is 3 mM and/or above (**Figure 3.2d**). Therefore, from these observations it can be concluded that presence of phenyl group in BDAC and higher pH (Concentration of NaOH above 3 mM) of the growth solution is indispensable for the high yield synthesis of Au NWs.

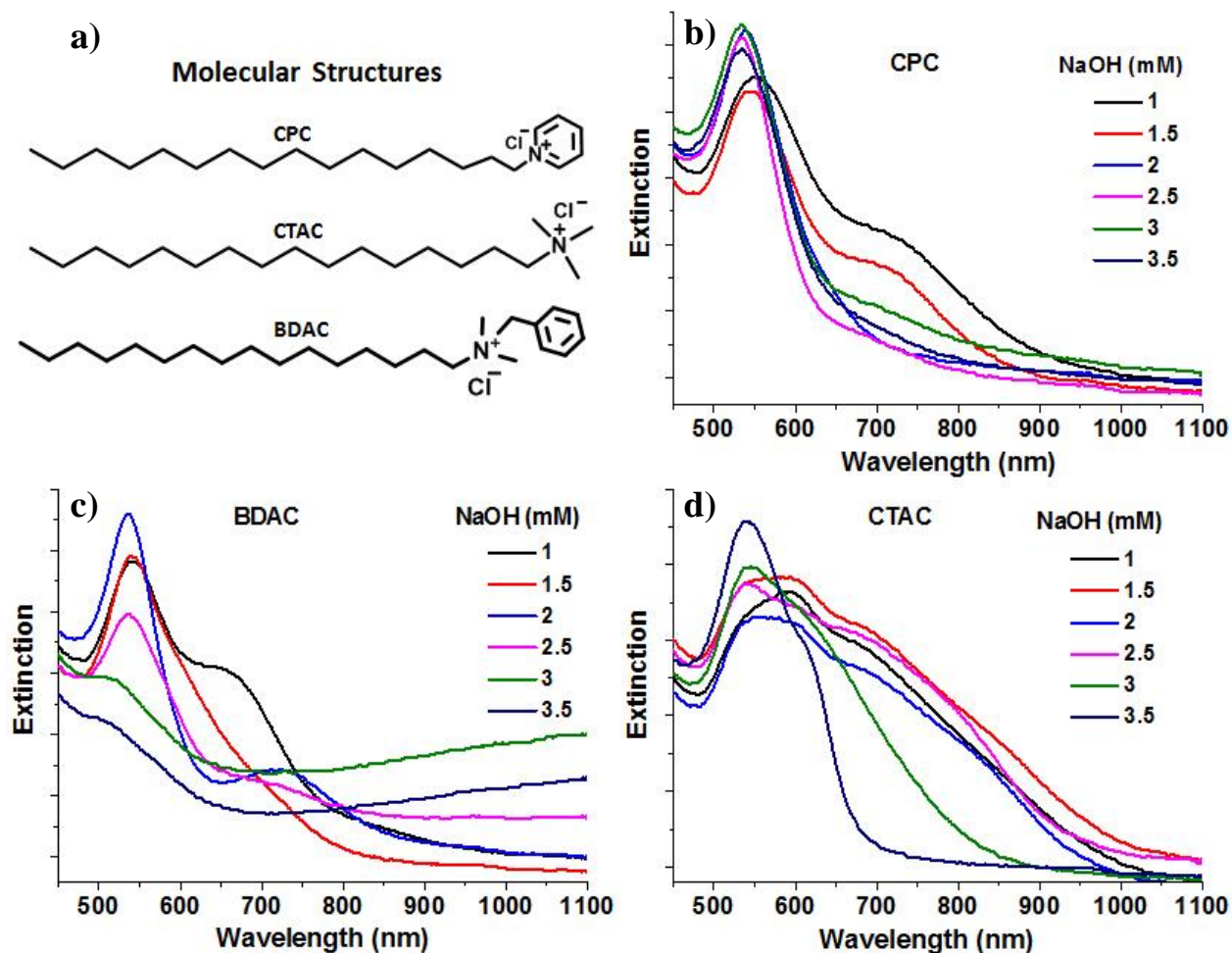


Figure 3.2: a) Molecular structures of surfactants used for the Au NWs synthesis. b-d) UV-vis spectra were recorded for the gold nanostructures synthesized with varying the amount of NaOH in presence of b) CPC, c) CTAC and d) BDAC surfactants in the growth solution.

To understand further about the role of BDAC during the growth of Au NWs, its concentration was varied from 0.02 M to 0.1 M (with the interval of 0.02) while keeping all other parameters

constant. UV-vis spectra and FE-SEM data revealed that increasing the concentration from 0.02, 0.04 to 0.1 M resulted in spherical, fragmented wires and complete nanowires structures respectively (**Figure 3.3**). It can be clearly seen from UV-vis spectra that minimum concentration of 0.06 M is required for the fabrication of well-defined Au NWs.

To understand the role of BDAC to an even greater extent, it is necessary to capture the nanostructures at their embryonic stage (after few seconds of growth initiation). But the stumbling block lies in the difficulty in separation of such small structures by centrifugation since the time taken in such a technique is sufficient for the full growth of a nanowire.

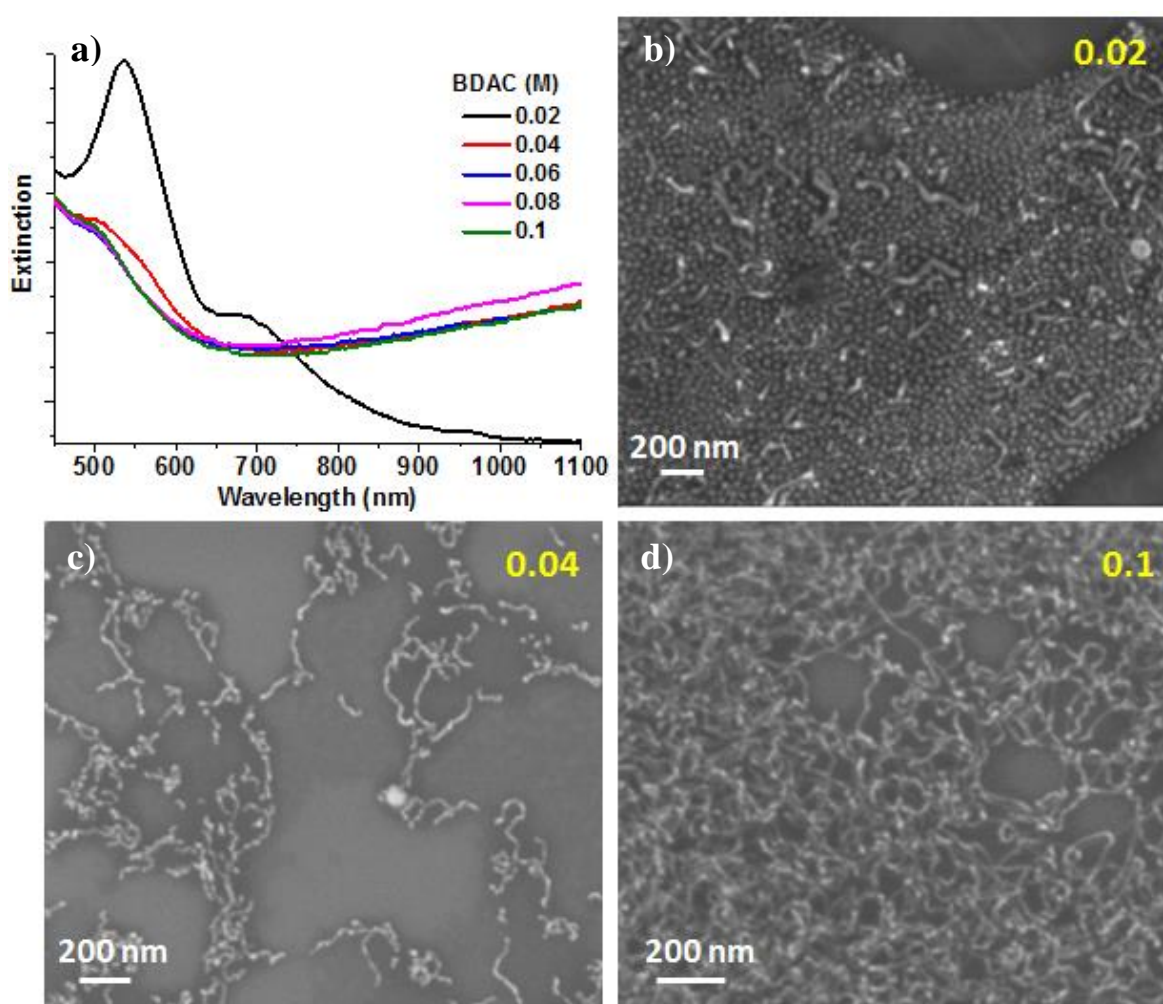


Figure 3.3: a) UV-vis spectra recorded for Au NWs synthesized at different concentrations of BDAC. FE-SEM images of samples prepared with b) 0.02, c) 0.04 and d) 0.1 M (labeled in yellow color) concentrations of BDAC.

An alternative way seemed to be varying the amount of HAuCl_4 to pinpoint the initial stages of Au NWs growth. UV-vis spectra (**Figure 3.4a**) showed that at 0.04 mM concentration of HAuCl_4 features does not match with that of typical Au NWs which can be correlated with FE-SEM image (**Figure 3.4b**) i.e. small wires with one spherical end. When the concentration is 0.2 mM, smaller Au NWs with no spherical end were observed. TSPR of Au NWs got red-shifted (sky blue arrow; **Figure 3.4a**) on increasing the concentration of HAuCl_4 which suggested the increment in width of wires.

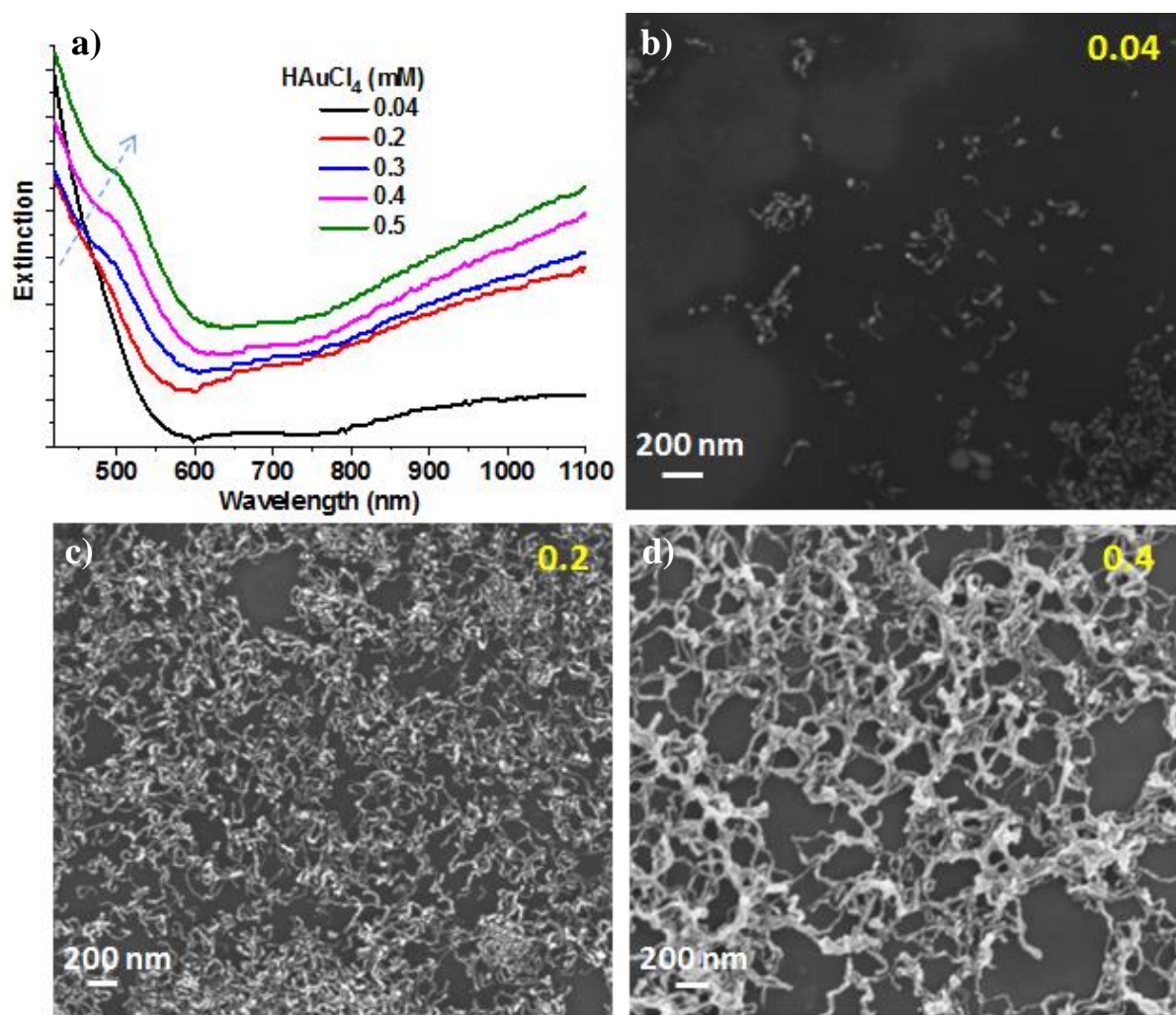


Figure 3.4: a) UV-vis spectra recorded for the Au NWs synthesized with varying the concentration of HAuCl_4 . FE-SEM images captured for the samples prepared with b) 0.04, c) 0.2 and d) 0.4 mM of HAuCl_4 .

As it is well known that on increasing the amount of AgNO_3 in the growth solution will lead to the formation of Au NRs with increased aspect ratio. Here, we varied the amount of AgNO_3 to know its significance in Au NWs synthesis. It is observed that at the concentration of 0.05 mM lead to the formation of spherical Au NPs under standard experimental conditions. This implies that AgNO_3 is playing a vital role in directing the one dimensional growth. And it was also observed that growth rate of Au NWs is getting increased with the amount of AgNO_3 .

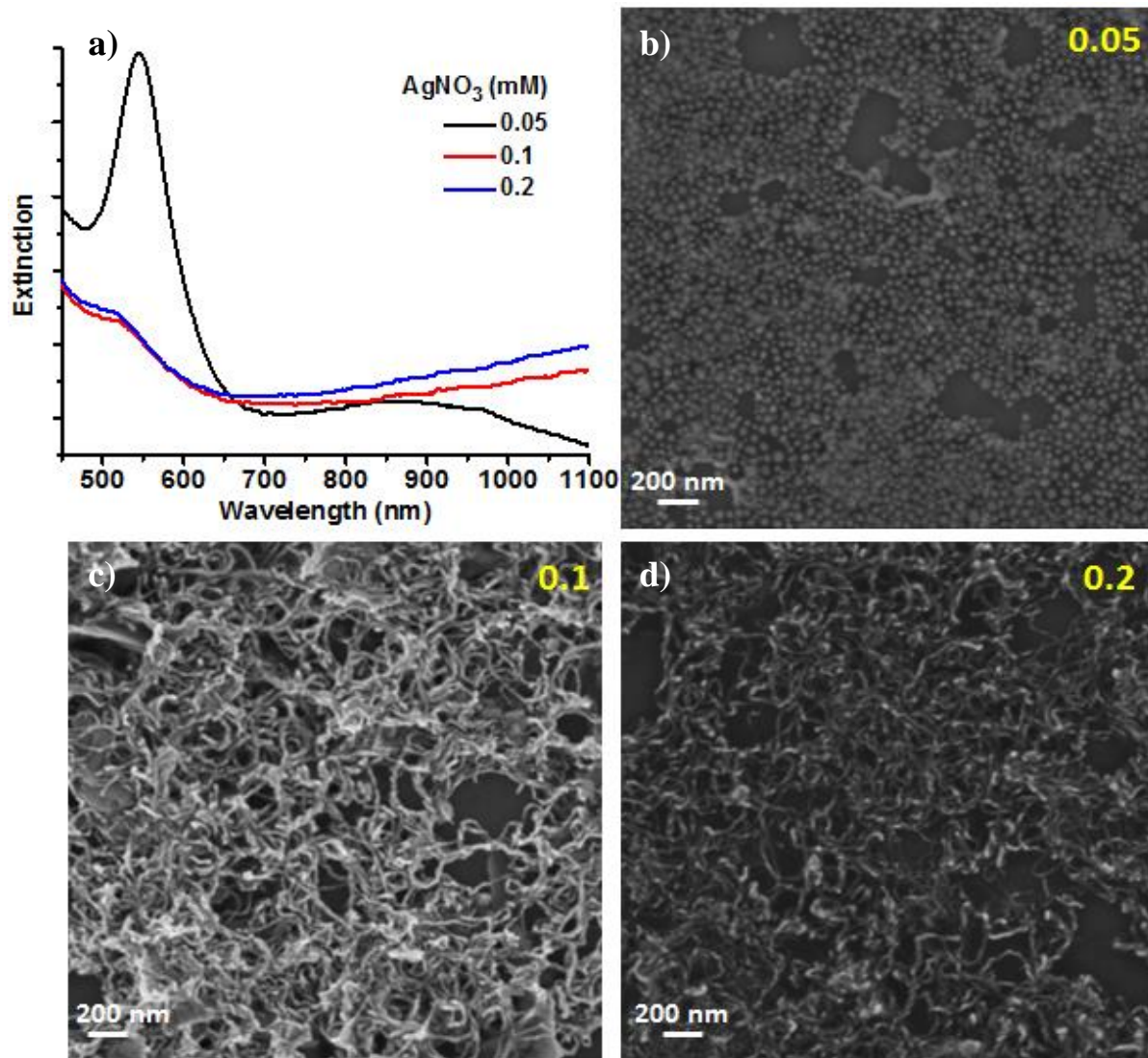


Figure 3.5: a) UV-vis recorded for the Au NWs synthesized with different amount of AgNO_3 . FE-SEM images corresponding to the samples fabricated with b) 0.05, c) 0.1 and d) 0.2 mM of AgNO_3 .

TEM image below (**Figure 3.6a**) shows that as synthesized Au NWs do not possess uniform width along the length. SAED measurement revealed that these Au NWs are poly-crystalline in nature.

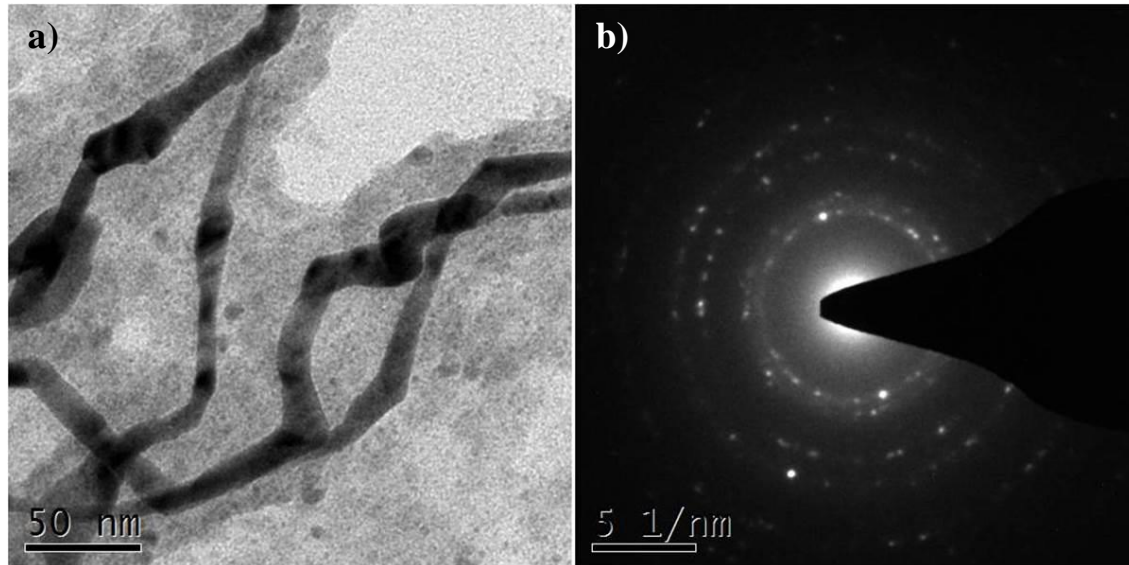


Figure 3.6: a) TEM image of Au NWs. b) SAED pattern recorded on image.

3.4 Summary and Conclusion

We have devised a single step and robust method which takes hardly 5 min for the synthesis of Au NWs by using tannic acid as mild reducing agent. Control experiments with other surfactants like CTAC and CPC did not lead to Au NWs structures formation. Therefore, the usage of BDAC with sufficient concentration in the reaction mixture is a decisive factor for the formation of Au NWs. We have also demonstrated that length of the nanowire segment can be tuned by varying the amount of HAuCl_4 . As per our knowledge, it is the fastest method developed for the synthesis of Au NWs, compared with the existing literature. However, detailed characterization of the Au NWs regarding its crystallinity requires extensive examination using spectroscopic and microscopic techniques such as PXRD and HR-TEM. Our results not only enthuse the use of tannic acid such a benign reagent, but also promote the utilization of other structurally similar molecules (to tannic acid) in the synthesis of various metal nanostructures.

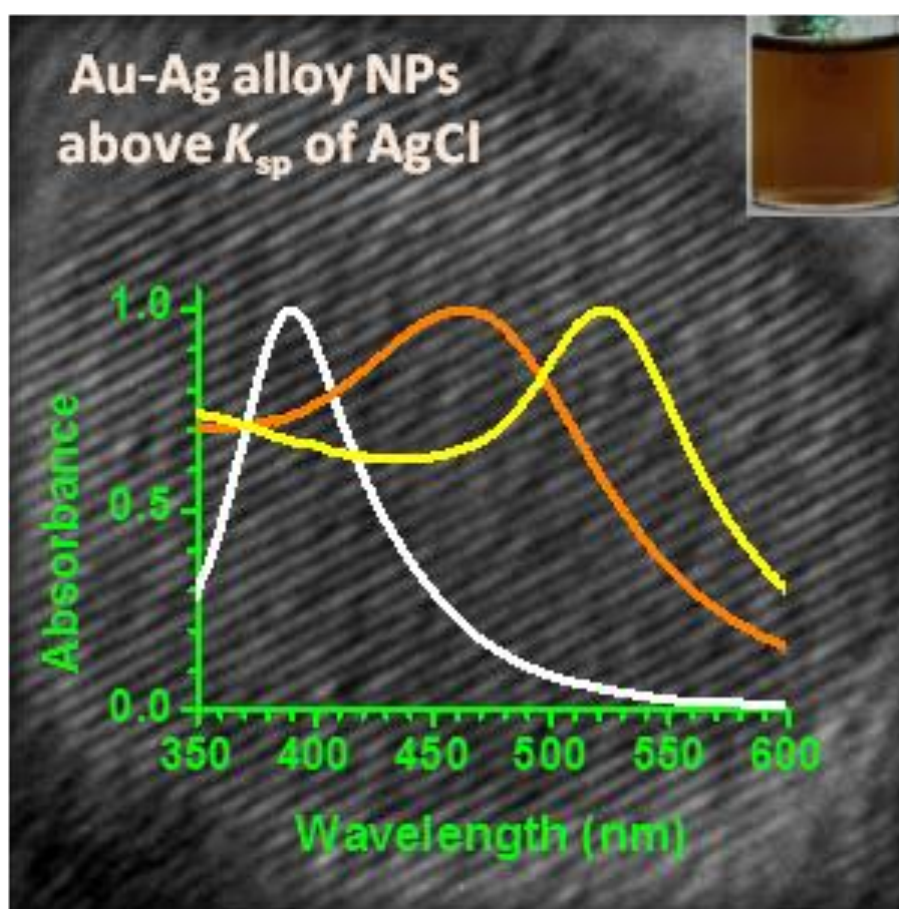
3.5 References

- (1) Chang, F.; Shan, S.; Petkov, V.; Skeete, Z.; Lu, A.; Ravid, J.; Wu, J.; Luo, J.; Yu, G.; Ren, Y.; Zhong, C.-J. Composition Tunability and (111)-Dominant Facets of Ultrathin Platinum–Gold Alloy Nanowires toward Enhanced Electrocatalysis. *J. Am. Chem. Soc.* **2016**, *138*, 12166.
- (2) Gong, S.; Zhao, Y.; Yap, L. W.; Shi, Q.; Wang, Y.; Bay, J. A. P. B.; Lai, D. T. H.; Uddin, H.; Cheng, W. Fabrication of Highly Transparent and Flexible NanoMesh Electrode via Self-assembly of Ultrathin Gold Nanowires. *Adv. Electr. Mater.* **2016**, *2*, 1600121.
- (3) Khan, A.; Lee, S.; Jang, T.; Xiong, Z.; Zhang, C.; Tang, J.; Guo, L. J.; Li, W.-D. High-Performance Flexible Transparent Electrode with an Embedded Metal Mesh Fabricated by Cost-Effective Solution Process. *Small* **2016**, *12*, 3021.
- (4) Gong, S.; Zhao, Y.; Shi, Q.; Wang, Y.; Yap, L. W.; Cheng, W. Self-assembled Ultrathin Gold Nanowires as Highly Transparent, Conductive and Stretchable Supercapacitor. *Electroanalysis* **2016**, *28*, 1298.
- (5) Guo, T.; Yu, G.; Zhang, Y.; Xiang, H.; Chang, F.; Zhong, C.-J. Synthesis of Ultralong, Monodispersed, and Surfactant-Free Gold Nanowire Catalysts: Growth Mechanism and Electrocatalytic Properties for Methanol Oxidation Reaction. *J. Phys. Chem. C* **2017**, *121*, 3108.
- (6) Wang, C.; Sun, S. Facile synthesis of ultrathin and single-crystalline Au nanowires. *Chem. Asian. J.* **2009**, *4*, 1028.
- (7) Wirtz, M.; Martin, C. R. Template-Fabricated Gold Nanowires and Nanotubes. *Adv. Mater.* **2003**, *15*, 455.
- (8) Yu, S.; Li, N.; Wharton, J.; Martin, C. R. Nano Wheat Fields Prepared by Plasma-Etching Gold Nanowire-Containing Membranes. *Nano Letters* **2003**, *3*, 815.
- (9) Halder, A.; Ravishankar, N. Ultrafine Single-Crystalline Gold Nanowire Arrays by Oriented Attachment. *Adv. Mater.* **2007**, *19*, 1854.
- (10) Kim, F.; Sohn, K.; Wu, J.; Huang, J. Chemical Synthesis of Gold Nanowires in Acidic Solutions. *J. Am. Chem. Soc.* **2008**, *130*, 14442.
- (11) Takahata, R.; Yamazoe, S.; Koyasu, K.; Tsukuda, T. Surface Plasmon Resonance in Gold Ultrathin Nanorods and Nanowires. *J. Am. Chem. Soc.* **2014**, *136*, 8489.
- (12) Zhou, M.; Lin, M.; Wang, Y.; Guo, X.; Guo, X.; Peng, L.; Ding, W. Organic-free synthesis of ultrathin gold nanowires as effective SERS substrates. *Chem. Commun.* **2015**, *51*, 11841.

- (13) Bai, H.; Xu, K.; Xu, Y.; Matsui, H. Fabrication of Au nanowires of uniform length and diameter using a monodisperse and rigid biomolecular template: collagen-like triple helix. *Angew. Chem., Int. Ed.* **2007**, *46*, 3319.
- (14) Huo, Z.; Tsung, C.-k.; Huang, W.; Zhang, X.; Yang, P. Sub-Two Nanometer Single Crystal Au Nanowires. *Nano Lett.* **2008**, *8*, 2041.
- (15) Feng, H.; Yang, Y.; You, Y.; Li, G.; Guo, J.; Yu, T.; Shen, Z.; Wu, T.; Xing, B. Simple and rapid synthesis of ultrathin gold nanowires, their self-assembly and application in surface-enhanced Raman scattering. *Chem. Commun.* **2009**, 1984.
- (16) Liu, R.; Liu, J.-f.; Jiang, G.-b. Use of Triton X-114 as a weak capping agent for one-pot aqueous phase synthesis of ultrathin noble metal nanowires and a primary study of their electrocatalytic activity. *Chem. Commun.* **2010**, *46*, 7010.
- (17) Ju, J.-J.; Lu, C.-X.; Jan, J.-S. Synthesis of Gold Nanowire Networks and Nanoparticles by Tyrosine Reduction of Chloroaurate. *J. Nanosci. Nanotechnol.* **2012**, *12*, 2802.
- (18) Li, C. C.; Chen, L. B.; Li, Q. H.; Wang, T. H. Seed-free, aqueous synthesis of gold nanowires. *CrystEngComm* **2012**, *14*, 7549.
- (19) Liu, H.; Cao, X.; Yang, J.; Gong, X.-Q.; Shi, X. Dendrimer-mediated hydrothermal synthesis of ultrathin gold nanowires. *Sci. Rep.* **2013**, *3*, 3181.
- (20) Wang, Y.-N.; Wei, W.-T.; Yang, C.-W.; Huang, M. H. Seed-Mediated Growth of Ultralong Gold Nanorods and Nanowires with a Wide Range of Length Tunability. *Langmuir* **2013**, *29*, 10491.
- (21) Qian, Z.; Park, S.-J. Silver Seeds and Aromatic Surfactants Facilitate the Growth of Anisotropic Metal Nanoparticles: Gold Triangular Nanoprisms and Ultrathin Nanowires. *Chem. Mater.* **2014**, *26*, 6172.

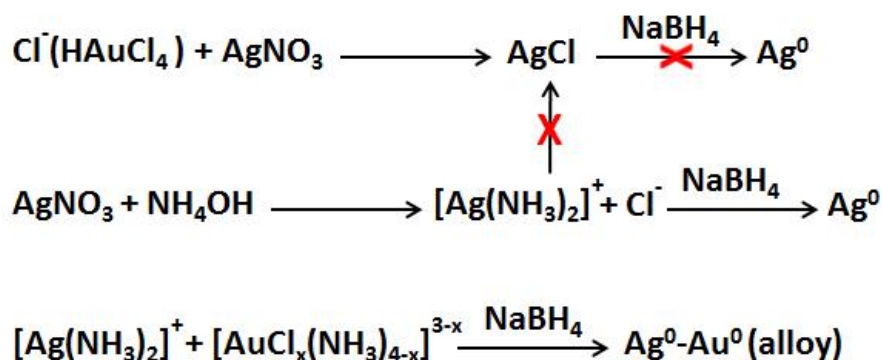
Chapter-4

Synthesis, Characterization and Applications of Au-Ag Alloy NPs



4.1 Introduction

Among various bimetallic alloy NPs, it is the Au–Ag combination which attracted extensive research in the recent past due to the composition-tunable physical, chemical and biological properties, and an easy synthetic methodology. On the one hand, Au–Ag alloy NPs retain superior plasmonic property due to the Ag component; and on the other hand, inert nature of the counterpart Au provides improved chemical stability.¹ Owing to the simplicity, co-reduction of commonly available stable salts like HAuCl_4 and AgNO_3 seems dominating ($E^0_{\text{Au(III)/Au(0)}} = 1.0 \text{ V}$ and $E^0_{\text{Ag(I)/Ag(0)}} = 0.8 \text{ V}$) the wet-chemical routes in synthesizing Au–Ag alloy NPs.^{2,3} However, the unavoidable problem of such a co-reduction reaction is the co-precipitation of AgCl (**Scheme 4.1**) in the course of formation of alloy NPs due to very poor solubility in water ($K_{\text{sp}} = 1.7 \times 10^{-10}$ at 25°C) which can adversely alter the composition of the alloy NPs from the initial feed vis-a-vis properties. The use of a strong reducing agent like NaBH_4 did not help in addressing this pertinent problem which is why the solution-phase synthesis of citrate stabilized Au–Ag alloy NPs warrant that the molar concentration of Ag be always kept below solubility product of AgCl .³



Scheme 4.1: Represents how NH_4OH can protect the Ag^+ from the formation of AgCl and thereby facilitate the reduction of Ag^+ and Au^{+3} simultaneously for the alloy NPs formation.

To overcome such an important problem of the co-reduction, two-phase reduction, complex functioning of proteins (bio-reduction) or polymers and special techniques like digestive ripening, sputter deposition on ionic liquids, capillary micro-reaction, or photosynthesis were found to be reliable alternatives.⁴⁻¹⁴ Another alarming concern of the Au–Ag alloy NPs is the phase-segregation of Ag on the outermost surface of the particle which has been previously concluded by various experiments as well as theoretical investigations.¹⁵⁻¹⁹ Thus, despite numbers of reported work in the synthesis and applications of Au–Ag alloy NPs, a

fundamental question remained overlooked -- “heterogeneous-alloy” or “homogeneous-alloy”? Here, we have taken an attempt to address the concept as well as importance of “homogeneous-alloying” of Au and Ag in sub-10-nm NPs by adopting a novel wet-chemistry approach and combining various complementary measurements on the NPs. Specifically, an additional use of NH_4OH solution in the co-reduction of HAuCl_4 and AgNO_3 (**Scheme 4.1**) in the presence of trisodium citrate (Na_3Ct) in aqueous medium enabled us to synthesize highly crystalline, SERS-active and biocompatible Au–Ag alloy NPs at ambient temperature with precisely tunable SPR, controllable catalytic-activity and high-chemical stability – just as per the feeding moles and well-above the solubility product of AgCl .

4.2 Materials/Methods

Gold (III) chloride trihydrate ($\text{HAuCl}_4 \cdot 3\text{H}_2\text{O}$), silver nitrate (AgNO_3), hydrogen peroxide (H_2O_2)(30%), ammonium hydroxide (NH_4OH) (29%), NaBH_4 , trisodium citrate (Na_3Ct), p-terphenyl-4, 4''-dithiol (TPDT), dodecanethiol (DDT), H_3PO_4 , p-nitrophenol and 3-(4, 5-dimethylthiazol-2-yl)-2,5-diphenyltetrazolium bromide (MTT) were purchased from Sigma-Aldrich. Dulbecco’s modified Eagle’s medium (DMEM), fetal bovine serum (FBS), phosphate buffered saline (PBS) and penicillin – streptomycin solution were purchased from Life Technologies (USA).

The synthesis of Au–Ag alloy NPs with compositions of 0:1, 1:3, 1:1, 3:1 and 1:0 (Au:Ag) is as follows. Five 25 mL round-bottom flasks were washed with aqua-regia and deionized water; filled with 0.625, 0.468, 0.3125, 0.156, and 0mL of AgNO_3 (4 mM) solutions; and treated with 40, 30, 20, 10, and 0 μL of NH_4OH (1 M), respectively. Each solution was diluted with appropriate amount of H_2O to make the total volume 10 mL. For each solution 100 μL of Na_3Ct (25 mM) was added followed by 0, 0.156, 0.3125, 0.468, and 0.625 mL of HAuCl_4 (4 mM) (same order as mentioned earlier) solution with vigorous stirring at room temperature. These colourless solutions turned colorful in 5s upon addition of 0.125 mL of NaBH_4 (0.02 mM), which indicates the formation of NPs. The total concentration of salts in each reaction mixture was kept for 0.25 mM.

UV–visible spectra of the solutions were recorded using a PerkinElmer Lambda-35 UV –visible spectrometer. TEM and FESEM images were recorded in TECHNAI T30 and ZEISS Ultra Plus microscopes, respectively. The room temperature and high-temperatures PXRD patterns were recorded using a Bruker D8 Advance diffractometer using $\text{Cu K}\alpha$ radiation

($\lambda=1.5406 \text{ \AA}$). SERS spectra were recorded on a high-resolution confocal Raman microscopy (Lab Ram HR, Horbia Jobin Yvon, France) using 633 nm laser.

4.3 Results and discussion

We demonstrate the problem of AgCl precipitation where subsequent use of NaBH_4 for the reduction of $\text{Ag}^+ \rightarrow \text{Ag}^0$ is apparently redundant so as to severely affecting the alloying of Au and Ag. Without NH_4OH , colour of the solutions of 3:1 and 1:1 feeding moles of Au:Ag do not exhibit the expected colour and in fact these solutions look like pure Au NPs solution (Figure 4.1a). As for the 1:3 feeding moles of Au:Ag, the solution shows intermediate colour and suggests formation of 1:1 Au–Ag alloy NPs.

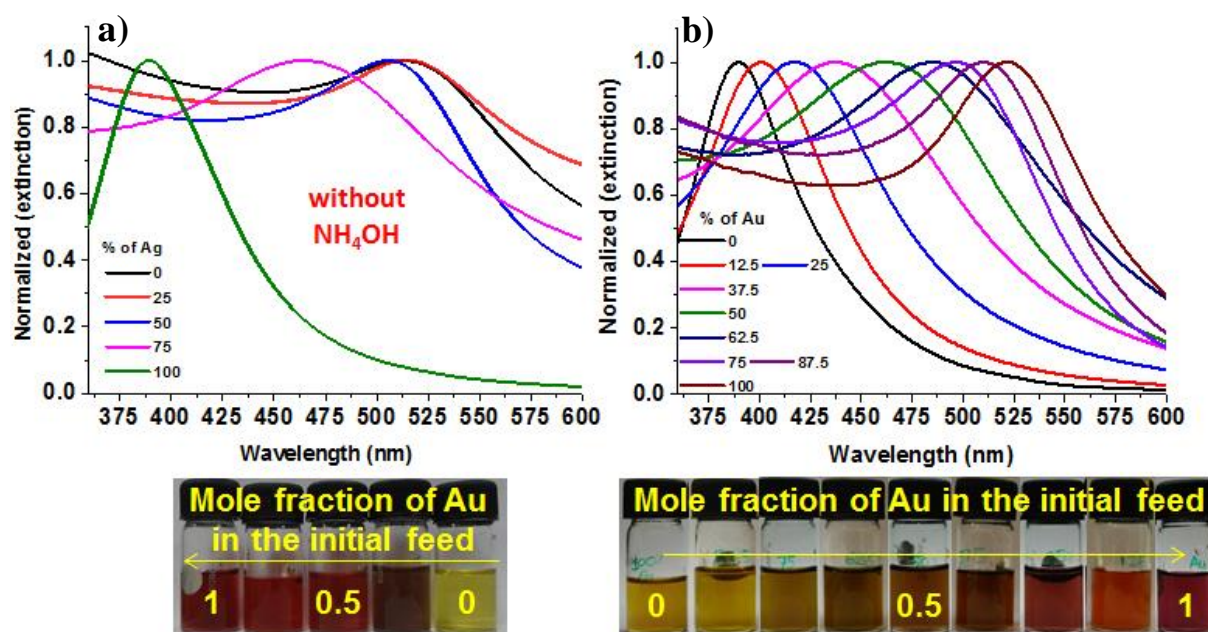


Figure 4.1: a) UV–vis absorption spectra (normalized) for the Au–Ag alloy NPs synthesized without using NH_4OH and respective optical images of the solutions. b) Normalized UV–vis spectra for the Au–Ag alloy NPs synthesized with NH_4OH by varying Au mole fraction. For a direct comparison cum visualization, optical photographs of the Au–Ag alloy NPs solutions are presented.

The respective UV–vis spectra (Figure 4.1a) reflect that alloying of Au and Ag in the NPs is certainly not as per the feeding moles of HAuCl_4 and AgNO_3 . However, it can be easily worked out by pre-addition of NH_4OH solution which effectively dissolved the AgCl precipitate in the form of soluble $[\text{Ag}(\text{NH}_3)_2]^+$ complex (i.e., basically Tollen’s reagent), followed by the addition of NaBH_4 . In the case of coreduction in the presence of NH_4OH ,

there is a gradual change, not only in the colour of the solutions but also in the absorption maxima (λ_{\max}) which strongly suggest the formation of Au–Ag alloy NPs as per the feeding moles of HAuCl_4 and AgNO_3 (**Figure 4.1b**). Instead of NH_4OH , the use of methylamine and/or ethylenediamine could only produce pure Ag NPs; not pure Au and Au–Ag alloy NPs. As for the stabilizer, we also tried several commonly used stabilizing agents, namely, poly(vinylpyrrolidone) (PVP), poly(ethylene glycol) (PEG), cyclodextrin, and glucose under similar experimental conditions to those of Na_3Ct ; however, in all those cases stable Au–Ag alloy NPs as good as with Na_3Ct could not be achieved.

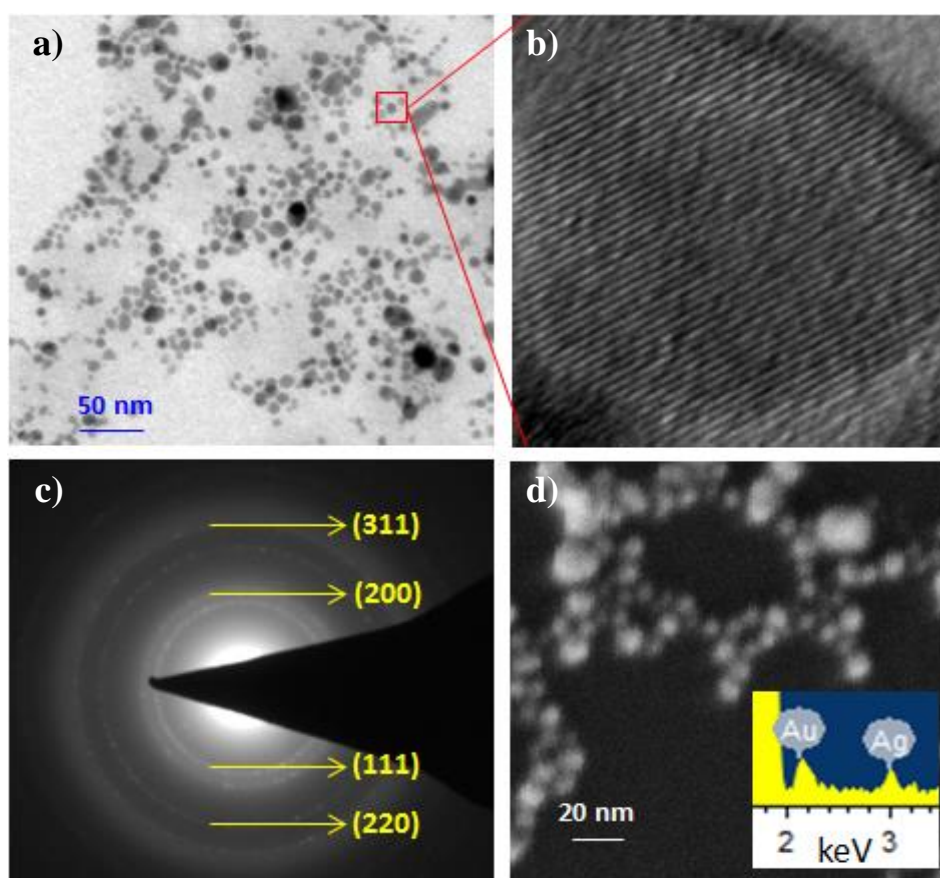


Figure 4.2: a) TEM image of Au–Ag (1:1) alloy NPs and b) a magnified view on single nanoparticle revealing a high-degree of crystallinity (almost single crystalline) where the $\langle 111 \rangle$ fcc lattice fringes are separated by $\sim 2.5 \text{ \AA}$. c) SAED pattern collected on the same zone where large-scale TEM image was taken. Various lattice planes are indicated by yellow arrows. d) FESEM image of the 1:1 alloy NPs sample from which elemental composition of $\sim 1:1$ (Au:Ag) was estimated by energy dispersive X-ray spectroscopy (EDXS) (inset).

TEM images (**Figure 4.2a**) of the 1:1 Au–Ag alloy NPs sample show the formation of spherical NPs with average diameter 6 nm. The overall contrast reveals the formation of

“homogeneously alloyed” NPs. The high-resolution TEM images clearly (**Figure 4.2b**) suggest a high-degree of crystallinity where one can even depict the well-defined fcc-lattice fringes which are separated by $\sim 2.5 \text{ \AA}$ (distance between (111) planes). The SAED pattern (**Figure 4.2c**) recorded on these alloy NPs exhibited bright fringes resulting out of the characteristic diffractions from various fcc-lattice planes namely (111), (200), (220), and (311).^{11,12} Earlier, the alloy NPs (prepared without NH_4OH) did reveal a considerable amount of structural defects.^{2,3} Also, in the present study, Au–Ag alloy NPs prepared without the use NH_4OH look far more disordered and well-defined atomic arrangements/fringes were not visible. The FESEM image of the 1:1 Au–Ag alloy NPs sample (**Figure 4.2d**) obtained with the use of NH_4OH supported the TEM observations and revealed spherical alloy NPs with average diameter sub-10 nm. Apart from NaBH_4 , other reducing agents like hydrazine (NH_2NH_2) and Na_3Ct (at $\sim 90^\circ \text{ C}$) were also attempted; however, it did not lead to the formation of homogeneous and truly alloyed Au–Ag NPs. We have also used tannic acid (earlier it was used to control the size of Ag NPs²⁰) along with Na_3Ct for the same experiment (NaBH_4 as reducing agent), but no improvement (i.e., above 10 nm) in particle size was observed.

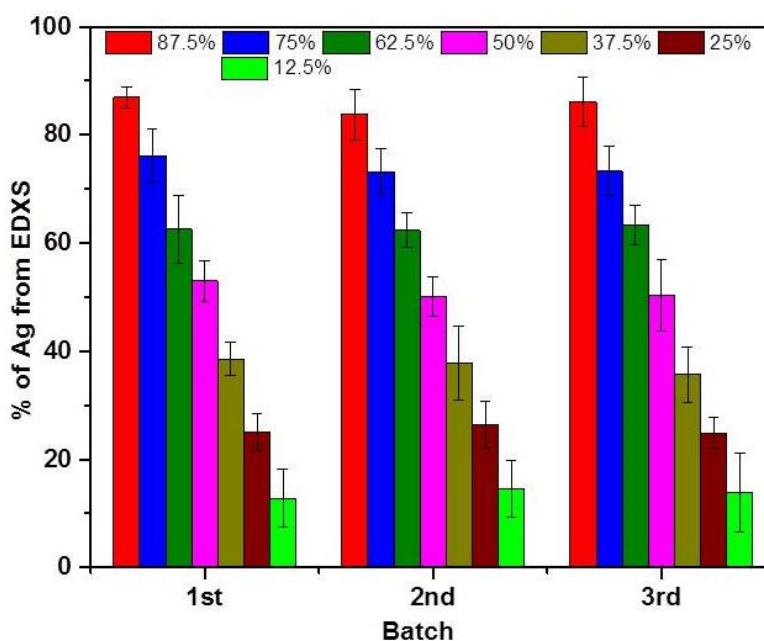


Figure 4.3: Verification of the elemental composition (%) on the Au–Ag alloy NPs from EDXS analysis with the initial feeding moles of Ag (%). Three batches of sample preparation were executed and overall, there was a very good match between feed and actual with a statistical average of more than three hundred EDXS analysis on Au–Ag alloy NPs covering seven different compositions.

Elemental signatures of both Au and Ag on the agglomerates of Au-Ag alloy NPs were confirmed by EDXS analysis and the composition was estimated to be $\sim 1:1$ – clearly as per the feeding moles. It is not only the 1:1 Au:Ag alloy NPs, for the 1:3 and 3:1 Au:Ag alloy NPs elemental compositions derived from EDXS data were also very much close to the initial moles of HAuCl_4 and AgNO_3 which justify claiming -as per feeding moles.

Statistically, we have carried out close to three hundred EDXS analysis on three batches of sample preparation and in each batch of samples seven sets of alloy compositions were verified. The exhaustive EDXS analysis is summarized in (Figure 4.3) and standard deviation for each of the seven alloy composition was found to be varied only by few percent. Without the use of NH_4OH , composition in the alloy NPs was not as per the feeding moles of HAuCl_4 and AgNO_3 ; specifically, with an initial mole ratio of Au:Ag $\sim 1:3$ resulted in the formation of Au–Ag alloy NPs with a final Au:Ag composition close to $\sim 1:1$ – as revealed by the EDXS data complementing the UV–vis spectrum (Figure 4.1a).

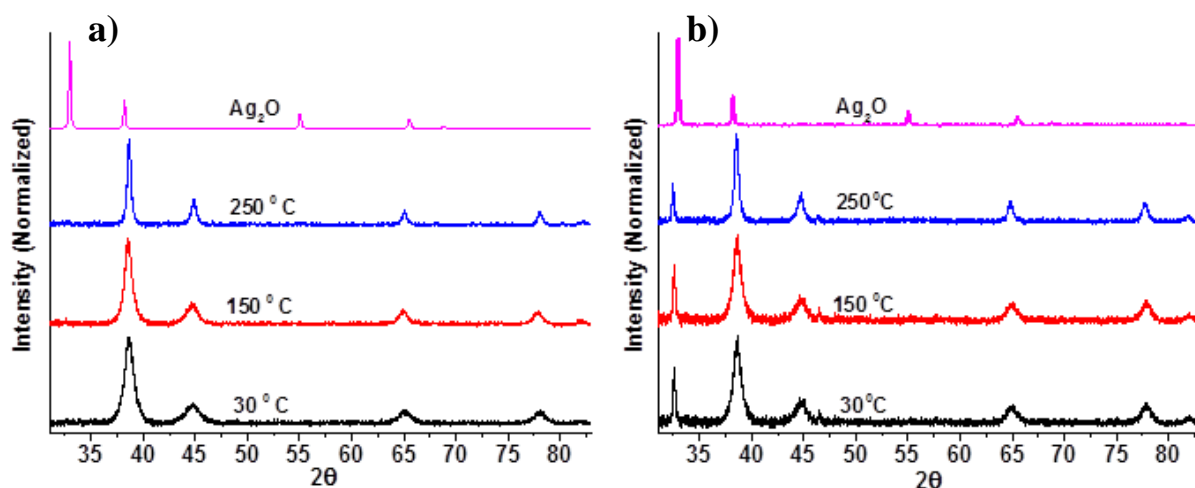


Figure 4.4: PXR D was measured at 30, 150 and 250 °C for (1:1) Au-Ag alloy NPs synthesized with (a) and without (b) using NH_4OH . The same measurement was done for Ag_2O at 30 °C.

PXR D pattern (Figure 4.4a) fully supported the SAED data by predominantly showing diffraction peaks which are characteristic of fcc-lattice.^{11,12} Even brightness of the SAED fringes corroborates the intensity of the respective PXR D peaks. Furthermore, we have recorded temperature-dependent PXR D patterns for (1:1) alloy NPs and realized that up to 250 °C the original pattern practically remained unchanged, thereby ruling out the presence of secondary-ordering due to phase-segregation and/or impurity.

Without NH_4OH , we could detect additional impurity peak characteristic of Ag_2O and/or AgCl at $2\theta \sim 32.5$ which persisted even after heating up to $250\text{ }^\circ\text{C}$ (**Figure 4.4b**).

So far in the literature, for the Au–Ag alloy NPs, a linear variation of the SPR peak (λ_{max}) with the compositional fraction (Au:Ag) was always observed and proposed to be the general expectation.^{2,3} Only recently, a theoretical model came up with the idea of a third-order function of composition with size-dependent coefficients.²¹ Note that according to Verbruggen *et al.*²¹ It is primarily the composition of alloy that determines the SPR wavelength, whereas particle size is of the secondary importance. Indeed, we have plotted the SPR peak values versus mole fraction of Au initially used (**Figure 4.5a**).

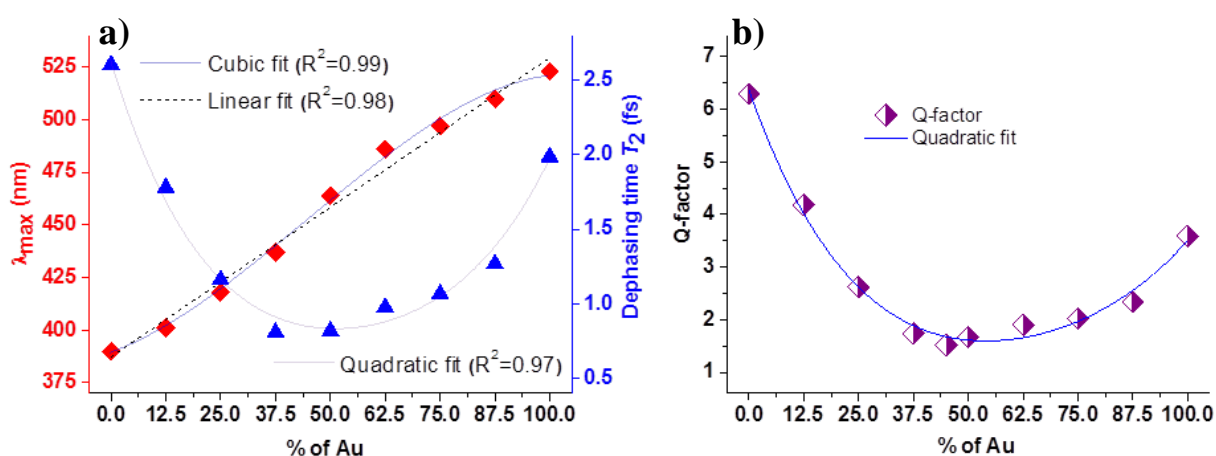


Figure 4.5: a) SPR wavelength (λ_{max}) and dephasing time (T_2) as a function of mole fraction of Au (%) in various Au–Ag alloy NPs. The dotted black (linear fit), blue (cubic fit), and violet (quadratic fit) curves are representing the plots for λ_{max} (orange diamonds) and T_2 (green triangles) against mole fraction of Au, respectively. b) Quadratic fit (blue) for the plot of Q-factor against mole fraction of Au in corresponding Au–Ag alloy NPs.

Although, it looks like that the trend can be apparently fitted linearly ($R_2 = 0.98$), however a third-order polynomial function gave a much better fit for a set of nine data points ($R_2 = 0.99$) and the nonlinearity is visibly much pronounced in the tails. An important issue follows is the compositional dependency of the plasmon bandwidth (Γ) -linear or nonlinear? Taking the two-level concept of molecular spectroscopy into consideration one can simply express the spectral width (Γ in eV) of plasmon band as²

$$\Gamma = 2\hbar/\pi T_2$$

Here T_2 is given by the following equation:

$$T_2^{-1} = T_1^{-1}/2 + T_2^{*-1}$$

(T_1 is the population relaxation time, both radiative and nonradiative; T_2 is the total dephasing time; and T_2^* is the pure dephasing time which is often much shorter than T_1).

Since in our experiments a homogeneous size distribution of the NPs was observed, a homogeneous spectral line broadening is expected where T_2 can be easily estimated from the measured widths of the plasmon bands by following the procedure described by Link *et al.*² In general, T_2 was in the range of few femtoseconds, relatively shorter for alloys than pure metals, and falling down below 1 fs for the 1:1 Au–Ag alloy NPs which is perhaps the shortest T_2 value known in the literature of plasmonic NPs and throws new challenges for complementary experiments, specifically frequency and time domain measurements.²² A plot of the composition dependent variations of T_2 exhibit a much more erratic behaviour – a quadratic polynomial fitting very well with the experimental data (**Figure 4.5a**). Surprisingly, such a trend was observed for thin- films alloys of Au and Ag having thickness in the range of few hundreds of nanometer.²³

Another important parameter is the quality factor (Q) which can be easily derived from the λ_{\max} (SPR peak) and Γ values (**Figure 4.5b**) by applying the following equation:²⁴

$$Q = \lambda_{\max}/\Gamma$$

In case of the particle plasmon, Q value represents the local-field enhancement which is basically linked to nonlinear applications like SERS (discussed below). Likewise T_2 , data on the variation of Q on the composition of Au–Ag alloy NPs can be better fitted with a quadratic polynomial. Again, considering alloy as a kind of impure material with respect to pure metals and by applying the Matthiessen's rule (resistivity proportional to sum of different scattering mechanisms) one would expect a linear dependency of T_2 or Q versus alloy composition which is clearly not the case we observe. Thus, SPR cannot be simply correlated with the free-electron-gas model -whether it is sub-10 nm Au–Ag alloy NPs or a 170–300 nm thin-film alloy of Au and Ag. To explain such an unusual trend, we need to look at the significantly different electronegativity values of Au and Ag whereby a charge-transfer mechanism ($\text{Ag}^{\delta+} \text{--} \text{Au}^{\delta-}$) could bring additional factor by redistributing the electron density across the NPs being maximum at the matching mole fraction (1:1).^{23,25}

Raman scattering of molecules adsorbed onto noble metallic nanostructures is dramatically enhanced which is known as SERS; and the enhancement factor (EF) can reach up to 10^{14} – 10^{15} thereby showcasing a very high-sensitivity of the SERS technique down to single-molecule level.^{26,27} Even, sophisticated X-ray based surface analytical tools fail to provide unprecedented information on the outermost surface layers compared to those of the interior of alloy NPs.^{15,16,18} In fact, Kim *et al.*^{15,16,18} have successfully proved by SERS that ~ 30 nm sized Au–Ag alloy NPs are indeed surface-enriched with Ag. Furthermore, Monte Carlo simulations suggested the surface segregation of Ag in sub-10 nm Au–Ag alloy NPs for a wide range of compositions, sizes, and temperatures.¹⁷ Thus, Au–Ag alloy NPs so far synthesized via various wet-chemical routes are “heterogeneous-alloy” or “homogeneous-alloy”? For the assessment of quality of Au–Ag alloy NPs with respect to composition as per the feeding moles and mixing homogeneity additional application oriented experiments were performed.

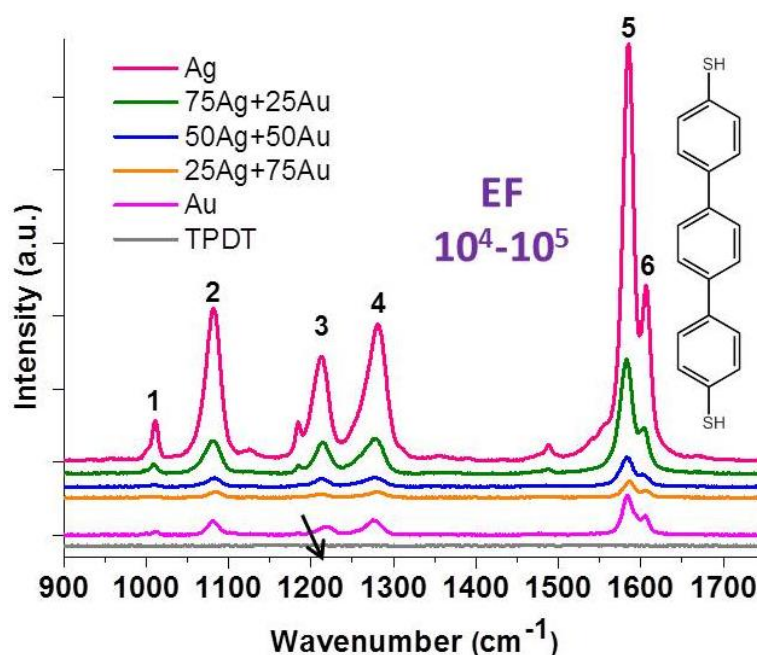


Figure 4.6: Untangling electromagnetic and chemical enhancement. SERS of TPDT (inset: molecular structure) in the presence of Au–Ag alloy NPs with various compositions and the arrow indicates the gradual reduction in the intensity of the peak at ~ 1182 cm^{-1} as the Ag fraction gradually decreases in Au–Ag alloy NPs.

We have measured the SERS spectra (**Figure 4.6**) for the Au–Ag alloy NPs (3:1; 1:1; and 1:3) along with those of pure Au and Ag NPs prepared under similar experimental conditions. The samples were prepared as follows; 1mL of TPDT solution (10 μM) in ethanol was added

to the mixture of 0.5 mL of water and 0.5 mL of NPs solution (as synthesized). These samples were kept for incubation for 6 h and then drop-casted on glass-slide, subsequently dried under high vacuum. Enhancement factor for each sample has been estimated from the average of five-data set on different spots and by considering the intensity of the peak at 1210 cm^{-1} . A significant enhancement of the Raman signal of terphenyl di-thiol (TPDT) molecules was observed for all the NPs; specifically for the pure Au and Ag NPs the analytical enhancement factors (AEFs) were estimated to be in the range of $\sim 5 \times 10^4$ and $\sim 5 \times 10^5$, respectively. From the exponential decay in the optical density with the increasing mole fraction of Au,² one would expect a similar trend in the nonlinear optical properties like SERS activity. However, the overall trend in enhancing the Raman signal of TPDT was as follows: $\text{Ag} > \text{Ag-Au (3:1)} > \text{Au} > \text{Ag-Au (1:1)} > \text{Ag-Au (1:3)}$, which corresponds well to the trend in the Q-factor values (**Figure 4.5b**) that are believed to be the figures of merit for enhancement in SERS signal (roughly proportional to Q^4).²⁶ The SERS spectra looked similar to each other; six major peaks were visible in all the systems and a negligible shift observed in the peak positions reflects similar bonding (covalent attachment to Au or Ag via S atom) and upright orientation of TPDT on the surface of all NPs.²⁸ However, few peaks of TPDT appeared characteristically on the Ag NPs and were apparently absent in the Au NPs which could be attributed to a chemical enhancement effect.²⁹ Specifically, the relative intensity ratio between the peaks at ~ 1185 and $\sim 1210\text{ cm}^{-1}$ gradually decreased reaching almost zero upon increasing the concentration of Au up to 100% which is remarkable and strongly supports formation of “homogeneously alloyed” NPs by ruling out the possibility of surface enrichment by Ag atoms.

To complement the SERS measurements, we have performed catalysis on the reduction conversion from p-nitrophenol to p-aminophenol at ambient conditions which is a rather common practice for checking the catalytic activity of unsupported Au NPs.^{8,30} Catalysis in general is very much surface-sensitive and the chosen reaction can be easily monitored by using UV-vis spectrophotometer as the reactant, intermediate and product have distinctive absorption characteristics (**Figure 4.7**). Since in our method we can precisely control the composition of Au in the alloy NPs, a controlled catalysis of the reaction is expected. Indeed, a gradual increase in the product conversion with increasing concentration of Au under a fixed time of 9 min (**Figure 4.7**) was observed. Note that particle sizes remained almost same in the concentration range of Au from 25 to 100%. On the contrary, Au-Ag alloy NPs prepared without the use of NH_4OH show an anomalous trend in the catalysis (data point

cannot be fitted linearly) which strongly supports the uncontrolled composition of Au in the alloy NPs. Thus, our results rule out the possibility of enrichment by Ag on the outermost surface layers of the Au–Ag alloy NPs. Citrate-stabilization on the NPs seems very much flexible –allowing not only the self-assembly of thiols on the surface but also providing active sites on the surface for catalysis.

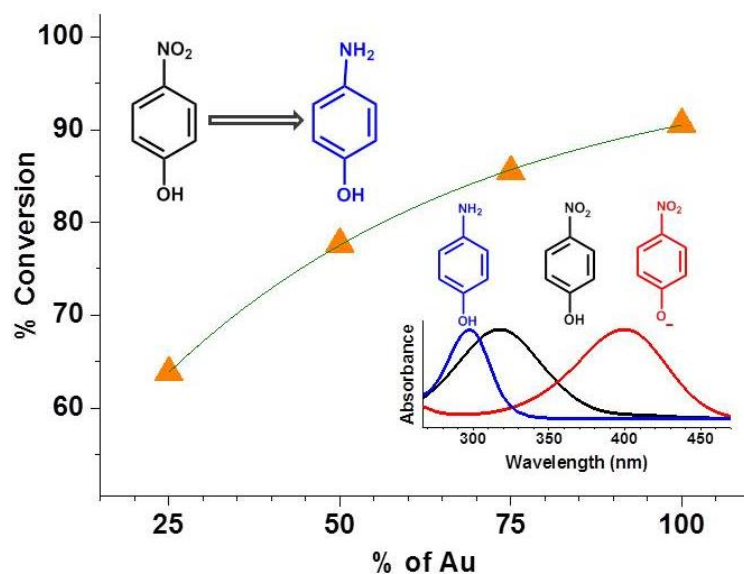


Figure 4.7: Controlled catalysis. The plot of % conversion of *p*-nitrophenol to *p*-aminophenol (after 9 min of duration) against mole fraction of Au in Au–Ag alloy NPs. Inset (left): scheme of *p*-nitrophenol to *p*-aminophenol conversion. Inset (right): absorption signatures of reactant (*p*-nitrophenol), intermediate (*p*-nitrophenoxide ion) and product (*p*-aminophenol).

To further strengthen our claim of “homogeneous-alloying” of Au and Ag in sub-10 nm particles, the potential cytotoxicity of different Au–Ag alloy NPs was evaluated in both HeLa (cervical carcinoma) and HEK293T (human embryonic kidney) cells using the MTT assay³¹ (**Figure 4.8**). All the NPs showed dose-dependent and similar effect on the cell viability in both HEK293T cells (**Figure 4.8a**) and HeLa cells (**Figure 4.8b**) when compared to the untreated cells.

Even at the maximum concentration (40%; v/v), more than 50% cells were viable for both the cell lines, thereby suggesting an acceptable level of biocompatibility for Au–Ag alloy NPs prepared by our method. As expected, the Ag NPs showed relative more cytotoxicity (by ~10%) than Au NPs; however, the present observation on the huge reduction (by ~50%) in the cytotoxicity of Ag NPs (size ~10 nm) compared to earlier reports (by ~100%) is noticeable.⁴² Despite having sub-10 nm size,³² a comparable level of biocompatibility for all

the NPs in cell lines derived from a cancerous (HeLa) and noncancerous (HEK293T) source is interesting and could possibly originate from a common fact - high-degree of crystallinity and uniformity in the distribution of Au and Ag atoms all throughout. These NPs are therefore promising for drug-delivery applications as well as medical diagnostics – from genomics to proteomics.³³

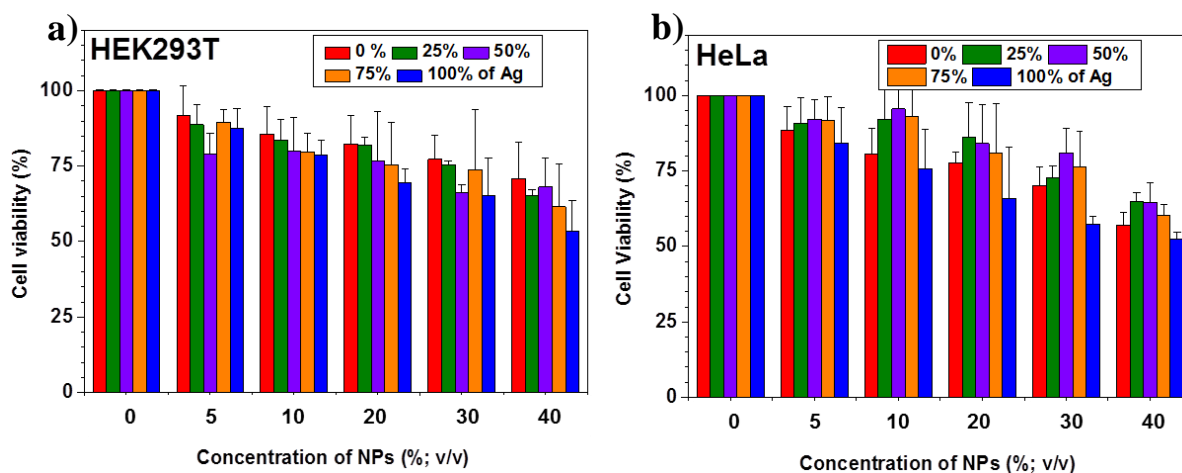


Figure 4.8: The potential cytotoxicity of pure Au and Ag and of Au–Ag alloy NPs in (a) HEK293T and (b) HeLa cells as revealed by the MTT assay. Pure Ag NPs exhibited an unusually good biocompatibility.

Because of poor solubility of metal salt precursors in nonpolar solvents such as hexane, cyclohexane, chloroform, and toluene, phase-transfer remained an important approach for obtaining stable dispersions of noble metal nanoparticles inorganic media and thereby paving the way forward toward applications in nanotechnology.³⁴ In a two-step method, Brust *et al.*³⁵ pioneered the methodology in producing Au NPs inorganic solvent by means of an alkanethiol and a phase transfer catalyst. Subsequently, stable dispersions of Au NPs in organic medium have been achieved upon using capping agents like alkanethiol,³⁶ aromatic thiol,³⁷ dialkyldisulfides,³⁸ thiolatedcyclodextrin,³⁹ and alkylamine.⁴⁰ Also, phase-transfer of preformed Au NPs in aqueous medium by means of surface modifications with suitable hydrophobic ligands was found to be reliable alternatives.⁴¹ Note that it is difficult to achieve homogeneously alloyed Au–Ag alloy NPs in organic solvents by Brust method. In order to explore the phase-transfer characteristics of the pure Au, Ag, and Au–Ag alloy NPs prepared by our method, we adopted the following procedure for four different organic solvents namely hexane, cyclohexane, chloroform and toluene. An amount of 0.5 mL of ethanol was added to 1 mL of NPs solution and stirred for 5 min. To this solution, 1.5 mL of organic

solvent, 50 μ L of 2 mM dodecanethiol (DDT) in respective organic solvent and 15 μ L of 0.1 mol H_3PO_4 (acted as an inducer^{34,42}) were added sequentially followed by stirring vigorously at room temperature 20 min. To our surprise, the Au–Ag alloy NPs (1:3; 1:1 and 3:1) got transferred to each of the organic solvents while pure Au and Ag NPs remained in the aqueous phase (**Figure 4.9**). One probable reason could be the particle size; which was in the range of ~ 10 nm for the pure Au and Ag NPs whereas those for each Au–Ag alloy system was ~ 6 nm. In line with previous reports, a common red-shift in the SPR of alloy NPs was noted thereby reflecting different dielectric surrounding of the NPs in the organic medium than in comparison to the aqueous medium.⁴³ Specifically, for the 3:1, 1:1, and 1:3 Au–Ag alloy NPs, the SPR values were changed from ~ 515 to ~ 525 nm, from ~ 472 to ~ 487 nm and from ~ 425 to ~ 445 nm; respectively. However, the consistency in the red-shift value of SPRs of various alloy NPs, for example, ~ 10 nm for 3:1 Au–Ag, ~ 15 nm for 1:1 Au–Ag and ~ 20 nm for 1:3 Au–Ag, irrespective of the different refractive index values of the organic solvents ($n_d \sim 1.37$, ~ 1.42 , ~ 1.44 and ~ 1.49 for hexane, cyclohexane, chloroform, and toluene; respectively⁴³) could primarily arise due to consistent formation of DDT self-assembled monolayers onto the particle surface. The controlled increment of red-shift is ca. 5 nm from 3:1 to 1:1 to 1:3 Au–Ag alloying is perhaps a reflection of the well-defined surface-structure of NPs and warrants further investigations.

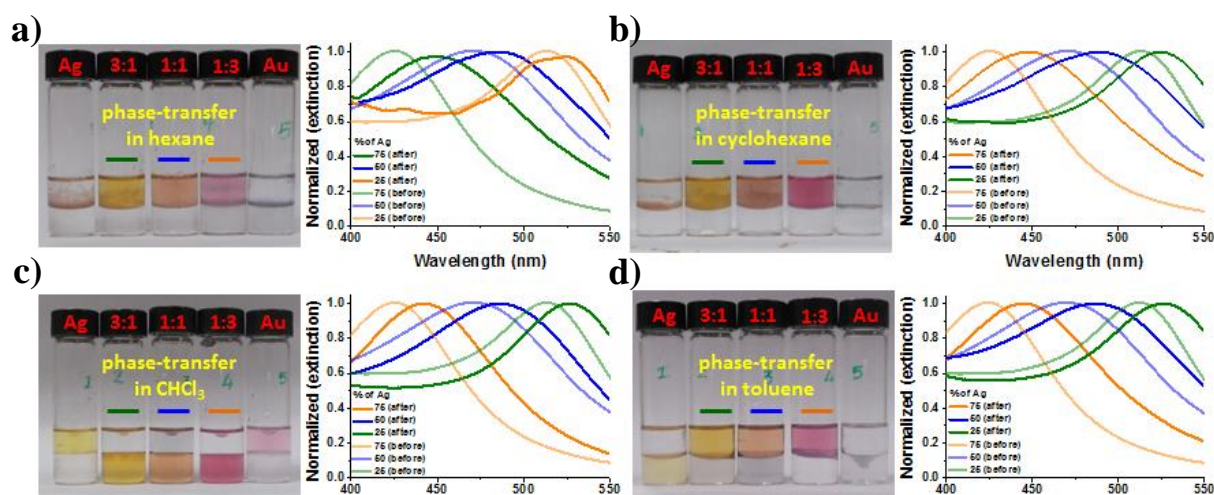


Figure 4.9: *a–d*) Optical photograph showing the transfer of 3:1, 1:1 and 1:3 Ag–Au alloy NPs from aqueous solution to hexane (a), cyclohexane (b), chloroform (c), and toluene (d) (left) and the respective UV–vis spectra (normalized), before and after phase-transfer (right). Notably, phase-transfer of pure Au and Ag NPs in those organic solvents could not be achieved under similar conditions which could primarily be due to larger particle size.

We present an observation on the electron-beam induced fusion of sub-10 nm self-assembled (with TPDT) Au–Ag alloy NPs in real-time at room temperature under a high-resolution 300 keV TEM (**Figure 4.10**). A scheme of e-beam fusion of NPs is shown in **Figure 4.10a**. Our observation on the e-beam fusion of NPs is consistent with previous report.⁴⁴ However, we have taken an attempt to shed new light in the seemingly simple and fundamentally important problem in fluid mechanics –coalescence singularity.⁴⁵

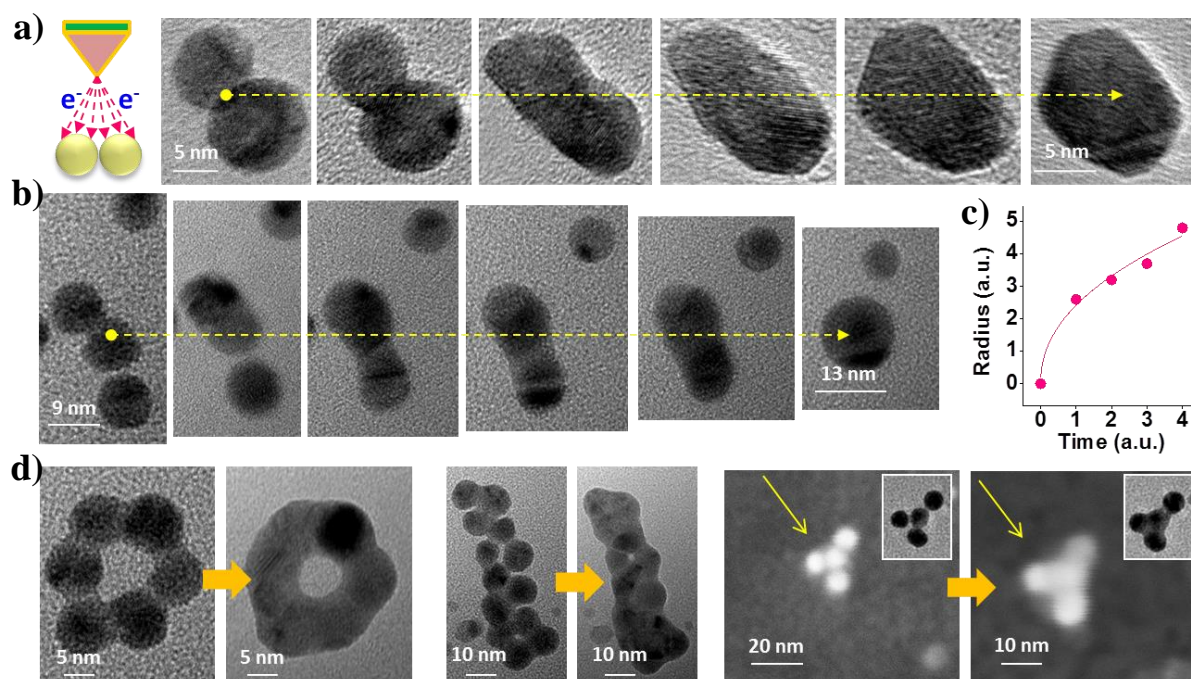


Figure 4.10: a) Scheme of electron bombardment on NPs. TEM images (300 kV) captured coalescence between two 1:1 Au–Ag alloy NPs with 1 min of interval time. b) TEM images showing fusion of 3-NPs into 1-NP upon 5 min of electron irradiation. c) Evolution of liquid-bridge radius against time. d) Circularly arranged mixture of Au and Ag NPs becoming a nanoring in 5 min of electron beam exposure. e) possibility of obtaining nanorod from the fusion of spherical NPs. f) Fusion of NPs under FESEM, images of group of Au NPs recorded at 0 min (left) and after 10 min (right) upon exposure to electron beam (20 kV) for ~15 min (inset: TEM observations complementing the FESEM data).

It is classically a finite-time singularity problem where the dynamics is directed by nonlinear partial differential equations. TEM image of NPs obtained from a mechanical mixture of pure Au and Ag NPs (Sigma-Aldrich, average size ~10 nm, and with TPDT) showed spherical Au and Ag NPs with average size ~sub-10 nm (**Figure 4.10**) and the self-assembly of Au NPs in the presence of TPDT as dimers/trimers and no larger aggregates was visible.⁴⁶ Specifically, a discriminative response of TPDT with respect to an aliphatic di-thiol analogue

(undecanedithiol, UDDT) in the self-assembly of Au and Ag NPs was observed (**Figure 4.11**). Remarkably, while zooming-in with converging electron-beam having accelerator voltage of 300 kV for performing high-resolution microscopy, we observed fusion of NPs initiating at a very small contact point which is reminiscent of coalescence of droplets. In fact, one can directly visualize the fusion of three spherical NPs of average diameter ~ 9 nm into one spherical NP of diameter ~ 13 nm which took place in 5 min of duration at room temperature. A subsequent follow-up question would be – is it a viscous or inertial coalescence? On the basis of theoretical modelling and experimental observations reported earlier it can be inferred that if the growth of the radius of the liquid-bridge r (see the dumbbell-like shape in **Figure 4.10b**) is linearly proportional to the time t then it is likely a viscous coalescence or if it follows a power-law ($r \propto t^\alpha$) then it is an inertial coalescence.⁴⁷ We have plotted the variation of r as a function of t and found that $r \propto t^{0.45}$ (**Figure 4.10c**) thereby directing toward the occurrence of an inertial coalescence –likewise fusion of Hg droplets.⁴⁸ Some exotic nanostructures which can be fabricated from spherical NPs and with the help of e-beam are presented in **Figure 4.10d** and **Figure 4.10e**. In **Figure 4.10f** we demonstrate e-beam (20 keV) fusion of NPs under FESEM truly complementing the results obtained under TEM. A combination of e-beam fusion and e-beam manipulation of NPs is expected to open-up new possibilities in experimenting with ensembles of NPs down to single NPs level.

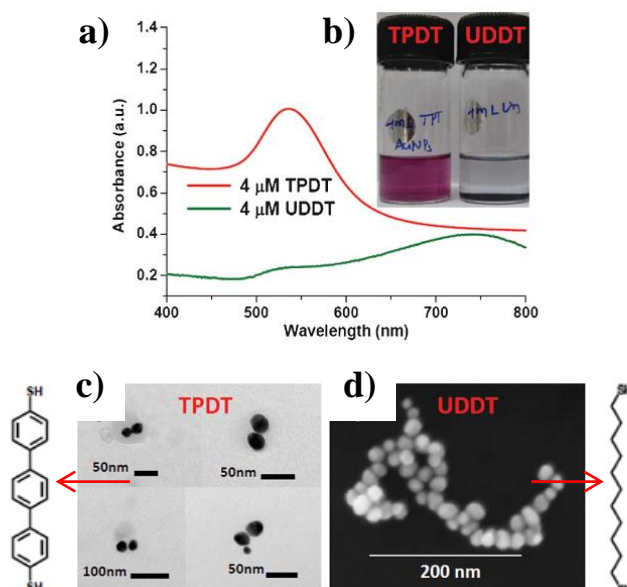


Figure 4.11: a) UV-vis spectra for the mixture of Au NPs solution and 4 μ M solutions of UDDT and TPDT. b) Optical photographs of the respective solution. c) TEM image of the TPDT-Au NPs system. d) FE-SEM images for the UDDT-Au NPs system.

It is known that addition of NH_4OH to a solution of AgNO_3 generates $[\text{Ag}(\text{NH}_3)_2]^+$ ions (so-called Tollen's reagent; pH ~ 10.0). Subsequently, addition of HAuCl_4 changed the pH of the solutions to ~ 9.5 , ~ 9.0 , and ~ 7.0 , for the 3:1, 1:1, and 1:3 (Ag: Au) systems, respectively. Usually, HAuCl_4 remained as $[\text{AuCl}_4]^-$ at pH ~ 3.0 and $[\text{Au}(\text{OH})_4]^-$ at pH ~ 12 ; and a gradual hydrolysis produce various intermediate species such as $[\text{AuCl}_3(\text{OH})]^-$ (pH ~ 6.0), $[\text{AuCl}_2(\text{OH})_2]^-$ (pH ~ 7.0) and $[\text{AuCl}(\text{OH})_3]^-$ (pH ~ 8.0).^{49,50} Upon addition of excess NH_4OH to HAuCl_4 solution, no characteristic metal-to-ligand (Au-Cl) charge-transfer band at ~ 290 nm was detected which indicates considerable replacement of the Cl^- ligands by the OH^- ions and formation of $[\text{Au}(\text{NH}_3)_4]^+$ species in the solution. However, such an ammoniacal solution of HAuCl_4 did not allow stable AuNPs formation. On the contrary, a solution of HAuCl_4 in excess NaOH where $[\text{Au}(\text{OH})_4]^-$ seems to be the predominant species, did form stable Au NPs. Furthermore, the onset of NPs formation took place very rapidly, started almost immediately upon the addition of NaBH_4 (relatively stronger reducing agent) to the reaction mixture of HAuCl_4 , AgNO_3 , Na_3Cit and NH_4OH . As the mole fraction of Au was increased, the evolution of Au-Ag alloy NPs growth somewhat slowed down. Specifically, the time required to reach ultimate color of the corresponding Au-Ag alloy NPs solutions with varied feeding moles of 0:1, 1:3, 1:1, 3:1 and 1:0 were ca. 10 s, 30 s, 2 min, 15 min, and 30 min, respectively (beyond these time scales there was no change in the color of the respective solutions which could be detected optically). Considering the pH values measured in our method, we would be in favour of assigning $[\text{AuCl}_2(\text{NH}_3)_2]^-$ and/or $[\text{AuCl}(\text{NH}_3)_3]^-$ as the active species⁵¹ in conjunction with $[\text{Ag}(\text{NH}_3)_2]^+$; possibly as an ion-pair intermediate (**Scheme 4.1**). Notably, from these intermediate species the reduction potential to Au^0 and Ag^0 is only ~ 0.42 and ~ 0.38 V, respectively.⁵¹ Thus, significant lowering of the reductions potential values and bringing them closer to each other by means of NH_4OH and the use of relatively stronger reducing agents like NaBH_4 could be the main driving forces for such a precise control over the composition of the alloy NPs above the solubility product of AgCl .

In the conceptual framework of Au-Ag alloy NPs, bringing chemical stability with the help of Au counterpart remained one of the main aspects. To test chemical stability, alloy NPs prepared were subjected to corrosive chemical environment, namely a mixture of 30% H_2O_2 and 29% NH_4OH (1:1; v/v) for about an hour. 30 μL of corrosive solution was added to 2 mL solution of each set of NPs. The SPR peak of pure Ag NPs solution was vanished as expected. However, the SPR peaks of all alloy NPs including pure Au NPs solutions were retained; though SPR intensities were modulated depending on the amount of Ag.

Remarkably, the SPR peak position which is predominantly dependent on the composition (since all NPs were sub-10 nm) was almost unaltered. For Ag-rich (>75%) NPs, there was red-shift of SPR due to surface-etching, as by default there is more Ag on the surface region. As for Au-rich (>75%) NPs, we could not find any change in the SPR peak position besides observing an onset of aggregation of Au NPs. This experiment suggests that such-prepared Au–Ag alloy NPs can withstand corrosive chemical environments and no pre-thermal treatment at high-temperatures close to melting points of Au and Ag is required as recently demonstrated by Gao *et. al.*¹ Thus, our coreduction approach at room-temperature using NH₄OH does lead to the formation of homogeneously alloyed as well as chemically stable Au–Ag NPs as per feeding moles.

4.4 Summary and Conclusions

We have presented a robust wet-chemical co-reduction for producing citrate-stabilized “homogeneously alloyed” Au–Ag NPs with average size sub-10 nm and as per the feeding moles of HAuCl₄ and AgNO₃. A decade long problem in the standard NaBH₄ co-reduction was solved by exploring the power of wet chemistry in the usage of NH₄OH; and the alloying of Au and Ag was achieved well-above the solubility product of AgCl. Compositional dependency of the SPR could be best fitted with a third-order polynomial and the quality factor (Q) followed a quadratic trend. At the matching mole fraction (1:1), the Au–Ag alloy NPs were found to be highly damped where the dephasing time (T₂) was estimated to be extremely short (below 1 fs). The SERS enhancement factors earned with these alloy NPs were pretty good (10⁴–10⁵). Remarkably, all alloy NPs showed high-stability in corrosive chemical environment. An acceptable level of biocompatibility in human cell lines tested, including pure Ag NPs is noteworthy. A possible mechanism involving the formation of an ion-pair intermediate consists of Au and Ag complexes has been proposed. Our method is not limited to the Au–Ag combination but can be employed in the synthesis of various bimetallic and trimetallic alloy NPs. The results are expected to stimulate future investigations in the development of multifunctional “homogeneously alloyed” NPs with high-performance capability.

4.5 References

- (1) Gao, C.; Hu, Y.; Wang, M.; Chi, M.; Yin, Y. Fully Alloyed Ag/Au Nanospheres: Combining the Plasmonic Property of Ag with the Stability of Au. *J. Am Chem. Soc.* **2014**, *136*, 7474.
- (2) Link, S.; Wang, Z. L.; El-Sayed, M. A. Alloy formation of gold-silver nanoparticles and the dependence of the plasmon absorption on their composition. *J. Phys. Chem. B* **1999**, *103*, 3529.
- (3) Mallin, M. P.; Murphy, C. J. Solution-phase synthesis of sub-10 nm Au-Ag alloy nanoparticles. *Nano Lett.* **2002**, *2*, 1235.
- (4) Singh, A. V.; Bandgar, B. M.; Kasture, M.; Prasad, B. L. V.; Sastry, M. Synthesis of gold, silver and their alloy nanoparticles using bovine serum albumin as foaming and stabilizing agent. *J. Mater. Chem.* **2005**, *15*, 5115.
- (5) Kariuki, N. N.; Luo, J.; Maye, M. M.; Hassan, S. A.; Menard, T.; Naslund, H. R.; Lin, Y. H.; Wang, C. M.; Engelhard, M. H.; Zhong, C. J. Composition-controlled synthesis of bimetallic gold-silver nanoparticles. *Langmuir* **2004**, *20*, 11240.
- (6) Zhang, M.-X.; Cui, R.; Zhao, J.-Y.; Zhang, Z.-L.; Pang, D.-W. Synthesis of sub-5 nm Au-Ag alloy nanoparticles using bio-reducing agent in aqueous solution. *J. Mater. Chem.* **2011**, *21*, 17080.
- (7) Zhang, G.; Du, M.; Li, Q.; Li, X.; Huang, J.; Jiang, X.; Sun, D. Green synthesis of Au-Ag alloy nanoparticles using *Cacumen platycladi* extract. *RSC Adv.* **2013**, *3*, 1878.
- (8) Shin, K. S.; Kim, J. H.; Kim, I. H.; Kim, K. Novel fabrication and catalytic application of poly(ethylenimine)-stabilized gold-silver alloy nanoparticles. *J. Nanopart. Res.* **2012**, *14*.
- (9) Zhang, H.; Haba, M.; Okumura, M.; Akita, T.; Hashimoto, S.; Toshima, N. Novel Formation of Ag/Au Bimetallic Nanoparticles by Physical Mixture of Monometallic Nanoparticles in Dispersions and Their Application to Catalysts for Aerobic Glucose Oxidation. *Langmuir* **2013**, *29*, 10330.
- (10) Chen, D. H.; Chen, C. J. Formation and characterization of Au-Ag bimetallic nanoparticles in water-in-oil microemulsions. *J. Mater. Chem.* **2002**, *12*, 1557.
- (11) Zhang, Q.; Lee, J. Y.; Yang, J.; Boothroyd, C.; Zhang, J. Size and composition tunable Ag-Au alloy nanoparticles by replacement reactions. *Nanotechnology* **2007**, *18*.
- (12) Smetana, A. B.; Klabunde, K. J.; Sorensen, C. M.; Ponce, A. A.; Mwale, B. Low-temperature metallic alloying of copper and silver nanoparticles with gold nanoparticles through digestive ripening. *J. Phys. Chem. B* **2006**, *110*, 2155.

- (13) Okazaki, K.-i.; Kiyama, T.; Hirahara, K.; Tanaka, N.; Kuwabata, S.; Torimoto, T. Single-step synthesis of gold-silver alloy nanoparticles in ionic liquids by a sputter deposition technique. *Chem. Commun.* **2008**, 691.
- (14) AbdelHamid, A. A.; Al-Ghobashy, M. A.; Fawzy, M.; Mohamed, M. B.; Abdel-Mottaleb, M. M. S. A. Phytosynthesis of Au, Ag, and Au-Ag Bimetallic Nanoparticles Using Aqueous Extract of Sago Pondweed (*Potamogeton pectinatus* L.). *ACS Sustainable. Chem. Eng.* **2013**, *1*, 1520.
- (15) Kim, K.; Kim, K. L.; Lee, S. J. Surface enrichment of Ag atoms in Au/Ag alloy nanoparticles revealed by surface enhanced Raman scattering spectroscopy. *Chem. Phys. Lett.* **2005**, *403*, 77.
- (16) Manzhos, R. A.; Krivenko, A. G.; Doronin, S. V.; Choba, M. A.; Safonov, V. A. Surface segregation of silver atoms on Au-Ag alloys according to data of laser-heating induced temperature potential shifts, XPS and conventional electrochemical methods. *J. Electroanal. Chem.* **2013**, *704*, 175.
- (17) Deng, L.; Hu, W.; Deng, H.; Xiao, S.; Tang, J. Au-Ag Bimetallic Nanoparticles: Surface Segregation and Atomic-Scale Structure. *J. Phys. Chem. C* **2011**, *115*, 11355.
- (18) Kim, K.; Kim, K. L.; Choi, J.-Y.; Lee, H. B.; Shin, K. S. Surface Enrichment of Ag Atoms in Au/Ag Alloy Nanoparticles Revealed by Surface-Enhanced Raman Scattering of 2,6-Dimethylphenyl Isocyanide. *J. Phys. Chem. C* **2010**, *114*, 3448.
- (19) Rodriguez-Gonzalez, B.; Sanchez-Iglesias, A.; Giersig, M.; Liz-Marzan, L. M. AuAg bimetallic nanoparticles: formation, silica-coating and selective etching. *Faraday Discuss.* **2004**, *125*, 133.
- (20) Bastus, N. G.; Merkoci, F.; Piella, J.; Puntès, V. Synthesis of Highly Monodisperse Citrate-Stabilized Silver Nanoparticles of up to 200 nm: Kinetic Control and Catalytic Properties. *Chem. Mater.* **2014**, *26*, 2836.
- (21) Verbruggen, S. W.; Keulemans, M.; Martens, J. A.; Lenaerts, S. Predicting the Surface Plasmon Resonance Wavelength of Gold-Silver Alloy Nanoparticles. *J. Phys. Chem. C* **2013**, *117*, 19142.
- (22) Maier, S. A. *Plasmonics: fundamentals and applications*; Springer Science & Business Media, 2007.
- (23) Pena-Rodriguez, O.; Caro, M.; Rivera, A.; Olivares, J.; Manuel Perlado, J.; Caro, A. Optical properties of Au-Ag alloys: An ellipsometric study. *Opt. Mater. Exp.* **2014**, *4*, 403.

- (24) Sonnichsen, C.; Franzl, T.; Wilk, T.; von Plessen, G.; Feldmann, J.; Wilson, O.; Mulvaney, P. Drastic reduction of plasmon damping in gold nanorods. *Phys. Rev. Lett.* **2002**, *88*.
- (25) Nishijima, Y.; Akiyama, S. Unusual optical properties of the Au/Ag alloy at the matching mole fraction. *Opt. Mater. Exp.* **2012**, *2*, 1226.
- (26) Kneipp, K.; Wang, Y.; Kneipp, H.; Perelman, L. T.; Itzkan, I.; Dasari, R.; Feld, M. S. Single molecule detection using surface-enhanced Raman scattering (SERS). *Phys. Rev. Lett.* **1997**, *78*, 1667.
- (27) Nie, S. M.; Emery, S. R. Probing single molecules and single nanoparticles by surface-enhanced Raman scattering. *Science* **1997**, *275*, 1102.
- (28) Siegfried, T.; Kind, M.; Terfort, A.; Martin, O. J. F.; Zharnikov, M.; Ballav, N.; Sigg, H. Reusable plasmonic substrates fabricated by interference lithography: a platform for systematic sensing studies. *J. Raman Spectrosc.* **2013**, *44*, 170.
- (29) Saikin, S. K.; Chu, Y.; Rappoport, D.; Crozier, K. B.; Aspuru-Guzik, A. Separation of Electromagnetic and Chemical Contributions to Surface-Enhanced Raman Spectra on Nanoengineered Plasmonic Substrates. *J. Phys. Chem. Lett.* **2010**, *1*, 2740.
- (30) Wu, T.; Zhang, L.; Gao, J.; Liu, Y.; Gao, C.; Yan, J. Fabrication of graphene oxide decorated with Au-Ag alloy nanoparticles and its superior catalytic performance for the reduction of 4-nitrophenol. *J. Mater. Chem. A* **2013**, *1*, 7384.
- (31) Mosmann, T. Rapid Colorimetric Assay For Cellular Growth and Survival - Application to Proliferation and Cytotoxicity Assays. *J. Immunol. Meth.* **1983**, *65*, 55.
- (32) Shang, L.; Nienhaus, K.; Nienhaus, G. U. Engineered nanoparticles interacting with cells: size matters. *J. Nanobiotech.* **2014**, *12*.
- (33) Larginho, M.; Baptista, P. V. Gold and silver nanoparticles for clinical diagnostics - From genomics to proteomics. *J. Proteomics* **2012**, *75*, 2811.
- (34) Yang, J.; Lee, J. Y.; Ying, J. Y. Phase transfer and its applications in nanotechnology. *Chem. Soc. Rev.* **2011**, *40*, 1672.
- (35) Brust, M.; Walker, M.; Bethell, D.; Schiffrin, D. J.; Whyman, R. Synthesis of thiol-derivatised gold nanoparticles in a two-phase Liquid-Liquid system. *J. Chem. Soc., Chem. Commun.* **1994**, 801.
- (36) Leff, D. V.; Ohara, P. C.; Heath, J. R.; Gelbart, W. M. THERMODYNAMIC CONTROL OF GOLD NANOCRYSTAL SIZE - EXPERIMENT AND THEORY. *J. Phys. Chem.* **1995**, *99*, 7036.

- (37) Johnson, S. R.; Evans, S. D.; Mahon, S. W.; Ulman, A. Alkanethiol molecules containing an aromatic moiety self-assembled onto gold clusters. *Langmuir* **1997**, *13*, 51.
- (38) Porter, L. A.; Ji, D.; Westcott, S. L.; Graupe, M.; Czernuszewicz, R. S.; Halas, N. J.; Lee, T. R. Gold and silver nanoparticles functionalized by the adsorption of dialkyl disulfides. *Langmuir* **1998**, *14*, 7378.
- (39) Liu, J.; Xu, R. L.; Kaifer, A. E. In situ modification of the surface of gold colloidal particles. Preparation of cyclodextrin-based rotaxanes supported on gold nanospheres. *Langmuir* **1998**, *14*, 7337.
- (40) Kumar, A.; Mukherjee, P.; Guha, A.; Adyantaya, S. D.; Mandale, A. B.; Kumar, R.; Sastry, M. Amphoterization of colloidal gold particles by capping with valine molecules and their phase transfer from water to toluene by electrostatic coordination with fatty amine molecules. *Langmuir* **2000**, *16*, 9775.
- (41) Zhu, H. F.; Tao, C.; Zheng, S. P.; Wu, S. K.; Li, J. B. Effect of alkyl chain length on phase transfer of surfactant capped Au nanoparticles across the water/toluene interface. *Colloids Surf., A* **2005**, *256*, 17.
- (42) Wang, W.; Efrima, S.; Regev, O. Directing oleate stabilized nanosized silver colloids into organic phases. *Langmuir* **1998**, *14*, 602.
- (43) Templeton, A. C.; Pietron, J. J.; Murray, R. W.; Mulvaney, P. Solvent refractive index and core charge influences on the surface plasmon absorbance of alkanethiolate monolayer-protected gold clusters. *J. Phys. Chem. B* **2000**, *104*, 564.
- (44) Jose-Yacaman, M.; Gutierrez-Wing, C.; Miki, M.; Yang, D. Q.; Piyakis, K. N.; Sacher, E. Surface diffusion and coalescence of mobile metal nanoparticles. *J. Phys. Chem. B* **2005**, *109*, 9703.
- (45) Eggers, J.; Lister, J. R.; Stone, H. A. Coalescence of liquid drops. *J. Fluid Mech.* **1999**, *401*, 293.
- (46) Rajendra, R.; Ballav, N. Discriminative response of aliphatic and aromatic dithiol in the self-assembly of gold nanoparticles. *RSC Adv.* **2013**, *3*, 15622.
- (47) Aarts, D.; Lekkerkerker, H. N. W.; Guo, H.; Wegdam, G. H.; Bonn, D. Hydrodynamics of droplet coalescence. *Phys. Rev. Lett.* **2005**, *95*.
- (48) Menchaca-Rocha, A.; Martinez-Davalos, A.; Nunez, R.; Popinet, S.; Zaleski, S. Coalescence of liquid drops by surface tension. *Phys. Rev. E* **2001**, *63*, art. no.
- (49) Ji, X.; Song, X.; Li, J.; Bai, Y.; Yang, W.; Peng, X. Size control of gold nanocrystals in citrate reduction: The third role of citrate. *J. Am Chem. Soc.* **2007**, *129*, 13939.

(50) Wang, S.; Qian, K.; Bi, X.; Huang, W. Influence of Speciation of Aqueous HAuCl_4 on the Synthesis, Structure, and Property of Au Colloids. *J. Phys. Chem. C* **2009**, *113*, 6505.

(51) Mironov, I. V. About the stability of $\text{Au}(\text{NH}_3)_4^{3+}$ in aqueous solution. *Russ J Inorg Chem+* **2008**, *53*, 655.